Concentration of Ammonium from Dilute Aqueous Solutions using Commercially Available Reverse Osmosis Membranes

by

Tolulope David Awobusuyi

A thesis submitted to the Faculty of Graduate and Post-Doctoral Studies in partial fulfillment of the requirements for the degree of

Master of Applied Science, Chemical Engineering

Department of Chemical and Biological Engineering

Faculty of Engineering

University of Ottawa

February 2016

Abstract

Several commercially available reverse osmosis (RO) membranes were characterized with aqueous solutions of ammonium sulfate, potassium triphosphate, and mixtures of these two salts at different feed concentrations, compositions and pressures. The objective of this study was to investigate the rejection of these solutes, in particular the ammonium ion (NH_4^+), by different RO membranes. The aqueous solutions were assumed to come from an anaerobic digester via a process, currently under investigation by CHFour Biogas Inc., to maintain low concentrations of ammonia in the digester in order to maximize the biogas production. The ammonium ions present in the liquid produced from the process are then concentrated using membrane separation. The concentrated ammonium solution would be a valuable fertilizer that could be used by agriculture.

The membranes were characterized with three models: the solution-diffusion model, the Kedem-Katchalsky model, also known as the irreversible thermodynamics model, and the Donnan Steric Pore Model (DSPM). The solution-diffusion and irreversible thermodynamics models were found to be inadequate for proper membrane characterization and the use of the DSPM model yielded membrane properties in good agreement with those found in already existing literature. The pore radius of investigated membranes ranged from 0.39 to 0.51 nm. The effect of pH on membrane surface charge was also studied, with the conclusion that increases in pH led to increasingly negative surface charges. This affected the transport of individual ions through the membrane due to preferential passage of the counter-ions. The effects of applied pressure on the stoichiometric nature of salt rejections were also studied.

The minimal observed rejection from the range of experiments carried out using ammonium sulfate was 93%Non-stoichiometric rejections of ions were also observed in the experiments with single and multiple solutes. Furthermore, the rejection of ammonium ions in the presence of other ions (K^+, SO_4^{2-}, PO_4^{3-}) increased as feed concentration increased, which was a result of the synergistic effects of feed pH and ionic interactions. The minimum NH_4^+ rejection in the presence of other ions was 95.4%, which suitability using RO membranes for concentration of ammonium from dilute aqueous solutions.

Résumé

Plusieurs membranes d'osmose inverse disponibles commercialement ont été caractérisées en utilisant des solutions aqueuses de sulfate d'ammonium, triphosphate de potassium, ainsi que des mélanges de ces deux composés à différentes compositions, concentrations et pressions. L'objectif de ce projet était de déterminer et quantifier la rejection de ces sels, en particulier l'ion ammonium (NH_4^+), par les membranes d'osmose inverse testées. Il a été supposé que les solutions aqueuses provenaient d'un digesteur anaérobique par un procédé, qui est présentement en développement chez CHFour Biogas Inc., afin de maintenir des concentrations d'ammoniac basses dans le digesteur avec le but de maximiser la production de biogaz. Les ions ammonium qui sont présents dans le liquide produit par le procédé sont par la suite concentrés en utilisant des méthodes de séparation membranaire. Le résultat est une solution concentré d'ammonium qui pourrait être un engrais de grande valeur dans l'industrie agroalimentaire.

Les membranes ont été caractérisées en utilisant trois modèles : le modèle solution-diffusion, le modèle Kedem-Katchalsky (aussi connu comme le modèle de la thermodynamique irréversible), et le Donnan Steric Pore Model (DSPM). Il a été conclu que les modèles solution-diffusion et de la thermodynamique irréversible sont inadéquats pour la caractérisation des membranes. Cependant, les propriétés de membrane obtenue avec le modèle DSPM étaient en bon accord avec ceux trouvés dans la littérature existante. La taille moyenne des pores de la membrane a été déterminé comme étant 0.39 a 0.51 nm. L'effet du pH sur la charge à la surface de la membrane a aussi été étudié. Il a été déterminé qu'en augmentant le pH, la charge dominante à la surface devenait de plus en plus négative. Cela a affecté le transport des ions à travers la membrane en raison du passage préférentiel des contre-ions. L'effet de la pression sur la nature stoichiométrique de la rejection de sel a aussi été étudié.

La rejection minimale obtenue par les expériences performé avec du sulfate d'ammonium était de 93 pourcent, ce qui indique que le procédé proposé est en effet faisable. Rejets non stoechiométriques d' ions ont également été observées , ce qui était une raison majeure pour discréditer le modèle solution -diffusion et de la thermodynamique irreversible. De plus, la rejection d'ions ammonium en présence des autres ions qui sont retrouvés dans le digestat anaérobie (K^+, SO_4^{2-}, PO_4^{3-}) était supérieure à des

concentrations d'alimentation plus élevées. Ceci était un résultat des effets synergiques du pH de l'alimentation et des interactions ioniques. La rejection minimale de NH_4^+ en présence des autres ions était de 95.4 pourcent.

Thesis Acknowledgement

It takes a village to raise a child, so the African saying goes. This thesis is my child, and the following people were instrumental to both bringing it to its full term and my growth as an individual and researcher during this period.

1. Dr. Boguslaw Kruczek and Dr. F. Handan Tezel, for the invaluable knowledge, direction and perseverance; the gift of confidence; the love of research; and role models by whose lives a man can measure himself.
2. CHFour Biogas and NSERC, for funding and patience with the progress of this thesis.
3. My parents and family. Obviously.
4. Sid Ypma, Kirstin Johnson, and the Linlathen Board, for the gift of wisdom and the encouragement to seek for meaning in all I do. Down the rabbit hole I tumble, and let the cards fall where they may.
5. Dr. Nimal DeSilva and the researchers at the Geochemistry Laboratory, ARC, for helping with the most important measurements regardless of the demanding nature of the request.
6. David Carter, for starting the project and serving as a minor supervisor and a second set of more experienced eyes.
7. Haoyu Wu, for being the ultimate encouragement and an inspiration beyond the pale.
8. The lab technicians of the Department of Chemical Engineering: Franco Ziroldo, Lou Tremblay, and Gerard Nina. Without their technical expertise this work would not have been completed.
9. The graduate students in Office D218: Thank you for being good sounding boards and effective foils to my more harebrained ideas.
10. Music: Jazz, black music, neo-soul, folk. Without these, days in the lab wore the soul down to a nub.

Statement of contributions of collaborators

I hereby declare that I, Tolulope David Awobusuyi, am the sole author of this thesis and that no part of the work presented in this document has been submitted or accepted for any other degree.

Dr. Boguslaw Kruczek and Dr. F. Handan Tezel supervised this thesis. Both provided continued guidance during the course of the work carried out and editorial comments to the final version of this thesis. David Carter and Lauren Rose co-authored the paper on characterization of RO membranes using ammonium sulfate and the basic solution-diffusion model. The role of the author of this thesis was to carry out experiments in the laboratory, to determine the correct way of calculating osmotic pressures for all experiments, and to edit several versions of the paper before publication. An M.Eng. report was also submitted by the author of this thesis from the work done.

The responsibilities designated and carried out by the author, Tolulope Awobusuyi, in completion of this thesis were:

1. Carry out experiments studies to determine the feasibility of using reverse osmosis and low pressure reverse osmosis membranes to concentrate ammonia as found in anaerobic digestate,
2. Characterize the membranes using phenomenological (solution-diffusion and Kedem-Katchalsky) and mechanistic (Donnan steric pore model) models,
3. Characterize the membranes using pure water, ammonium sulphate, and tripotassium phosphate,
4. Determine the stoichiometric nature or otherwise of the rejection of ions comprising a solute and the effect of pH on the stoichiometric nature, and
5. Prepare a written thesis in partial fulfillment of the requirements for obtaining a M.A.Sc. degree in Chemical Engineering.

Table of Contents

List of Figures

List of Tables

Chapter 1: Introduction

1.1 Overview

Anaerobic digestion is a method used in the treatment of waste products from farms and municipalities. The process converts organic matter to methane [1] and also produces biomass, which is a good plant fertilizer. Ammonia (NH_3) and ammonium $(NH_4)^+$ are also produced in the digester by the degradation of nitrogen-containing substances. But the presence of high concentrations of free ammonia is considered toxic to the digestion process [2]. Ammonia is also required in the production of N-type fertilizers, which encourages the removal of ammonia from the system. The ammonia produced can be removed by denitrifying the gas mixtures from the digester and can either be used in the production of fertilizer [1] or liquefied and reformed to hydrogen gas [3]. Ammonia can also be continuously removed from the digester by scrubbing the gas from the digester [4]. After the gas mixture is scrubbed and the ammonia has dissolved in water, the ammonia-containing solution is acidified by the addition of sulfuric acid to produce ammonium sulfate. Ammonium is removed by feeding the effluent to a membrane process. To reject high amounts of NH_4^+ ions in the retentate, which would be used as fertilizer, membranes with high solute rejections must be used.

A number of membrane processes can be used to concentrate NH_4^+ ions in the retentate: reverse osmosis (RO), low-pressure reverse osmosis (LPRO), nanofiltration (NF), ultrafiltration (UF), and microfiltration (MF). Of the processes mentioned above, reverse osmosis and nanofiltration are the most commonly used as they have high solute rejections [5], [6]. Intensive research in this field has led to the design of reverse osmosis membranes with greater chemical and mechanical stabilities [5], increased water fluxes [5], and high solute rejections, which reduce operating costs [5], [6]. LPRO/NF membranes are also widely used as they provide high fluxes at lower pressures when compared to RO membranes [7], but these occur at lower solute rejections than observed for commercial RO membranes [7], [8].

Understanding membrane performance is crucial to improving the effectiveness of membranes used for separation. This is usually done using transport models for membrane characterization [9], and these models are classified into two broad groups.

Phenomenological models describe the membrane performance in terms of experimentally measureable parameters such as permeate fluxes and solute rejections and neglect transport mechanisms within the membrane, while mechanistic models relate the membrane structure and polymer properties to its performance, providing information on physical (pore radius and effective membrane thickness) and chemical (membrane surface charge generated by the nature of the feed and feed pH) properties observed for the membranes.

1.2 Objectives

This thesis aims to study the effectiveness of using reverse osmosis (RO) and low-pressure reverse osmosis (LPRO) membranes in the removal of ammonium from anaerobic digester effluent as a method of producing N-type fertilizers with the rejected portion of the effluent. Three LPRO and two RO membranes were characterized using aqueous solutions of ammonium sulfate, but testing with other solutions (tripotassium phosphate and a mixture of tripotassium phosphate and ammonium sulfate) was carried out using only LPRO membranes. The membranes were also characterized using both phenomenological and mechanistic models with the experimental results of the salts tested, and from these the membrane properties (pore radius, effective membrane thickness and solute and solvent permeances) were determined. The influence of feed pressure and pH on ionic rejections for ions comprising ammonium sulfate and tripotassium phosphate was also observed.

This thesis is divided into six chapters. Chapter 1 is an introduction, which gives a summary of the thesis objectives and the work carried out. Chapter 2 is a literature review on membrane technology. Chapters 3 to 5 comprise the work carried out for this thesis in paper format. Chapter 3 focuses on the use of RO membranes in the rejection of ammonium sulfate. Chapter 4 focuses on the comparison of phenomenological models and the observation of non-stoichiometric transport through the membranes. Chapter 5 focuses on the use of the Donnan steric pore model to determine the membrane properties using acidic and alkaline pH salts. A general conclusion based on the limitations and challenges faced during the course of the thesis is provided in Chapter 6.

1.3 References

[1] D. M. Babson, K. Bellman, S. Prakash, and D. E. Fennell, "Anaerobic digestion for methane generation and ammonia reforming for hydrogen production: Athermodynamic energy balance of a model system to demonstrate net energy feasibility," *Biomass and Bioenergy*, vol. 56, pp. 493–505, 2013.

[2] L. Appels, J. Baeyens, J. Degrève, and R. Dewil, "Principles and potential of the anaerobic digestion of waste-activated sludge," *Prog. Energy Combust. Sci.*, vol. 34, no. 6, pp. 755–781, 2008.

[3] J. H. Kim, D. H. Um, and O. C. Kwon, "Hydrogen production from burning and reforming of ammonia in a microreforming system," *Energy Convers. Manag.*, vol. 56, pp. 184–191, 2012.

[4] S. H. Byeon, B. K. Lee, and B. Raj Mohan, "Removal of ammonia and particulate matter using a modified turbulent wet scrubbing system," *Sep. Purif. Technol.*, vol. 98, pp. 221–229, 2012.

[5] K. P. Lee, T. C. Arnot, and D. Mattia, "A review of reverse osmosis membrane materials for desalination-Development to date and future potential," *J. Memb. Sci.*, vol. 370, no. 1–2, pp. 1–22, 2011.

[6] B. Peñate and L. García-Rodríguez, "Current trends and future prospects in the design of seawater reverse osmosis desalination technology," *Desalination*, vol. 284, pp. 1–8, 2012.

[7] N. Hilal, H. Al-Zoubi, N. a. Darwish, a. W. Mohammad, and M. Abu Arabi, "A comprehensive review of nanofiltration membranes: Treatment, pretreatment, modelling, and atomic force microscopy," *Desalination*, vol. 170, no. 3, pp. 281–308, 2004.

[8] B. Van der Bruggen, M. Mänttäri, and M. Nyström, "Drawbacks of applying nanofiltration and how to avoid them: A review," *Sep. Purif. Technol.*, vol. 63, no. 2, pp. 251–263, 2008.

[9] J. Wang, D. S. Dlamini, A. K. Mishra, M. T. M. Pendergast, M. C. Y. Wong, B. B. Mamba, V. Freger, A. R. D. Verliefde, and E. M. V Hoek, "A critical review of transport through osmotic membranes," *J. Memb. Sci.*, vol. 454, pp. 516–537, 2014.

Chapter 2: Literature review

2.1 Overview

Anaerobic digestion is a commonly used waste treatment process that simultaneously produces methane and biomass, both alternative energy sources [1], [2]. The production of methane is a result of bacterial activity on organic matter in the digestate feed, which contains food products, manure, dead plants, and other carbon-containing compounds. The particulars of the process are influenced by the pH of the digestate, the temperature at which anaerobic digestion is taking place, and the digester retention time. In the presence of nitrogen-containing matter the initial degradation stage produces ammonia gas and ammonium ions, and increased production of these compounds results in a decrease in methanogenic activity of the bacteria. Ammonia, as an inhibitor to methane production via methanogenesis and the digestion process [2]–[4], is an undesired product and can be removed by reacting the anaerobic digestate with sulfuric acid. This creates ammonium sulfate in solution, which can be concentrated using membranes. The concentrate can be used as fertilizer for plants, which is important to the maintenance of sustainable farms.

The most common methods of ammonia removal from anaerobic digestate are ion-exchange [5] and membrane contacting [4]. Existing literature proves that ammonium sulfate can be produced by contacting ammonia found in aqueous solutions with sulfuric acid in a membrane contactor with high rates of ammonia removal [4], [6]. Literature also shows increased methane yield for anaerobic digesters equipped with a membrane contactor for high organic loading rates and increased hydrogen sulfide content [3]. These results, along with the reduced operating costs of membrane reactors, make membrane contacting and stripping with sulfuric acid an economically attractive proposition when compared to existing forms of ammonia removal.

Solids content in anaerobic digestate is a major inhibitor to membrane performance as fouling leads to decline in permeate fluxes across the membranes [7], [8]. A lot of the solids in anaerobic digestate being larger than 100 μm [9], both coarse and fine filtration steps are necessary to prepare the anaerobic digestate for use with membranes. An existing study reported significant flux reductions for reverse osmosis

experiments conducted with digestate filtered to 100-µm particle size as compared to experiments using deionized water [10]. In the paper, these reductions in flux were caused by fouling and were more pronounced at lower ionic concentrations. Masse et al., in their review article, write that manure for reverse osmosis treatment has to undergo multiple pretreatment steps, and it is the usual practice to filter manure down to 10-µm particles before contacting it with reverse osmosis (RO) or low pressure reverse osmosis (LPRO) membranes [8].

2.2 Membranes: Types, Characterization models, and Commercial uses

2.2.1 Membrane types

Membrane classification is based on certain properties intrinsic to the membranes: the materials used in the membrane fabrication, the pore sizes of the membranes, and the membrane structure. Materials used in membrane fabrication are ceramics, polymers, glass, and metal alloys [11], [12]. The materials used depend on the desired application, and in the case of RO/LPRO separations the overwhelming majority of the membranes are polymeric in nature [11]–[13]. Common polymers include: polysulfones [11], [12], [14], [15], polyamides, polyfuranes [12], [16]–[18], and cellulose acetate[19]–[24].

Another common classification method is the pore size method. This is based on the understanding that solute rejection is primarily a result of size exclusion. In this classification the membranes are either porous (ultrafiltration and microfiltration) or dense (reverse osmosis and nanofiltration). The distinctions are not clear-cut, leading to more specific classifications such as low-pressure reverse osmosis (LPRO), which falls between reverse osmosis and nanofiltration. The pore sizes also determine the rejection performance of the membranes.

2.2.2 Characterization models

Currently available models for characterizing RO/LPRO membranes do not always provide adequate descriptions for the membrane properties. Solute rejections usually depend on the combined interactions of sieving, electrical and dielectric effects [25]–[27], and the interrelationship among these three effects is not always understood. These limitations, along with the complexities involved in understanding the electrical

transport mechanisms, require complex modeling before ionic transport through membranes can be properly interpreted.

Models can be grouped according to the following criteria: membrane porosity and model dependence on transport mechanisms across the membrane. Dense membranes are classified as non-porous, and according to Wang: “separation is a result of differences in solubility and diffusivity of permeates.” [13]. The most common models used in characterizing these membranes are the solution-diffusion and the irreversible thermodynamics model. The pore flow model is the most common model used in describing transport through a porous membrane [13].

Model classification according to dependence on transport mechanisms result in two classes of models: mechanistic and phenomenological models. The mechanistic models account for ion transport through the membrane. According to Ahmed (2013), these models “integrate the physical and chemical factors of both the membrane and the solution to deliver a complete picture of the interactions between the filtering solution and the membrane” [27]. These are used especially with NF/LPRO membranes, as literature on the subject agrees that sieving, electrical and dielectric effects govern the rejection abilities of liquid separation membranes in addition to size exclusion [27]–[29], and any model used in characterization must take these into consideration. Ionic transport as a function of electrostatic interaction on the membrane surface is accounted for by the presence of fixed charge groups on the membrane surface, which interact with charged solutes in the feed [30]. The extended Nernst-Planck equation takes these effects into account [27], [28], and is used in combination with a number of models: the space charge pore model and the Teorell-Meyer-Sievers (TMS) model being two examples [28], [31]. The TMS model assumes a uniformity in the ionic concentration and electrical potential across the pore, it being primarily concerned with ionic transportation in an axial direction, through the membrane [27], [30]. It is also regarded as a simpler model than the space-charge model [30]. The extended Nernst-Planck equation has also been combined with a concentration polarization model to determine the rejection characteristics of organic and inorganic compounds, with the conclusion that for charged inorganic compounds the contributions of the diffusive, convective, and electric field gradient transport mechanisms are important parameters [28], [32]. It was also concluded

that uncharged organic compounds were primarily transported by the diffusive and convective mechanisms [32].

The ubiquity of the extended Nernst-Planck equation in mechanistic modeling can be attributed to two characteristics: its ability to describe the various ionic transport mechanisms present in membrane separation and the ease with which it can be combined with other models. Most recently it has been combined with the Donnan-steric pore model (DSPM) to account for hindered transport and the effects of the combined presence of electrical and size exclusion (sieving/steric) mechanisms [27], [33]. Notable findings include a variable membrane charge density that was dependent on the salt type, ionic concentration, and ion adsorption [27], [34], and the influence of valence charges on ionic rejections [34]. Of singular importance is the correlation between the mechanistic and phenomenological models with respect to describing transport through the membrane. Cuartas-Uribe reported that the rejections predicted by the DSPM and the irreversible thermodynamics models corroborated experimental findings using single and mixed electrolytes in a NF setup [27], [35].

The phenomenological models can be described as "mechanism-independent" [27], and do not describe ionic transport through the membrane [33]. The membrane is assumed to be a black box and near to equilibrium during solvent transport [13], [33]. Two of the most commonly used models in the characterization of RO/LPRO membranes, the solution-diffusion model and the Kedem-Katchalsky model, are phenomenological in nature. The solution-diffusion model, while being the most common model used in the characterization of polymeric membranes, has been shown to have limitations with respect to characterizing RO and LPRO membranes as it does not account for convective transport through the membranes [36], [37]. This problem is rectified by the use of the Kedem-Katchalsky model or modifications to this model, such as the Spiegler-Kedem-Katchalsky model or a combination of the Spiegler-Kedem combination with liquid film theory [13], [27]. The use of phenomenological models has been shown to successfully predict separation performance of RO/LPRO/NF membranes, which is a reason for their enduring use [33].

2.2.3 Commercial uses

RO/LPRO has seen extensive use in industrial processes requiring separation or concentration with a high degree of efficiency. Notable applications of RO/LPRO/NF include desalination [12], [16], [38]; the purification of ground water, wastewater [39]–[41], and industrial effluents; pharmaceutical separations requiring high rejections of specific ions or compounds [37], [42], [43]; ammonia removal from animal waste products on farms [44], [45]. The focus of this thesis is the investigation of ammonia removal from animal wastes using RO and LPRO membranes as a commercially feasible application. Considering the objectives of the work done in this thesis, only the applications of membranes in the wastewater treatment and ion removal from waste will be discussed further.

Ground water, wastewater, and industrial effluents

Strict laws regarding the ionic content of water disposed into the world's oceans demand that wastewater fed to the water bodies are in compliance with environmental regulations provided by national or international laws. To this end, industries have to ensure that wastewater produced from facilities are routinely treated, and there is ongoing research into the most effective methods of treatment available.

The application of membrane separation processes to the removal of organics and particulate matter present in groundwater, wastewater, and industrial effluents has been extensively studied and documented [27], [46]. High multivalent ion rejections of Ca^{2+}, Mg^{2+}, and SO_4^{2-}, equal to or greater than 80 percent, have been routinely observed for RO/NF membranes in studies detailing the rejections of these ions in industrial processes [46]–[48]. In pulp and paper industries, membrane separation processes are routinely used to remove contaminants such as COD and multivalent ions like Ca^2 in the process effluents [46], [47], [49]. In wastewater treatment, where the removal of contaminants is prioritized, membrane technology has been proven to yield water removal rates greater than 95% [27], [50]. Membrane separation processes are also applied for their abilities to produce high-purity permeates, as they are able to effectively reject most of the ions, bacteria, and viruses present in wastewater [11], [30], [46], [51].

RO/LPRO/NF processes have also been used in the purification of dye-containing effluents [40], [41], [52]. Rejections above 90 percent have been observed for color removal for processes using NF [27], [41], [53], and dye rejections using RO/LPRO/NF processes are usually in the 99th percentile [39]–[41], [54]. COD removal using RO/LPRO membranes is also excellent, with a 98 % average COD removal recorded for RO/LPRO processes [41]. A comparison of the physicochemical processes used for dye and COD removals indicates that membrane separation processes outperform other techniques, with Chitosan adsorption being the only process yielding similar results [41], [55].

Ammonia removal from animal waste

Anaerobic digestate, which comprises manure, farm wastes, and occasionally municipal wastes, is high in ammonia content, and this poses substantial problems to methane production in the digesters and environmental compliance during and after digestate disposal. Ammonia in anaerobic digesters is a product of converted organic nitrogen [56], and in the form of ammonia gas is known as a major inhibitor to methane production [1], [57], [58]. Ammonia inhibition is such an important factor in anaerobic digestion that uncontrolled ammonia activity is known to cause digestate failure [44], [58], and because of this valuable effort has been expended on ammonia removal processes from anaerobic digesters. Added to this are ammonia's negative effects on the environment: nitrogen-containing matter produces 1.5 to 2.6 tons of CO_2 per ton of nitrogen [45]; and ammonia in nature is directly responsible for eutrophication [44].

Some of the most common technologies proposed for ammonia removal are ion exchange [5], [58], electrochemistry [58], gas stripping using air or steam, membrane contacting [4], fuel cells [58], and membrane technology [44], [45]. Membrane technology promises rejections as high as the other methods used while operating at reduced costs. Membrane technology is also an attractive alternative because of its environmentally benign nature: as it requires no external chemicals for operation it produces no new waste of its own. The compactness of membrane modules is an added attractiveness to the process: with the use of spiral wound modules large effective surface

areas can be packed into compact modules, leading to optimization in equipment area and reduced capital costs.

RO and LPRO membranes are used in the rejection of ammonium ions in anaerobic digestate and aqueous solutions because they have been shown to reject as much as 97% of the ammonium content present in the feed [19], [44]. RO and LPRO membranes generally have higher rejection rates than NF membranes. Some NF membranes, for example, have shown 30% ammonium rejections and other NF membranes have shown ammonium rejections as high as 82% [44], [45]. This large variation in ammonium rejections is arguably due to the differences in pH, membrane morphology, ion-ion interaction, and ion-membrane interaction across the available membranes. A series of tests using NF270 shows that the ammonium rejection increases with an increase in pH [45]. This was attributed to the combined effects of the surface charge of the membrane in relation to the NH_4^+ ion, the presence of phosphorus-containing ions in the dairy manure, and the changes in the membrane morphology with increasing pH [45].

Desalination

Perhaps the most common application of RO/LPRO membranes today, desalination involves the purification of seawater by membrane separation processes to provide potable water for communities [59]. It is an increasingly common method for providing potable water to large communities in arid regions of the world, where water scarcity is chronic and increasingly severe due to population explosions. It is estimated that at least 300 million people worldwide depend on desalination for their daily water intake, solely or in part [60]. The usefulness of desalination is most appreciated in Israel, where it provides a quarter of the nation's water supply [61]. In 2009, there were more than 15,000 desalination plants in operation worldwide, and the total production capacity of these plants was 37 million m^3 of water per day [16]. In 2015 that number is approximately 66 million m^3/day with over 17,000 plants in 150 countries [60], [61].

Desalination processes are widely applied for many reasons. RO processes are popular because the rejection abilities of RO membranes are high for many of the ions

found in seawater and brackish water. The processes also require no chemical additives for the processes [62], leading to the production of environmentally benign wastes.

As membrane separation processes separate solutes from the solvent by the preferential permeation of solvent through the membrane, the retentate portion is more concentrated than the incoming feed. Desalination plants are no exception to this behavior [63], and solute concentration in the retentate is considered to be a major environmental issue as it could disturb the ecological balance of the water body the retentate is introduced to [63], [64]. Other environmental issues are the dangers of impingement and entrainment of aquatic organisms in the vicinities of the desalination plants [18], [64]; noise pollution [63]; and the presence of pretreatment residuals, such as antiscalants and coagulants [18], [64]. These issues are addressed in the WHO Desalination for Safe Water Supply, Guidance for the Health and Environmental Aspects Applicable to Desalination report, published in 2007 [18], and include such solutions as: careful site selection away from oil and gas plants and further offshore [18], [64]; improved dispersion techniques for the retentate stream [63]; and continued monitoring of the impact of desalination on marine waters [18].

2.3 Conclusions

The influence of membrane separation processes on modern society is far-reaching: from the desalination plants of the Arabian Gulf to the manufacture of fertilizer from anaerobic digestate in Europe and North America, and the astonishing success of the process can be attributed to its ability to deliver high ionic rejections for applications requiring a high degree of purity. The application of membrane to the removal of ammonia from animal wastes is especially promising for this thesis, as high rejections have been observed. Being a relatively new field, however, the mechanisms involved in solute and solvent transport are not completely understood, and the gaps in knowledge are most revealing in models used in membrane characterization. Modeling is challenging because the parameters affecting membrane performance are not always adequately defined, leading to a plentitude of models available to the researcher or engineer seeking to use RO/NF technology for a given purpose. Another limitation is the considerable

overlap between the characteristics that determine the class any given membrane belongs to, which makes any attempt at a limpid classification of the membranes difficult.

Despite the gaps in knowledge, membrane separation processes have showed consistently better performances in separation applications than a lot of currently available technology. A simplified design schematic, lower energy requirements, compact packing via the tubular configuration, and reduced recurring costs are the advantages of the processes, and the resulting predominance of RO/LPRO/NF membranes in desalination is an indicator of the potential inherent in membrane studies as a major process in chemical engineering.

2.4 References

[1] Y. Chen, J. J. Cheng, and K. S. Creamer, "Inhibition of anaerobic digestion process: A review," *Bioresour. Technol.*, vol. 99, no. 10, pp. 4044–4064, 2008.

[2] O. Yenigün and B. Demirel, "Ammonia inhibition in anaerobic digestion: A review," *Process Biochem.*, vol. 48, no. 5–6, pp. 901–911, 2013.

[3] B. Lauterböck, M. Nikolausz, Z. Lv, M. Baumgartner, G. Liebhard, and W. Fuchs, "Improvement of anaerobic digestion performance by continuous nitrogen removal with a membrane contactor treating a substrate rich in ammonia and sulfide," *Bioresour. Technol.*, vol. 158, pp. 209–216, 2014.

[4] B. Lauterböck, M. Ortner, R. Haider, and W. Fuchs, "Counteracting ammonia inhibition in anaerobic digestion by removal with a hollow fiber membrane contactor," *Water Res.*, vol. 46, no. 15, pp. 4861–4869, 2012.

[5] T. Wirthensohn, F. Waeger, L. Jelinek, and W. Fuchs, "Ammonium removal from anaerobic digester effluent by ion exchange," *Water Sci. Technol.*, vol. 60, no. 1, pp. 201–210, 2009.

[6] S. N. Ashrafizadeh and Z. Khorasani, "Ammonia removal from aqueous solutions using hollow-fiber membrane contactors," *Chem. Eng. J.*, vol. 162, no. 1, pp. 242–249, 2010.

[7] J. E. Kilduff, S. Mattaraj, and G. Belfort, "Flux decline during nanofiltration of naturally-occurring dissolved organic matter: Effects of osmotic pressure,

membrane permeability, and cake formation," *J. Memb. Sci.*, vol. 239, no. 1, pp. 39–53, 2004.

[8] L. Masse, D. I. Massé, and Y. Pellerin, "The use of membranes for the treatment of manure: a critical literature review," *Biosyst. Eng.*, vol. 98, no. 4, pp. 371–380, 2007.

[9] K. Koirala, P. M. Ndegwa, H. S. Joo, C. Frear, C. O. Stockle, J. H. Harrison, and V. Velsen, "Impact of Anaerobic Digestion of Liquid Dairy Manure on Ammonia Volatilization Process," *Trans. ASABE*, vol. 56, no. 5, pp. 1959–1966, 2013.

[10] L. Thörneby, K. Persson, and G. Trägårdh, "Treatment of Liquid Effluents from Dairy Cattle and Pigs using Reverse Osmosis," *J. Agric. Eng. Res.*, vol. 73, no. 2, pp. 159–170, 1999.

[11] A. Westgate, "Evaluation Of Novel Polyethersulfone Membranes Incorporating Charged Surface Modifying Macromolecules For The Removal Of Pharmaceuticals And Endocrine Disrupting Compounds From Drinking Water," University of Ottawa, 2008.

[12] K. P. Lee, T. C. Arnot, and D. Mattia, "A review of reverse osmosis membrane materials for desalination-Development to date and future potential," *J. Memb. Sci.*, vol. 370, no. 1–2, pp. 1–22, 2011.

[13] J. Wang, D. S. Dlamini, A. K. Mishra, M. T. M. Pendergast, M. C. Y. Wong, B. B. Mamba, V. Freger, A. R. D. Verliefde, and E. M. V Hoek, "A critical review of transport through osmotic membranes," *J. Memb. Sci.*, vol. 454, pp. 516–537, 2014.

[14] D. Libotean, J. Giralt, R. Rallo, Y. Cohen, F. Giralt, H. F. Ridgway, G. Rodriguez, and D. Phipps, "Organic compounds passage through RO membranes," *J. Memb. Sci.*, vol. 313, no. 1–2, pp. 23–43, 2008.

[15] M. E. Williams, "A Brief Review of Reverse Osmosis Membrane Technology," in *Engineering*, 2003, pp. 1–29.

[16] L. F. Greenlee, D. F. Lawler, B. D. Freeman, B. Marrot, and P. Moulin, "Reverse osmosis desalination: Water sources, technology, and today's challenges," *Water Res.*, vol. 43, no. 9, pp. 2317–2348, 2009.

[17] R. W. Baker, *Membrane Technology and Applications*, 2nd Editio. West Sussex:

John Wiley & Sons, Ltd, 2004.

[18] WHO, “Desalination for Safe Water Supply- Guidance for the Health and Environmental Aspects Applicable to Desalination,” *Public Heal. Environ. World Heal. Organ. Geneva 2007 World Heal.*, p. 173, 2007.

[19] A. Bódalo, J. L. Gómez, E. Gómez, G. León, and M. Tejera, “Ammonium removal from aqueous solutions by reverse osmosis using cellulose acetate membranes,” *Desalination*, vol. 184, no. 1–3, pp. 149–155, 2005.

[20] S. Basu, A. L. Khan, A. Cano-Odena, C. Liu, and I. F. J. Vankelecom, “Membrane-based technologies for biogas separations.,” *R. Soc. Chem.*, vol. 39, no. 2, pp. 750–768, 2010.

[21] N. G. Voros, Z. B. Maroulis, and D. Marinos-Kouris, “Salt and water permeability in reverse osmosis membranes,” *Desalination*, vol. 104, no. 3, pp. 141–154, 1996.

[22] D. Carter, L. Rose, T. Awobusuyi, M. Gauthier, F. H. Tezel, and B. Kruczek, “Characterization of commercial RO membranes for the concentration of ammonia converted to ammonium sulfate from anaerobic digesters,” *Desalination*, vol. 368, pp. 127–134, 2015.

[23] Y. Zhao and J. S. Taylor, “Incorporation of osmotic pressure in an integrated incremental model for predicting RO or NF permeate concentration,” *Desalination*, vol. 174, no. 2, pp. 145–159, 2005.

[24] D. R. Paul, “Reformulation of the solution-diffusion theory of reverse osmosis,” *J. Memb. Sci.*, vol. 241, no. 2, pp. 371–386, 2004.

[25] A. E. Yaroshchuk, “The role of imperfections in the solute transfer in nanofiltration,” *J. Memb. Sci.*, vol. 239, no. 1, pp. 9–15, 2004.

[26] C. Bellona, J. E. Drewes, P. Xu, and G. Amy, “Factors affecting the rejection of organic solutes during NF/RO treatment - A literature review,” *Water Res.*, vol. 38, no. 12, pp. 2795–2809, 2004.

[27] F. N. Ahmed, “Modified Spiegler-Kedem Model to Predict the Rejection and Flux of Nanofiltration Processes at High NaCl Concentrations,” University of Ottawa, 2013.

[28] W. R. Bowen, a. W. Mohammad, and N. Hilal, “Characterisation of nanofiltration membranes for predictive purposes - Use of salts, uncharged solutes and atomic

force microscopy," *J. Memb. Sci.*, vol. 126, no. 1, pp. 91–105, 1997.

[29] D. X. Wang, L. Wu, Z. D. Liao, X. L. Wang, Y. Tomi, M. Ando, and T. Shintani, "Modeling the separation performance of nanofiltration membranes for the mixed salts solution with Mg2+ and Ca2+," *J. Memb. Sci.*, vol. 284, no. 1–2, pp. 384–392, 2006.

[30] L. D. Nghiem, "Removal of emerging trace organic contaminants by nanofiltration and reverse osmosis," University of Wollongong, 2005.

[31] X.-L. Wang, W.-J. Shang, D.-X. Wang, L. Wu, and C.-H. Tu, "Characterization and applications of nanofiltration membranes: State of the art," *Desalination*, vol. 236, no. 1–3, pp. 316–326, 2009.

[32] Y. Yoon and R. M. Lueptow, "Removal of organic contaminants by RO and NF membranes," *J. Memb. Sci.*, vol. 261, no. 1–2, pp. 76–86, 2005.

[33] W. R. Bowen and J. S. Welfoot, "Modelling the performance of membrane nanofiltration-critical assessment and model development," *Chem. Eng. Sci.*, vol. 57, no. 7, pp. 1121–1137, 2002.

[34] J. Schaep, C. Vandecasteele, a. W. Mohammad, and W. R. Bowen, "Analysis of the Salt Retention of Nanofiltration Membranes Using the Donnan–Steric Partitioning Pore Model," *Sep. Sci. Technol.*, vol. 34, no. 15, pp. 3009–3030, 1999.

[35] B. Cuartas-Uribe, M. C. Vincent-Vela, S. Álvarez-Blanco, M. I. Alcaina-Miranda, and E. Soriano-Costa, "Prediction of solute rejection in nanofiltration processes using different mathematical models," *Desalination*, vol. 200, no. 1–3, pp. 144–145, 2006.

[36] B. Van der Bruggen, M. Mänttäri, and M. Nyström, "Drawbacks of applying nanofiltration and how to avoid them: A review," *Sep. Purif. Technol.*, vol. 63, no. 2, pp. 251–263, 2008.

[37] a. M. Hidalgo, G. León, M. Gómez, M. D. Murcia, D. S. Barbosa, and P. Blanco, "Application of the solution-diffusion model for the removal of atrazine using a nanofiltration membrane," *Desalin. Water Treat.*, vol. 51, no. 10–12, pp. 2244–2252, 2013.

[38] C. Fritzmann, J. Löwenberg, T. Wintgens, and T. Melin, "State-of-the-art of reverse osmosis desalination," *Desalination*, vol. 216, no. 1–3, pp. 1–76, 2007.

[39] S. K. Nataraj, K. M. Hosamani, and T. M. Aminabhavi, “Distillery wastewater treatment by the membrane-based nanofiltration and reverse osmosis processes,” *Water Res.*, vol. 40, no. 12, pp. 2349–2356, 2006.

[40] N. Al-Bastaki, “Removal of methyl orange dye and Na2so4 salt from synthetic waste water using reverse osmosis,” *Chem. Eng. Process. Process Intensif.*, vol. 43, no. 12, pp. 1561–1567, 2004.

[41] S. Mohana, B. K. Acharya, and D. Madamwar, “Distillery spent wash: Treatment technologies and potential applications,” *J. Hazard. Mater.*, vol. 163, no. 1, pp. 12–25, 2009.

[42] A. M. Comerton, R. C. Andrews, D. M. Bagley, and C. Hao, “The rejection of endocrine disrupting and pharmaceutically active compounds by NF and RO membranes as a function of compound and water matrix properties,” *J. Memb. Sci.*, vol. 313, no. 1–2, pp. 323–335, 2008.

[43] L. D. Nghiem and S. Hawkes, “Effects of membrane fouling on the nanofiltration of pharmaceutically active compounds (PhACs): Mechanisms and role of membrane pore size,” *Sep. Purif. Technol.*, vol. 57, no. 1, pp. 176–184, 2007.

[44] D. . Nurdan Doruk, “A Novel Solution for Biogas Applications in Poultry Industry: CLAMBS approach,” *J. Bioprocess. Biotech.*, vol. 05, no. 02, 2015.

[45] M. L. Gerardo, N. H. M. Aljohani, D. L. Oatley-Radcliffe, and R. W. Lovitt, “Moving towards sustainable resources: recovery and fractionation of nutrients from dairy manure digestate using membranes,” *Water Res.*, vol. 80, pp. 80–89, 2015.

[46] N. Hilal, H. Al-Zoubi, N. a. Darwish, a. W. Mohammad, and M. Abu Arabi, “A comprehensive review of nanofiltration membranes: Treatment, pretreatment, modelling, and atomic force microscopy,” *Desalination*, vol. 170, no. 3, pp. 281–308, 2004.

[47] Y. Kaya, Z. B. Gönder, I. Vergili, and H. Barlas, “The effect of transmembrane pressure and pH on treatment of paper machine process waters by using a two-step nanofiltration process: Flux decline analysis,” *Desalination*, vol. 250, no. 1, pp. 150–157, 2010.

[48] C. Bartels, R. Franks, S. Rybar, M. Schierach, and M. Wilf, “The effect of feed

ionic strength on salt passage through reverse osmosis membranes," *Desalination*, vol. 184, no. 1–3, pp. 185–195, 2005.

[49] M. Mänttäri, M. Kallioinen, a. Pihlajamäki, and M. Nyström, "Industrial membrane processes in the treatment of process waters and liquors," *Water Sci. Technol.*, vol. 62, no. 7, p. 1653, 2010.

[50] R. Rautenbach, T. Linn, and L. Eilers, "Treatment of severely contaminated waste water by a combination of RO, high-pressure RO and NF - Potential and limits of the process," *J. Memb. Sci.*, vol. 174, no. 2, pp. 231–241, 2000.

[51] T. Wintgens, M. Gallenkemper, and T. Melin, "Endocrine disrupter removal from wastewater using membrane bioreactor and nanofiltration technology," *Desalination*, vol. 146, no. 1–3, pp. 387–391, 2002.

[52] C. S. Slater, R. C. Ahlert, and C. G. Uchrin, "Applications of reverse osmosis to complex industrial wastewater treatment," *Desalination*, vol. 48, no. 2, pp. 171–187, 1983.

[53] Z. Ji, Y. He, and G. Zhang, "Treatment of wastewater during the production of reactive dyestuff using a spiral nanofiltration membrane system," *Desalination*, vol. 201, pp. 255–266, 2006.

[54] M. G. Buonomenna, L. C. Lopez, P. Favia, R. d'Agostino, a. Gordano, and E. Drioli, "New PVDF membranes: The effect of plasma surface modification on retention in nanofiltration of aqueous solution containing organic compounds," *Water Res.*, vol. 41, no. 19, pp. 4309–4316, 2007.

[55] I. G. Lalov, I. I. Guerginov, M. A. Krysteva, and K. Fartsov, "Treatment of waste water from distilleries with chitosan," *Water Res.*, vol. 34, no. 5, pp. 1503–1506, 2000.

[56] D. M. Babson, K. Bellman, S. Prakash, and D. E. Fennell, "Anaerobic digestion for methane generation and ammonia reforming for hydrogen production: Athermodynamic energy balance of a model system to demonstrate net energy feasibility," *Biomass and Bioenergy*, vol. 56, pp. 493–505, 2013.

[57] L. Appels, J. Baeyens, J. Degrève, and R. Dewil, "Principles and potential of the anaerobic digestion of waste-activated sludge," *Prog. Energy Combust. Sci.*, vol. 34, no. 6, pp. 755–781, 2008.

[58] J. Desloover, A. Abate Woldeyohannis, W. Verstraete, N. Boon, and K. Rabaey, "Electrochemical resource recovery from digestate to prevent ammonia toxicity during anaerobic digestion," *Environ. Sci. Technol.*, vol. 46, no. 21, pp. 12209–12216, 2012.

[59] B. Peñate and L. García-Rodríguez, "Current trends and future prospects in the design of seawater reverse osmosis desalination technology," *Desalination*, vol. 284, pp. 1–8, 2012.

[60] I. D. Association, "Desalination by the Numbers | IDA," *Desalination 101*, 2014. [Online]. Available: http://idadesal.org/desalination-101/desalination-by-the-numbers/. [Accessed: 13-Oct-2015].

[61] A. Little, "Can Desalination Counter California's Drought? - The New Yorker," *New Yorker*, 2015. [Online]. Available: http://www.newyorker.com/tech/elements/can-desalination-counter-the-drought. [Accessed: 13-Oct-2015].

[62] I. Koyuncu, D. Topacik, M. Turan, M. S. Celik, and H. Z. Sarikaya, "Application of the membrane technology to control ammonia in surface water," *Water Sci. Technol. Water Supply*, vol. 1, no. 1, pp. 117–124, 2001.

[63] R. Einav, K. Harussi, and D. Perry, "The footprint of the desalination processes on the environment," *Desalination*, vol. 152, no. 1–3, pp. 141–154, 2003.

[64] S. Lattemann and T. Höpner, "Environmental impact and impact assessment of seawater desalination," *Desalination*, vol. 220, no. 1–3, pp. 1–15, 2008.

Chapter 3: Characterization and Optimization of a Membrane Separation Process for the Concentration of Ammonium from Anaerobic Digesters as Ammonium Sulfate to be used as Fertilizer and Enhance Biogas Production.

D. Carter, L. Rose, T. Awobusuyi, M. Gauthier, F.H. Tezel, B. Kruczek*

Department of Chemical and Biological Engineering
University of Ottawa
161 Louis Pasteur, Ottawa, Ontario K1N 6N5, Canada

+ **Published in *Desalination*, April 2015. DOI: 10.1016/j.desal.2015.03.040**

* **To whom correspondence should be addressed.**

Tel: + 613 562-5800 ext. 2047
Fax: +1 613 562-5172
E-mail: bkruczek@uottawa.ca

Abstract

Commercially available thin film composite (TFC) polyamide membrane (GE AG) and asymmetric cellulose acetate membrane (GE CE) have been characterized using different concentrations of ammonium sulfate, up to 40 $g \cdot l^{-1}$, in order to determine their suitability for the concentration of ammonium as ammonium sulfate from anaerobic digester digestate. At the manufacturer specified pressures of 1550 kPa and 2900 kPa, the solvent permeances for the GE AG and the GE CE membranes were found to be 2.1×10^{-5} and 7.4×10^{-6} $l \cdot m^{-2} \cdot h^{-1} \cdot Pa^{-1}$, respectively. These permeances were practically independent of feed concentration. At the same time, both membranes showed excellent solute rejections, which decreased slightly with feed concentration, but were generally greater than 0.99. Consequently, the lower pressure GE AG membranes were considered to be more suitable for the separation of ammonium sulfate, and they were further tested at pressures exceeding the manufacturer specified value. These experiments revealed a slight decrease in solvent permeance for up to 17%, as well as a slight decrease in solute rejection, which was 0.97 or greater. Given these results, both membranes studied in this research are suitable for future investigations; first using multi- ion aqueous solutions and then pre-treated anaerobic digester digestate.

Keywords: Reverse osmosis, anaerobic digester, ammonium sulfate, polyamide membrane, cellulose acetate membrane.

Highlights

- Removal of ammonium sulfate from anaerobic digestate using RO membranes.
- Rejection of ammonium sulfate in excess of 0.99 by GE AG and GE CE membranes.
- Inadequacy of basic solution-diffusion model to explain permeances and rejections.

3.1 Introduction

Background

The implementation of a diverse range of sustainable energy producing technologies is required in order to mitigate the effects of global warming [1,2], and satisfy the energy needs of a growing world population. In this study, the application of a membrane separation process to further improve the economic feasibility of one type of sustainable energy technology, the anaerobic digestion of organic material to produce biogas, is investigated. Anaerobic digestion of biomass has been successfully utilized for many decades as away to produce methane, which can be used to generate heat, and/or electricity. In this process, organic materials such as plant waste, manure, and restaurant leftovers are degraded by microbial organisms including methanogens, which in the absence of oxygen convert these substrates to microbial biomass, carbon dioxide (CO_2) and methane (CH_4) [3]. When a significant amount of nitrogen is present in the organic feed sources, as is the case for animal manure, this nitrogen is converted to ammonium (NH_4^+), which is dissolved in the liquid inside the anaerobic digester. This liquid contains other components, including sodium, magnesium, potassium and phosphate, as well as some suspended solids, and is known as the digestate. The ammonium content of the digestate is of particular interest for two reasons. Firstly, free ammonia (NH_3), and ammonium (NH_4^+), exist in equilibrium, and have been shown to be responsible for inhibiting methanogenesis [4–6]. Secondly, ammonia and ammonium are a source of nitrogen that is easily absorbed by plants, and consequently could be used as fertilizers.

In order to minimize the inhibitory effect of ammonium on the production of biogas, its concentration in digestate is usually kept below 3.9 $g \cdot l^{-1}$ [7]. However, concentrations as high as 7.2 $g \cdot l^{-1}$ have also been reported [8]. According to Chen et al. [3], a 50% decrease in methane production may be caused, depending on the origin of digestate, by the total amount of ammonia and ammonium nitrogen (TAN) ranging from 1.7 to 14 $g \cdot l^{-1}$. It is therefore necessary to reduce the concentration of TAN in the digestate to maximize biogas production. The simplest way to maintain a low concentration of TAN in digestate is routine purging. However, due to its toxicity to marine life, the discharge of ammonia is strictly regulated in most countries. For example, in Canada the maximum concentration of ammonia in a discharged stream

cannot exceed 1.25 $mg \cdot l^{-1}$ at 15 °C [9]. Alternatively, discharged streams containing ammonia could be used as fertilizers. However, if ammonia is not converted into a stable form and sufficiently concentrated, the costs for storage and transport to neighboring farms, where it can be used as a liquid fertilizer, become significant and economically unfavorable. Therefore, to realize the potential of ammonia present in digestate, its concentration must be in- creased as much as possible once it has been removed from the digestate. To this end, several methods of removing and concentrating TAN from digestate have been investigated. These include, the application of hollow fiber membranes [10], vibrating reverse osmosis membranes [11], absorption [12], and steam stripping [13]. Alternatively, TAN present in digestate could be transformed into a stable form, and then separated. This can be achieved by acidifying digestate with sulfuric acid to convert TAN into a stable ammonium sulfate solution. In this form, the ammonium sulfate separated from digestate can be used as a fertilizer, and is a product that can be readily sold. In 2013 alone, Canada imported 116,000 metric tonnes of ammonium sulfate, up from 82,000 metric tonnes in 2009 [14]. In this paper, two commercially available membranes that are designed to be used for desalination are characterized using aqueous feed solutions of ammonium sulfate that represents the ideal form of acidified digestate. While the separation of ammonium sulfate from aqueous solution using reverse osmosis membranes is not expected to be challenging, the information on this separation is very limited. On the other hand, the separation of ammonium sulfate from aqueous solutions may potentially become another important application of membranes used in desalination processes. In this study, the effects of feed concentration and feed pressure on solvent and solute permeances are investigated. The results of these characterization experiments can then be used to model the performance of a full scale process consisting of spiral wound membrane elements, and the economic feasibility of a particular membrane.

3.2 Experimental

3.2.1 Setup & Equipment

Experiments were conducted using the setup whose process flow diagram (PFD) is shown in Fig. 3.1. The pressure gauges have a maximum pressure rating of 10,500 kPa, and the valves and fittings are made of 316 stainless steel, and are of Swagelok make. The pump (P-101) is a Hydracell F-20 single piston diaphragm pump with metallic heads. It has a maximum rated pressure and flow rate of 7000 kPa and 3.63 l per minute at 1750 rpm. The pump is connected to a JRP 0.5 hp motor. The feed tank is made of high density polyethylene (HDPE) and has a maximum capacity of 19 l. Feed solutions were made using 99.997% ammonium sulfate purchased from Sigma Aldrich and deionized water. The feed solution is cooled inside the tank using a 316 stain- less steel cooling element, containing ethylene glycol and water as a refrigerant. The external motor cooling fan is a 4 foot high pedestal fan. The static cells are made of 316 stainless steel, and were manufactured in house at University of Ottawa. The conductivity meter used to measure the concentration of ammonium sulfate is a CON 6+conductivity meter that was purchased from Oakton instruments. The rotameters are acrylic, and are able to measure permeate and retentate flow rates of 0.1–1.0 LPM and 0.4–4.0 LPM, respectively. To measure lower permeate flow rates, a measured mass of permeate was collected in a pre-defined period of time. Three static membrane cells were connected in parallel in order to eliminate any performance biases that may arise from defects in a single membrane, and to ensure that the feed stream composition entering each membrane was constant. The two membranes investigated in this study were General Electric (GE) thin film composite (TFC) polyamide membrane and GE asymmetric cellulose acetate membrane. The membranes were purchased from Sterlitech (Kent, USA) as flat sheet circular membranes with diameter of 47mm. The two membranes were chosen such that different material types, operating pressures, and expected fluxes could be compared. Spiral wound modules were not experimentally investigated in this study, but are expected to be used for the full scale process, and therefore their identification codes have been used. The polyamide membrane will be referred to as GE AG, and the cellulose acetate membrane will be referred to as GE CE. A summary of the membrane properties is shown in Table 3.1.

Table 3.1: Selected properties of interest for the membranes used in this study when tested using 2 $g \cdot l^{-1}$ NaCl.

Membrane ID	GE AG	GE CE
Membrane material	Polyamide	Cellulose acetate
Contact angle	63.5±1.7°[a]	59.1°[b]
Flux[c,d]	43.8–44.6 $l \cdot m^{-2} \cdot h^{-1}$@ 1550 kPa	37.1–40.1 $l \cdot m^{-2} \cdot h^{-1}$@ 2900 kPa
NaCl rejection[c]	0.995	0.970
Total thickness	0.15mm	0.15 mm

[a] As measured by Akin and Temelli [15].
[b] As measured by McCutcheon and Elimelech for the active layer [16].
[c] As reported for GE spiral wound membrane elements similar to the TFC membranes used in this study. Values are based on 24 hour permeation experiments at 25 °C with aqueous solution of NaCl (2 $g \cdot l^{-1}$) at pH=7.5for GE AG and pH=6.5 for GE CE.
[d] Individual element flux may vary +25%/−15%. The ranges shown encompass the performance of different modules, which use the same membrane, but different outer-wrappings.

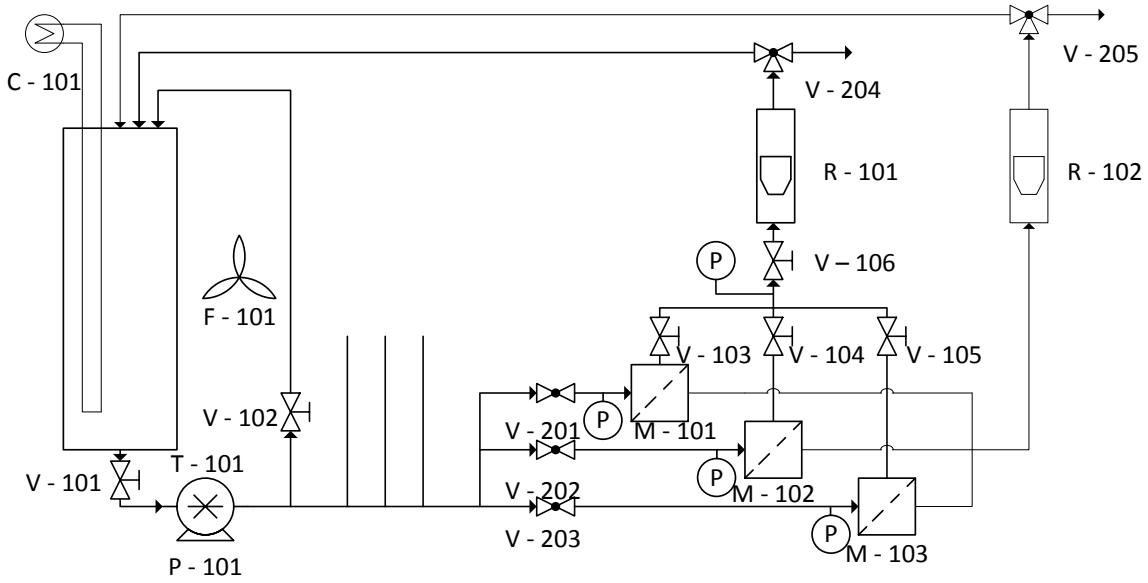

Figure 3.1: A schematic of the lab scale setup where P – 101 is the hydracell diaphragm pump, V – 100 series valves are metering valves, V – 200 series valves are globe valves, M – 101 to M – 103 are membrane elements, R – 101 and R – 102 are the rotameters on the retentate and feed side, respectively, and C – 101 is the tank cooling system. F – 101 is the pedestal fan.

3.2.2 Deionized water permeation experiments

The relationship between the flux and the applied pressure for each membrane was determined using deionized water in order to compare the flat sheet membranes used in this investigation to the manufacturer's specifications for spiral wound membrane modules. This was achieved by operating the pump at its maximum setting and closing the metering valve, V-106, as required to achieve the desired applied pressures. The exact permeate flow rate was then measured until steady state was achieved by collecting a volume of permeate in a predefined period of time and measuring its mass. The flux J_V [$l \cdot m^{-2} \cdot h^{-1}$] at each applied pressure was then calculated from:

$$J = \frac{V}{A_m} \tag{1}$$

where V [$l \cdot h^{-1}$] is the experimentally determined permeate flow rate and A_m [m^2] is the membrane area. The total membrane area, applied pressure, and stream flow rates were all subject to experimental noise. In order to calculate their influence on the overall uncertainty standard error equations were used.

3.2.3 Deionized water and ammonium sulfate permeation experiments

The membranes used in this study have been characterized by their manufacturer using NaCl. To the best knowledge of the authors, characterization data for aqueous ammonium sulfate containing solutions for the selected membranes have not been reported in the literature. Assuming the applicability of the solution-diffusion model, the rate equations for the transport of water J_V [$l \cdot m^{-2} \cdot h^{-1}$] and solute j_i [$g \cdot m^{-2} \cdot h^{-1}$] are described by:

$$J_V = \overline{P}_{H_2O} \left(\Delta P - \Delta \pi \right) \tag{2}$$

$$j_i = \overline{P}_{(NH_4)_2SO_4} \left(C_f - C_p \right) \tag{3}$$

where $\overline{P}_{H_2O}$ [$l \cdot m^{-2} \cdot h^{-1} \cdot Pa^{-1}$] is the permeance of water across the membrane, $\overline{P}_{(NH_4)_2SO_4}$ [$l \cdot m^{-2} \cdot h^{-1}$] is the permeance of solute across the membrane, ΔP [Pa] is the pressure differential across the membrane; feed side pressure – permeate side pressure, and $\Delta \pi$ [Pa] is the osmotic pressure differential across the membrane; feed side – permeate side. C_f and C_p [$g \cdot l^{-1}$] are the solute concentrations on the feed and permeate sides of the membrane, respectively.

In order to calculate the osmotic pressure as required for Eq. (2), the modified Van Hoff't equation was used:

$$\pi = i\phi CRT \tag{6}$$

where i [-] is the number of ions produced during dissociation, C [mol·m^{-3}] is the concentration of $(NH_4)_2SO_4$, R [J·mol^{-1}·K^{-1}] is the universal gas constant, T [K] is the temperature, and ϕ [-] is the osmotic coefficient, which is tabulated for various pressures and temperatures by El Guendouzi et al. [17]. This equation shows that at a solute concentration of 40 g·l^{-1}, the osmotic pressure is approximately 1600 kPa at room temperature. The osmotic coefficients reported by El Guendozi et al. [17] at 298.15 K are reproduced in Table 3.2.

The solute rejection R_s [-], which is used to quantify the separation of each membrane regardless of physical properties, is calculated using the following equation:

$$R_s = 1 - \frac{C_p}{C_f} \tag{7}$$

where C_p and C_f [g·l^{-1}] are the concentration of $(NH_4)_2SO_4$ in the permeate and feed, respectively.

Table 3.2: Osmotic coefficients reported by Guendouzi et al. [17] for $(NH_4)_2SO_4$ at 298.15 K.

$(NH_4)_2SO_4$ concentration		Calculated osmotic coefficients	Osmotic pressure
[mol·kg^{-1}]	[g·kg^{-1}]	ϕ [−]	[kPa]
[0.1]	[13.2]	0.773	575
[0.2]	[26.4]	0.729	1084
[0.3]	[39.6]	0.708	1580
[0.4]	[52.9]	0.689	2049

Experiments were conducted for multiple feed concentrations of $(NH_4)_2SO_4$, and at multiple applied pressures. Each experiment was conducted over a period of 8 h, which was sufficient to reach steady state conditions. The latter was confirmed by a constant permeation rate and constant concentration of each stream with respect to time. As there were no other solutes present in the system, the concentration of $(NH_4)_2SO_4$ in feed and

permeate were determined based on the experimentally-measured conductivity of the respective solutions.

3.3 Results and Discussion

3.3.1 Deionized water permeation experiment results

The deionized water flux for each membrane was measured and compared to the manufacturer's given flux. The results are shown in Fig. 3.2. The corresponding pure water permeances at different pressures are shown in Fig. 3.3. The uncertainties shown in Figs. 3.2 and 3.3 were calculated using standard error equations. The magnitude of the uncertainties is largely dependent on the actual membrane area. The diameter of the membrane was determined based on the size of the O rings used to ensure that the feed does not bypass the membrane, which was 43mm±2mm. For comparison, the flux given by the manufacturer at the conditions detailed in Table 3.1 for spiral wound membrane elements are shown as hollow points in Figs. 3.2 and 3.3.

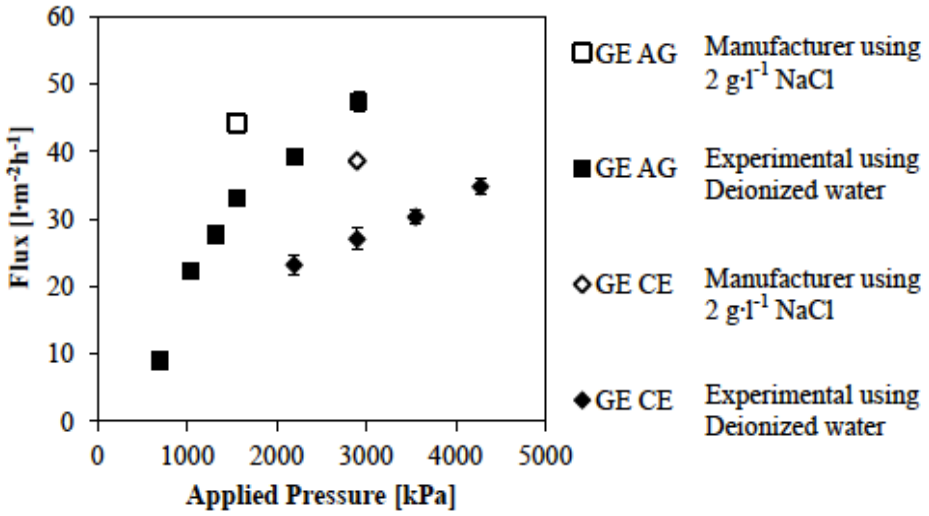

Figure 3.2: The deionized water flux for the membranes as function of the applied pressures. The manufacturer's data are shown for comparison.

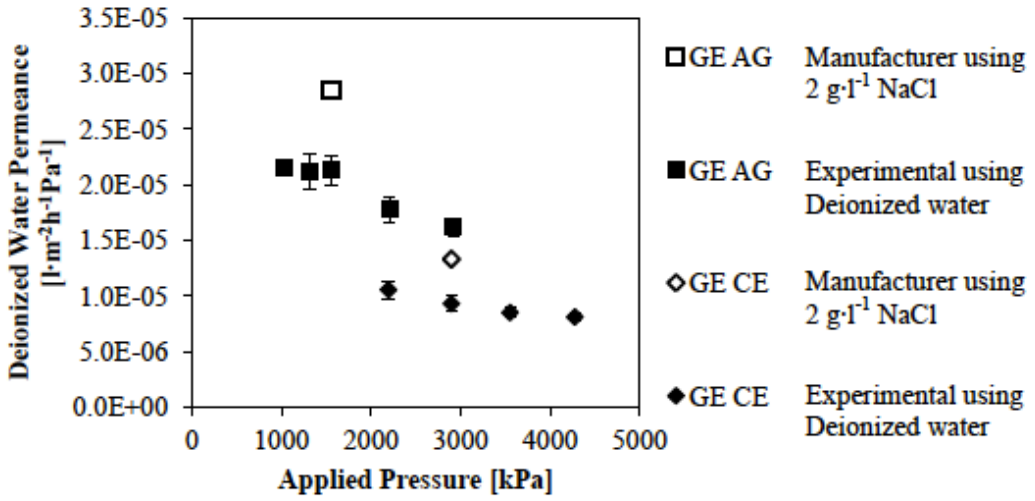

Figure 3.3: The deionized water permeances for the membranes investigated as a function of the applied pressure. The manufacturer's given fluxes are shown for comparison.

Fig. 3.2 shows that the experimentally determined flux for the GE CE membrane is lower than that given by the manufacturer, which is reasoned to be caused by membrane compaction. Evidence confirming membrane compaction can be seen in Fig. 3.3, which shows that as the applied pressure increases, the water permeance decreases. This observed behavior is caused by membrane densification resulting from rearrangement of polymeric chains under external pressure, which leads to a decrease in diffusion coefficient for water in the membrane [18,19]. For the GE CE membrane, the maximum flux of 34.8 $l \cdot m^{-2} \cdot h^{-1}$ (Fig. 3.2) was achieved at the maximum applied pressure investigated, 4300 kPa, which has a corresponding permeance of 8.1×10^{-6} $l \cdot m^{-2} \cdot h^{-1} \cdot Pa^{-1}$. This permeance, despite compaction, is within an order of magnitude of both the manufacturer's given permeance of 1.3×10^{-5} $l \cdot m^{-2} \cdot h^{-1}$, and the highest experimental permeance of 1.1×10^{-5} $l \cdot m^{-2} \cdot h^{-1} \cdot Pa^{-1}$ that was observed at the lowest applied pressure of 2200 kPa.

As with the GE CE membrane, the flux for the GE AG membrane is also less than the manufacturer's given value. Again, membrane compaction appears to be responsible for this behavior, which is supported by the decreasing trend in permeance as a function of the applied pressure (Fig. 3.3). The highest flux of 47.4 $l \cdot m^{-2} \cdot h^{-1}$, and the lowest water permeance of 1.6×10^{-5} $l \cdot m^{-2} \cdot h^{-1} \cdot Pa^{-1}$ were observed at the highest applied pressure of

2900 kPa. Pure water permeation tests confirmed that the GE AG membrane permeability is twice as much as the GE CE membrane permeability, which was expected based on the manufacturer's data.

3.3.2 Fluxes for various concentrations of $(NH_4)_2SO_4$ at manufacturer specified applied pressure

There is limited data available in the literature on the separation of $(NH_4)_2SO_4$ from aqueous solutions using membranes. Therefore these experiments were carried out to verify the suitability of the selected membranes for this separation. The effect of $(NH_4)_2SO_4$ concentration at a given feed concentration and manufacturer specified pressure on solvent flux is shown in Fig. 3.4. The flux uncertainties are calculated as explained for the deionized water permeation experiments, and the feed concentration uncertainties are the variation between the expected feed composition based on the amount of $(NH_4)_2SO_4$ added to the feed tank, and the feed composition measured by the conductivity meter. All calculations that require $(NH_4)_2SO_4$ concentration have been carried out using the values from conductivity measurements.

As expected from Eqs. (2) and (4), the water flux for both membranes decreases as the feed concentration of $(NH_4)_2SO_4$ increases, which is evident for both membranes in Fig. 3.4. However, the rate of the flux decrease with increase in feed concentration is greater for the GE AG membrane than for the GE CE membrane. At feed concentrations smaller than 20 $g \cdot l^{-1}$, the flux of the GE AG membrane is greater than that of the GE CE membrane, but at feed concentrations greater than 20 $g \cdot l^{-1}$ the situation becomes exactly the opposite. The slope of the plot in Fig. 3.4 is higher for GE AG membrane according to Eq. (2), since the solvent permeance, P_{H2O} is higher for this membrane, as can be seen in Fig. 3.5.

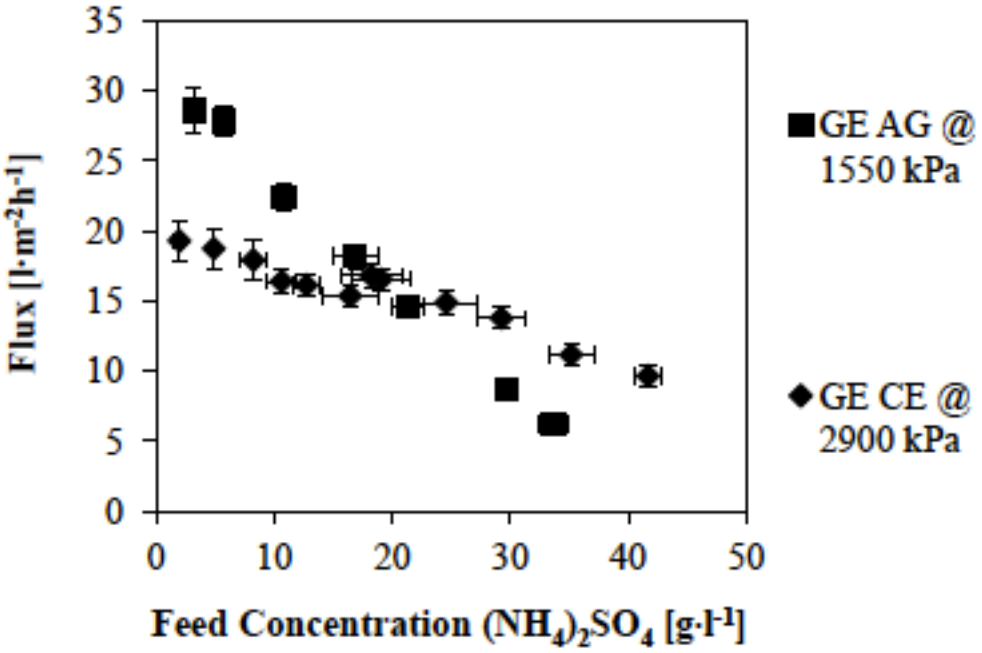

Figure 3.4: The flux for membranes investigated at the manufacturer specified applied pressures, under multiple feed concentrations of $(NH_4)_2SO_4$. The GE CE membrane was tested at an applied pressure of 2950 ± 150 kPa and 22 ± 2°C, and GE AG at 1550 ± 150 kPa and 22 ± 2°C.

Of particular note is the apparent jump in flux the GE CE membranes at the feed concentration of 19 $g \cdot l^{-1}$. This jump occurred after one of the three membranes was replaced following the experiment at a feed concentration of 16.45 $g \cdot l^{-1}$. The existence of this jump indicates that the unused GE CE membrane was noticeably more permeable than those already tested in permeation experiments. The latter is also indicated by a considerable discrepancy between the largest solvent flux for the GE CE membranes (19.3 $l \cdot m^{-2} \cdot h^{-1}$) at the lowest feed concentration and the flux observed in pure water permeation test (27 $l \cdot m^{-2} \cdot h^{-1}$) at the same feed pressure. On the other hand, in the case of the GE AG membranes, the largest flux at the lowest feed concentration and that in the experiment with pure water at the same feed pressure was more comparable (33 $l.m^{-2} \cdot h^{-1}$ vs. 28.6 $l.m^{-2} \cdot h^{-1}$). In both cases, prior to experiments with feed solutions containing $(NH_4)_2SO_4$, the membranes were exposed to pressures greater than those recommended by the manufacturer.

Solvent fluxes reported in Fig. 3.4 were used to determine the corresponding solvent permeances from Eq. (2). The osmotic pressure gradient required by Eq. (2) was calculated from Eq. (4) using the experimental concentrations, and the concentration-dependent osmotic coefficients listed in Table 3.2. The effect of feed concentration on solvent permeance for both membranes at their manufacturer recommended pressures is presented in Fig. 3.5. According to the solution- diffusion model, solvent permeance should be independent of feed con- centration. This effect is generally seen for the GE CE membrane at all feed concentrations from 0 to 40 $g \cdot l^{-1}$, and for the GE AG membrane at feed concentrations less than 30 $g \cdot l^{-1}$. At the two largest feed concentrations, the solvent permeance is up to 50% greater than the value at low feed concentrations for GE AG membrane. One possible explanation of this unexpected behavior was overestimation of the osmotic pressure gradient, which would lead to underestimation of the actual driving force and thus an overestimation of the solvent permeance. On the other hand, this behavior was not observed for the GE CE membrane. Therefore, this unexpected behavior is most likely a consequence of the diminished fluxes shown by the GE AG membranes at high feed concentrations, which is exacerbated as the osmotic pressure approaches the applied pressure. At these conditions a small error in the experimental flux may have a great effect on the calculated solvent permeance.

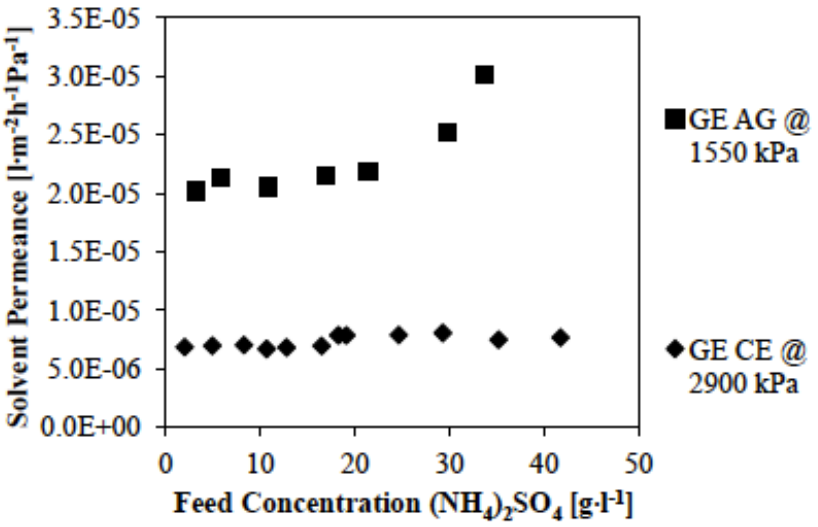

Figure 3.5: The solvent permeance for membranes investigated at the manufacturer specified applied pressures, under multiple feed concentrations of $(NH_4)_2SO_4$. The GE CE membrane was tested at an applied pressure of 2950 ± 150 kPa and 22 ± 2°C, and GE AG at 1550 ± 150 kPa and 22 ± 2°C.

Solvent permeance of 2.1×10^{-5} $l \cdot m^{-2} \cdot h^{-1} \cdot Pa^{-1}$ for the GE AG membrane at feed concentrations up to 30 $g \cdot l^{-1}$ is practically the same as the value from the pure water permeation experiment at the same feed pressure (see Fig. 3.3). On the other hand, for the GE CE membrane, the average solvent permeance of 6.9×10^{-6} $l \cdot m^{-2} \cdot h^{-1} \cdot Pa^{-1}$ from the experiments at low feed concentrations is considerably smaller than 9.6×10^{-6} $l \cdot m^{-2} \cdot h^{-1} \cdot Pa^{-1}$ observed in the experiment with pure water at the same feed pressure (see Fig. 3.3). In addition, the previously mentioned jump in solvent flux seen in Fig. 3.4 translates to an increase in solvent permeance by approximately 1×10^{-6} $l \cdot m^{-2} \cdot h^{-1} \cdot Pa^{-1}$ to 7.9 $l \cdot m^{-2} \cdot h^{-1} \cdot Pa^{-1}$. This increase, as previously mentioned, was a result of replacing one of the three membranes with the fresh one. Consequently, if all three membranes were replaced, the average permeance is expected to be comparable to the value from the pure water permeation experiment at the same feed pressure. While both membrane types were subject to compaction, which is clearly evident in Fig. 3.3, it appears that the exposure of the GE CE membranes to pressures greater than that recommended by the manufacturer led to irreversible compaction. On the other hand, after exposure

of the GE AG membranes to pressures greater than that recommended by the manufacturer, solvent permeance returned to the original value, which suggests a reversible compaction in the GE AG membranes. The latter membranes were further tested at pressures greater than the manufacturer's specified value, which will be discussed in Section 3.4.

3.3.3 Permeate compositions for various concentrations of $(NH_4)_2SO_4$ at manufacturer specified applied pressure

The permeate composition for each membrane when subjected to increasing feed concentrations of $(NH_4)_2SO_4$ was measured in addition to the flux, in order to investigate the effect of feed concentration on solute rejection. The permeate concentrations and solute rejections are shown in Fig. 3.6. The permeate concentration uncertainties were determined by the fluctuation seen in permeate composition when each experiment had reached steady state. The magnitude of this uncertainty increases as the feed concentration increases, and is most clearly seen for the GE AG membrane experiments.

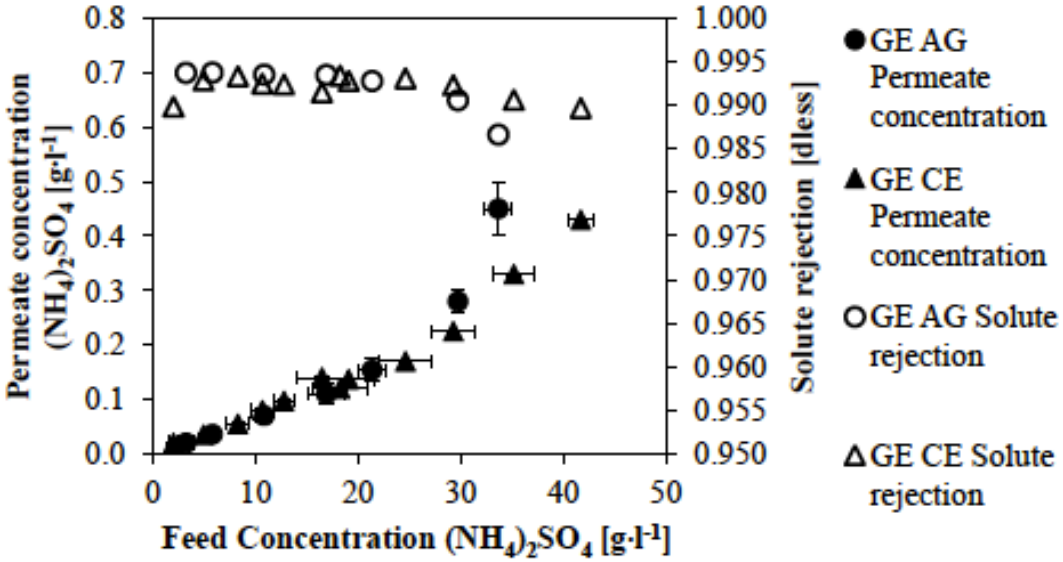

Figure 3.6: The permeate composition and the solute rejection for the membranes investigated at the manufacturer specified applied pressures, under multiple feed concentrations of $(NH_4)_2SO_4$. The GE CE membrane was tested at an applied pressure of 2950 ± 150 kPa and 22 ± 2°C, and GE AG at 1550 ± 150 kPa and 22 ± 2°C.

According to the solution diffusion model, the transport of solute is driven by the concentration gradient across the membrane. Therefore, as the concentration of the feed increases, the rate of the transport of solute increases. At the same time, the rate of the transport of solvent de- creases, because of an increase in the osmotic pressure gradient, which diminishes the driving force for the transport of solvent. Consequently, the solute concentration in permeate was expected to increase with feed concentration with an upward deviation from linearity. This effect is seen in Fig. 3.6, in particular at higher feed concentrations. Therefore, considering Eq. (5), the solute rejection was expected to decrease with increasing feed concentration. According to Fig. 3.6, the solute rejection of both membranes does indeed slightly decrease with feed concentration. However, the variation in solute rejection with feed concentration, which is approximately 0.005 (0.5%), is very small. More importantly, for both membranes, the solute rejection, regardless of the feed concentration is generally 0.99 or greater. This indicates an excellent potential of the selected membranes for the separation of ammonium sulfate from aqueous solutions at the manufacturer recommended pressures.

According to the manufacturer, the solute rejections for NaCl with the polyamide GE AG membrane and cellulose acetate GE CE membrane are 0.995 and 0.97, respectively. Thus the experimentally observed rejections of $(NH_4)_2SO_4$ for the GE AG membrane are comparable, while those for the GE CE membrane are greater than the value for NaCl provided by the membrane manufacturer. It is important to emphasize that NaCl dissociates into 2 monovalent ions, while $(NH_4)_2SO_4$ dissociates into monovalent and multivalent ions. Traditionally, the need to separate monovalent or multivalent ions determines whether a nanofiltration (NF) or reverse osmosis (RO) membrane is used, as NF membranes are able to reject multivalent salts, such as $(NH_4)_2SO_4$, while RO membranes are typically necessary to reject monovalent salts such as NaCl. Given this information, and the fact that the molecular weight of $(NH_4)_2SO_4$ is greater than that of NaCl (132.14 $g \cdot mol^{-1}$ vs. 58.44 $g \cdot mol^{-1}$), a very good rejection of $(NH_4)_2SO_4$ by both membranes was expected. However, it should also be emphasized that the NaCl rejections provided were for relatively low salt concentration of 2 $g.l^{-1}$, while the separation tests presented in Fig. 3.6 were carried out at much greater feed concentrations (up to 40 $g.l^{-1}$). This further proves the excellent potential of the selected membranes for

the separation and concentration of ammonium sulfate. It has been shown by others that experiments conducted using NaCl can be used to predict the performance of the same membrane to concentrate different ions using empirical correlations at feed concentrations that are less than 0.1 $mol \cdot l^{-1}$ [20], and so the results of this study could also be used to develop similar models for solutions at greater concentrations.

Due to the limited available data in the literature for $(NH_4)_2SO_4$ containing solutions, the results of this study have been compared to those undertaken by others using different ammonium containing feed solutions. In the study conducted by Häyrynen et al. [21], which used reverse osmosis membranes to separate several contaminants including ammonium from mining wastewater using DOW SW30HR membranes, ammonium rejections were found to be between 0.828 and 0.909. Other investigated membranes gave rejections between 0.861 and 0.945 for the same samples. These rejections are much lower than those found in the current study; however, in the current study ammonium sulfate was the only salt in the feed solution. A separate study was conducted by Bodalo et al. [22], where cellulose acetate membranes were used to concentrate ammonium hydroxide from feeds of different concentrations. That study found rejections between 0.986 and 0.992, which is very close to the results reported here, but for a different solute. Another study was conducted by Kurama et al. [23] to remove high concentrations of ammonium as well as other contaminants from potable water using two stages of nanofiltration followed by two stages of reverse osmosis. In that study, a rejection of 0.969 was achieved, which is lower than the rejections found here, but again, their feed was composed of multiple contaminants. The membrane materials were not specified in that study, although the reverse osmosis membranes were low- pressure models of GE make.

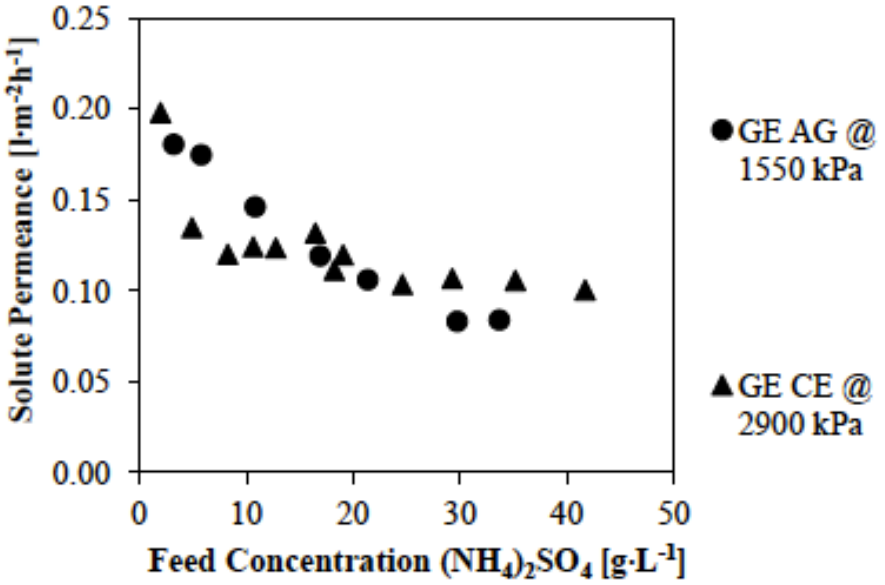

Figure 3.7: The solute permeance for the membranes investigated at the manufacturer specified applied pressures, under multiple feed concentrations of $(NH_4)_2SO_4$. The GE CE membrane was tested at an applied pressure of 2950 ± 150 kPa and 22 ± 2°C, and GE AG at 1550 ± 150 kPa and 22 ± 2°C.

Fig. 3.7 presents solute permeances as a function of feed concentrations that were determined from Eq. (3) using the experimental steady state fluxes and concentrations of feed and permeate in the experiments previously presented in Fig. 3.6. According to the solution-diffusion model, solute permeance should be constant. However, this is not the case in Fig. 3.7, in which solute permeance of both membranes decreases with increasing feed concentration. This effect appears to be more pronounced for the GE AG membrane than for the GE CE membrane. At the highest feed concentrations, the solute permeances were 0.10 and 0.08 $l \cdot m^{-2} \cdot h^{-1}$ for the GE CE and the GE AG membranes, respectively. A decrease in solute permeance with increasing feed concentration may indicate that solute is not only transported by concentration- driven diffusion, but also by pressure-driven flow along with the solvent. It has been mentioned previously that as the feed concentration in- creases, the increasing osmotic pressure gradient decreases the flux of solvent across the membrane (Fig. 3.4). Thus, on the one hand, as the feed concentration increases there is a greater concentration of solute in convectively transported solvent, but on the other hand, a decrease in solvent flux may lead to the overall decrease of the

fraction of solvent that is convectively transported across the membrane. Whatever the actual reason for the behavior seen in Fig. 3.7, an increase in solute permeance with decreasing feed concentration is very advantageous considering the application of the GE CE and GE AG membranes for the concentration of $(NH_4)_2SO_4$ from dilute solutions to as high a concentration as possible.

3.3.4 Effect of pressures exceeding the manufacturer specified pressure for membrane GE AG.

As shown in Fig. 3.2, both membranes were tested with deionized water at two feed pressures that were greater than the respective pressure values recommended by the manufacturer. It was then observed that exposure to pressures greater than that recommended by the manufacturer had led to irreversible compaction of the GE CE, but not for the GE AG membranes. Consequently, the GE AG membranes were also tested with different concentrations of ammonium sulfate at the same two pressures that exceeded the manufacturer's specification. The observed solvent fluxes as a function of feed concentration are shown in Fig. 3.8. Uncertainty for the feed concentration and solvent flux has been explained in Section 2.2, and the feed concentration uncertainty error bars have been removed for clarity.

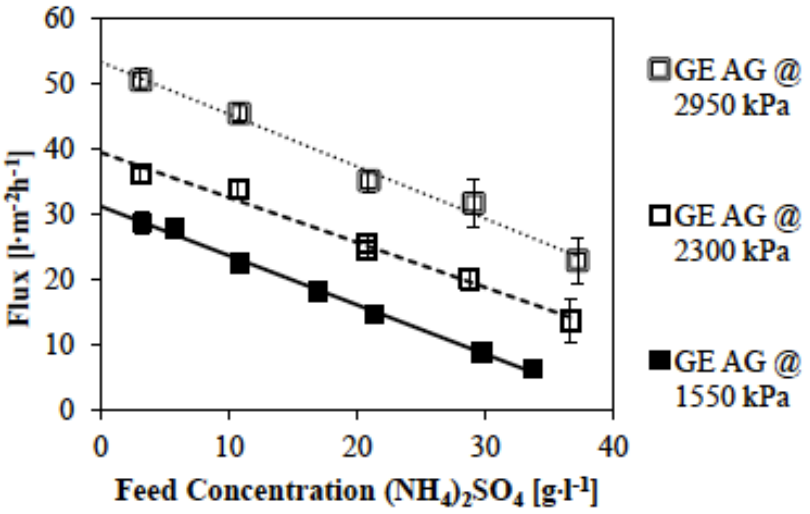

Figure 3.8: The flux for experiments conducted under multiple feed concentrations of $(NH_4)_2SO_4$ using GE AG membranes at three different pressures; 1550 ± 150 kPa and 22 ± 2°C, 2300 ± 150 kPa and 23 ± 2°C, and 2950 ± 200 kPa and 23 ± 2°C.

As expected, regardless of the feed concentration, the solvent flux increased with increasing feed pressure. Interestingly, the dependence of solvent flux on feed concentration appears to be the same at different feed pressures, which is indicated by approximately parallel trend lines for these pressures. Extrapolating the trend lines to a feed concentration equal to zero leads to the following fluxes: 31.0 $l \cdot m^{-2} \cdot h^{-1}$, 39.5 $l \cdot m^{-2} \cdot h^{-1}$, and 53.0 $l \cdot m^{-2} \cdot h^{-1}$ at pressures of 1550 kPa, 2300 kPa, and 2950 kPa, respectively. These values are remarkably similar to corresponding pure water fluxes of 33.1 $l \cdot m^{-2} \cdot h^{-1}$, 39.3 $l \cdot m^{-2} \cdot h^{-1}$, and 47.4 $l \cdot m^{-2} \cdot h^{-1}$ (from Fig. 3.2) which further suggests that the compaction undergone by the GE AG membranes was reversible.

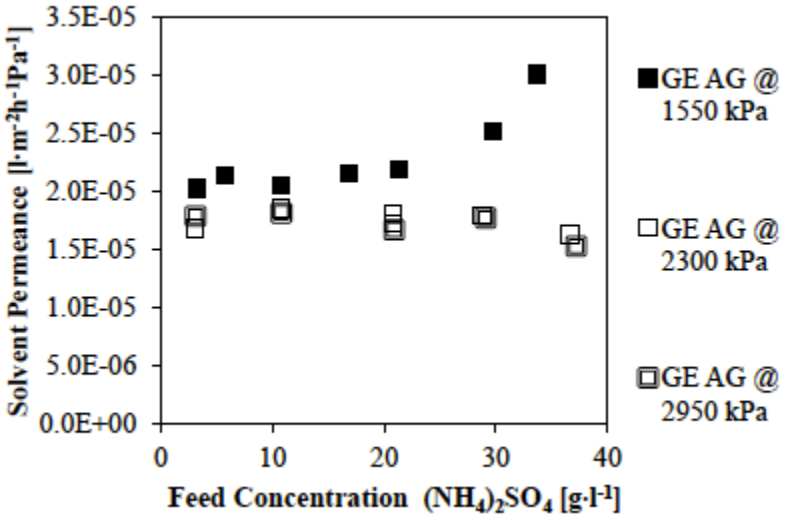

Figure 3.9: The solvent permeance for experiments conducted under multiple feed concentrations of $(NH_4)_2SO_4$ using GE AG membranes at three different pressures; 1550 ± 150 kPa and 22 ± 2°C, 2300 ± 150 kPa and 23 ± 2°C, and 2950 ± 200 kPa and 23 ± 2°C.

Fig. 3.9 presents solvent permeances as a function of increasing feed concentration at three different feed pressures, corresponding to the data shown in Fig. 3.8. As expected, due to membrane compaction, solvent permeances at 2300 kPa and 2950 kPa were lower

than the corresponding permeances at 1550 kPa. On the other hand, unlike Fig. 3.3 in which pure water permeance at 2300 kPa is clearly greater than that at 2950 kPa, there is little difference between solvent permeances at these two elevated pressures. Similar behavior has been observed by Arthanareeswaran et al. [18], using doped cellulose acetate membranes. In that study it was concluded that after exposing a membrane to high pressures for a long enough period, the flux stabilizes, which indicates that the membrane cannot compact anymore. Taking into account a considerable scatter in solvent permeances at the two elevated pressures, there is no clear trend between solvent permeance and feed concentration; thus solvent permeance could be considered as independent of feed concentration, which is expected in the solution-diffusion transport model. Unlike the experiments at 1550 kPa, the driving force for solvent transport across the membrane for the elevated feed pressure experiments was sufficiently larger even at the two highest feed concentrations, making the measurement of the permeation rate more reliable. Therefore, the previously noted in- crease in solvent permeance at the two highest feed concentrations for 1550 kPa feed pressure, seen in Figs. 3.5 and 3.9 should be disregarded.

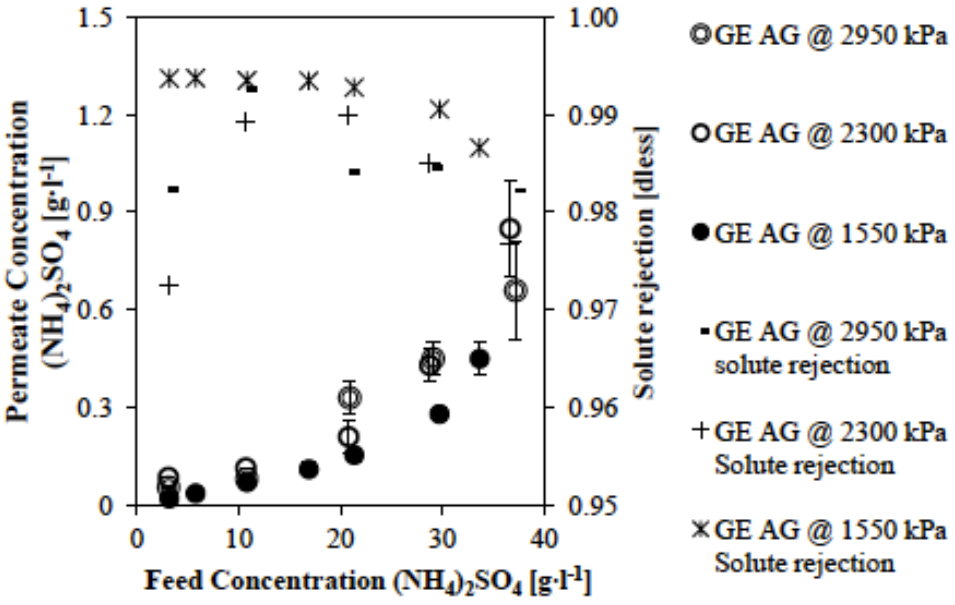

Figure 3.10: The permeate composition and the solute rejection for experiments conducted under multiple feed concentrations of $(NH_4)_2SO_4$ using GE AG membranes at three

different pressures; 1550 ± 150 kPa and 22 ± 2°C, 2300 ± 150 kPa and 23 ± 2°C, and 2950 ± 200 kPa and 23 ± 2°C.

Fig. 3.10 presents the extension of Fig. 3.6 for the GE AG membranes at two additional feed pressures of 2300 and 2950 kPa alongside the previously presented data at 1550 kPa. The effect of the feed concentration on the permeate concentration and solute rejection at 2300 and 2950 kPa are similar to what has been observed at 1550 kPa, but is more scattered. This scatter is particularly evident in the case of solute rejections at the lowest feed concentrations, and has resulted in some uncharacteristically low values. In general, in comparison to the experiments that were conducted at 1550 kPa, the permeate concentrations are greater while the solute rejections are lower in the experiments at the higher applied pressures. Despite this diminished separation, for all experiments at the applied pressures greater than those specified by the manufacturer, the permeate concentration did not increase beyond 0.85 $g \cdot l^{-1}$, and the solute rejection did not drop below 0.97.

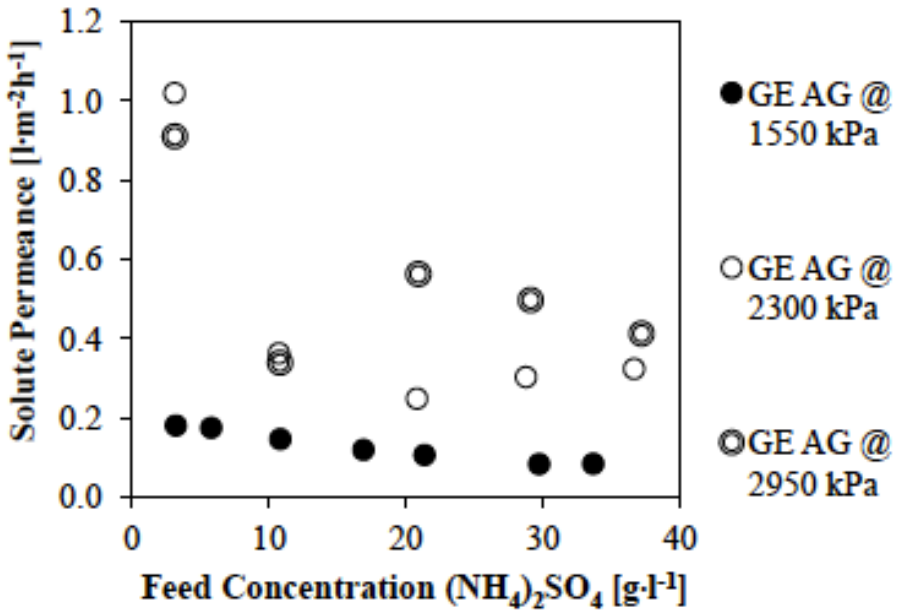

Figure 3.11: The solute permeance for experiments conducted under multiple feed concentrations of $(NH_4)_2SO_4$ using GE AG membranes at three different pressures; 1550 ± 150 kPa and 22 ± 2°C, 2300 ± 150 kPa and 23 ± 2°C, and 2950 ± 200 kPa and 23 ± 2°C.

Fig. 3.11 presents the solute permeances as a function of increasing feed concentration at three different feed pressures for the GE AG membranes, corresponding to the data shown in Fig. 3.10. Similar to the experiments at 1550 kPa, solute permeances at higher applied pressures can be seen to generally decrease with increasing feed concentration. Also, the solute permeances at 2300 kPa are lower than those at 2950 kPa for three out of five feed concentrations. At the other two feed concentrations, solute permeance is comparable or higher than can be seen at 2950 kPa. Nevertheless, the solute permeance at the highest feed con- centration is much lower than at the lowest feed concentration, for all applied pressures. Although there are many inconsistencies between the experiments carried out at pressures greater than the manufacturer recommended value, it can be concluded that solute permeances at 2300 kPa and 2950 kPa are considerably greater than those at 1550 kPa. The observed increase in permeate composition and solute permeance, as well as the resulting decrease in solute rejection at higher feed pressures is consistent with the previously noted dual solute transport mechanisms of solution diffusion and convective flow with solvent [24]. For a given feed concentration, increasing feed pressure increases the fraction of solute transported convectively. Thus, despite a constant driving force for concentration-driven diffusion, more solute appears at the permeate side because of an increase in the driving force for the convective transport of solvent across the membrane.

Experiments at different feed concentrations and feed pressures greater than the manufacturer's specified value indicate that despite some membrane compaction, the compaction effects for the GE AG membranes are not very significant. Consequently, solvent fluxes greater than the value specified for the NaCl separations are easily achieved and exceeded. At the same time, despite a decrease in solute rejection at higher feed pressures, the concentration of ammonium sulfate in permeate remains very low. This indicates that the GE AG membranes can be effectively operated not only at the manufacturer's recommended pressure, but also at the elevated feed pressures. Moreover, specification sheets for spiral wound elements from GE show that membranes of this type are designed to withstand higher applied pressures.

3.4 Conclusions

The ultimate goal of the research presented in this paper is to re- move ammonia from anaerobic digesters in order to enhance biogas production, and at the same time, to concentrate the removed ammonia, converted into a stable form of ammonium sulfate. The latter could be used as a liquid fertilizer. In the first phase of this research, the results of which are presented in this paper, two commercially available RO membranes, GE AG and GE CE membranes, were tested with aqueous solutions of ammonium sulfate at different feed concentrations and pressures. For the investigated range of feed concentrations (up to 40 $g \cdot l^{-1}$) both membranes showed excellent solute rejections of 0.99 or greater at the manufacturer specified pressures of 1550 kPa and 2900 kPa for the GE AG and GE CE membranes, respectively. On the other hand, the lower pressure GE AG membrane was three times more permeable than the higher pressure GE CE membrane (2.1×10^{-5} $l \cdot m^{-2} \cdot h^{-1} \cdot Pa^{-1}$ vs. 7.4×10^{-6} $l \cdot m^{-2} \cdot h^{-1} \cdot Pa^{-1}$). While both membranes were susceptible to compaction at pressures exceeding those specified by the manufacturer, the compaction effects were reversible for the GE AG membrane, but not for the GE CE membrane. As a result, the GE AG membrane is recommended for future studies with multi-ion aqueous solutions. The experimental results obtained in this study were interpreted in terms of a basic solution-diffusion model, which was found to be not entirely adequate to explain the observed results. In particular, solute permeance decreased with feed concentration at a given feed pressure, while solute rejection decreased with increased feed pressure at a given feed concentration. This suggests that in addition to concentration-driven diffusion, some solute was also transported convectively along with the solvent.

3.5 Acknowledgements

This research project was conducted in collaboration with CHFour Biogas Ltd, and was financially supported through the NSERC (Natural Sciences and Engineering Research Council) Engage program.

3.6 References

[1] IPCC, Climate Change 2014:Mitigation of Climate Change, 2014. (Expected publication date: October 2014).

[2] D.P. Van Vuuren, M.G. Den Elzen, P.L. Lucas, B. Eickhout, B.J. Strengers, B. van Ruijven,…, R. van Houdt, Stabilizing greenhouse gas concentrations at low levels: an assessment of reduction strategies and costs, Clim. Chang. 81 (2) (2007) 119–159.

[3] Y. Chen, J.J. Cheng, K.S. Creamer, Inhibition of anaerobic digestion process: a review, *Bioresour. Technol.* 99 (10) (2008) 4044–4064.

[4] R. Nakakubo, H.B. Møller, A.M. Nielsen, J. Matsuda, Ammonia inhibition of methanogenesis and identification of process indicators during anaerobic digestion, *Environ. Eng. Sci.* 25 (10) (2008) 1487–1496.

[5] J.J. Lay, Y.Y. Li, T. Noike, The influence of pH and ammonia concentration on the methane production in high-solids digestion processes, *Water Environ. Res.* 70 (5) (1998) 1075–1082.

[6] I.W. Koster,G. Lettinga, The influence of ammonium-nitrogen on the specific activity of pelletized methanogenic sludge, *Agric.Wastes* 9 (3) (1984) 205–216.

[7] F.Wäger-Baumann,W. Fuchs, Process variant for the treatment of anaerobic digester effluent with a membrane bioreactor, Environ. Eng. Sci. 28 (9) (2011) 611–617.

[8] T. Wirthensohn, F.Waeger, L. Jelinek,W. Fuchs, Ammonium removal from anaerobic digester effluent by ion exchange, *Water Sci. Technol.* 60 (1) (2009) 201–210.

[9] Fisheries Act: Wastewater Systems Effluent Regulations, Retrieved from the Government of Canada Justice Laws website, http://laws-lois.justice.gc.ca/eng/regulations/ sor-2012-139/index.html2012.

[10] B. Lauterbock,M. Ortner, R. Haider,W. Fuchs, Counteracting ammonia inhibition in anaerobic digestion by removal with a hollow fiber membrane contactor, *Water Res.* 46 (2012) 4861–4869.

[11] New Logic Research Inc. (n.d.) Biogas Effluent Treatment with VSEP. Retrieved from http://www.vsep.com/pdf/Membrane-Treatment-of-Biogas-Effluent-Case-Study. pdf.

[12] A. Jiang, T. Zhang, Q.B. Zhao, X. Li, S. Chen, C.S. Frear, Evaluation of an integrated ammonia stripping, recovery, and biogas scrubbing system for use with anaerobically digested dairy manure, *Biosyst. Eng.* 119 (2014) 117–126.

[13] L. Zeng, C.Mangan, X. Li, Ammonia recovery from anaerobically digested cattle manure by steam stripping, *Water Sci. Technol.* 54 (8) (2006) 137–145.

[14] Statistics Canada, Fertilizer Shipments to Canadian Agriculture and Export Markets, by Product Type and Fertilizer Year, Cumulative Data, Annual (Metric Tonnes), CANSIM (Database) Table 001–0068, 2014.

[15] O. Akin, F. Temelli, Probing the hydrophobicity of commercial reverse osmosis membranes produced by interfacial polymerization using contact angle, XPS, FTIR, FE-SEM and AFM, *Desalination* 278 (1) (2011) 387–396.

[16] J.R. McCutcheon, M. Elimelech, Influence of membrane support layer hydrophobicity on water flux in osmotically driven membrane processes, *J. Membr. Sci.* 318 (1) (2008) 458–466.

[17] M.E. El Guendouzi, A. Mounir, A. Dinane, Water activity, osmotic and activity coefficients of aqueous solutions of Li2SO4,Na2SO4,K2SO4, (NH4)2SO4, MgSO4, MnSO4, NiSO4, CuSO4,and ZnSO4 at T = 298.15 K, *J. Chem. Thermodyn.* 35 (2) (2003) 209–220.

[18] G. Arthanareeswaran, P. Thanikaivelan, K. Srinivasn, D. Mohan, M. Rajendran, Synthesis, characterization and thermal studies on cellulose acetate membranes with additive, *Eur. Polym. J.* 40 (9) (2004) 2153–2159.

[19] M. Sivakumar, D.R. Mohan, R. Rangarajan, Studies on cellulose acetate-polysulfone ultrafiltration membranes: II. Effect of additive concentration, *J. Membr. Sci.* 268 (2) (2006) 208–219.

[20] M. Khayet, J.I. Mengual, Effect of salt type on mass transfer in reverse

osmosis thin film composite membranes, *Desalination* 168 (2004) 383–390.

[21] K. Häyrynen, J. Langwaldt, E. Pongrácz, V. Väisänen, M.Mänttäri, R.L. Keiski, Separation of nutrients from mine water by reverse osmosis for subsequent biological treatment, *Miner. Eng.* 21 (1) (2008) 2–9.

[22] A. Bodalo, J.L. Gomez, E. Gomez, G. Leon, M. Tejera, Ammonium removal from aqueous solutions by reverse osmosis using cellulose acetate membranes, *Desalination* 184 (1) (2005) 149–155.

[23] H. Kurama, J. Poetzschke, R. Haseneder, The application of membrane filtration for the removal of ammonium ions from potable water, *Water Res.* 36 (11) (2002) 2905–2909.

[24] B. Shiyao, F.D.F. Talbot, T.D. Nguyen, T. Matsuura, S. Sourirajan, Surface force-pore flow model in predicting separation and concentration of polyhydric alcohols in aqueous solutions using cellulose acetate membranes, *Sep. Sci. Technol.* 23 (1–3) (1988) 77–90.

NOMENCLATURE

A_m	Membrane Area. [m^{-2}]
C	Concentration of ammonium sulfate used for the calculation of osmotic pressure. [$mol \cdot m^{-3}$]
C_f	Feed concentration of ammonium sulfate. [$g \cdot l^{-1}$]
C_p	Permeate stream concentration of ammonium sulfate. [$g \cdot l^{-1}$]
J_V	Experimentally determined flux of solvent. [$l \cdot m^{-2} \cdot h^{-1}$]
j_i	Flux of solute, ammonium sulfate. [$g \cdot m^{-2} \cdot h^{-1}$]
R	Universal gas constant. [$J \cdot mol^{-1} \cdot K^{-1}$]
R_s	Solute rejection. [dimensionless]
T	Temperature. [K]
V	Experimentally determined permeate flow rate. [$l \cdot h^{-1}$]
$\overline{P}_{H_2O}$	Permeance of solvent, water. [$l \cdot m^{-2} \cdot h^{-1} \cdot Pa^{-1}$]
$\overline{P}_{(NH_4)_2SO_4}$	Permeance of solute, ammonium sulfate. [$l \cdot m^{-2} \cdot h^{-1}$]
ΔP	Pressure differential across the membrane. [Pa]
$\Delta\pi$	Osmotic pressure differential across the membrane. [Pa]
Φ	Number of ions produced during dissociation. [dimensionless]

Chapter 4: Concentration of ammonium ion from mixed salt aqueous solutions using commercial LPRO membranes

Tolulope D. Awobusuyi, F. Handan Tezel, Boguslaw Kruczek

Department of Chemical and Biological Engineering, University of Ottawa, 161 Louis Pasteur, Ottawa, Ontario K1N 6N5, Canada

Abstract

Membrane technology is the preferred separation method for a wide selection of industries, including the agriculture and desalination industries, both of which require purity of the products. This is due to a number of advantages: higher separation efficiencies at lower costs, environmentally benign processes and materials, and low capital costs. Removal of ammonia from anaerobic digestate using membranes represents another potential application of membrane technology.

Our previous study had indicated excellent rejections of ammonium sulfate from aqueous solutions using commercial reverse osmosis (RO) membranes and suggested the possibility of using low-pressure reverse osmosis (LPRO) membranes for this application. In this paper the rejection of ammonium sulfate from single and mixed-salt [$(NH_4)_2SO_4$ + K_3PO_4] aqueous solutions is investigated using three commercial LPRO membranes. For both salts the rejections at feed concentration of 20 $g \cdot l^{-1}$ and feed pressure of 13.8 x 10^5 Pa were greater than 0.93. The rejections increased with an increase of feed pressure and a decrease of feed concentration; the highest rejections exceeded 99%. The analysis of ionic concentration of permeate-streams in mixed-salt experiments revealed non-stoichiometric transport of ions. In particular, the rejections of NH_4^+ ions exceeding 99% were observed even with a high total salt concentration in feed, which is very advantageous from the point of view of removing and concentration of ammonia from anaerobic digestate. The observed results are interpreted qualitatively using extended-Nernst-Plank transport model.

Keywords: low-pressure reverse osmosis, membrane separation, ionic rejections, solution-diffusion, Kedem-Katchalsky.

4.1 Introduction

Membrane separation processes are applied in many industries [1] for a variety of separation processes: desalination[2]–[5], agriculture [2], [6], [7], and healthcare industries [3], [7], [8]. These industries are generally involved in the production of high-purity chemical compounds and/or the production of waste considered hazardous to the environment, and efficient separation processes–as production and treatment steps–are a necessity [9]–[11]. Membrane separation processes have, over the last half-century, become a ubiquitous separation method, and perhaps the greatest testament to the pervasiveness of the technology is its dominance of the desalination industry. Between 2009 and 2015 the water production capacity of active desalination plants has gone from 37 million m^3/day [12] to approximately 66 million m^3/day [13], [14], and in Israel desalination plants alone produce a quarter of the national potable water supply [13]. Membrane separation processes are therefore important to contemporary society, and the importance of an understanding of the workings of the processes cannot be understated.

Anaerobic digestion is a common method used in the treatment of waste products from farms and municipalities. The process converts organic matter to methane [15] and also produces biomass. Ammonia is also produced by the degradation of nitrogen-containing substances, but the production of ammonia inhibits the production of methane in the digester [16]. Ammonia is generally removed by denitrifying the gas mixtures from the digester and can either be used in the production of fertilizer [15] or liquefied and reformed to hydrogen gas [17]. Some of the most common technologies used for ammonia removal are ion exchange [18], [19], electrochemical cells [19], gas stripping using air or steam, membrane contactors [20], and fuel cells [19]. While most of these processes may be efficient, they tend to have high operating costs and may also affect the environment in adverse ways. On the other hand, membrane separation technology promises rejections as high as the other methods while operating at reduced costs and with little effect on the environment [21], [22].

An alternative process design has ammonia continuously removed from the digester by scrubbing the gas mixture [23]. The next proposed step is the acidification of the scrubbed ammonia by the addition of sulfuric acid to produce ammonium sulfate. This is then concentrated by feeding the effluent to a reverse osmosis process using

spiral-wound membranes, and the concentrated retentate can be used as an N-type fertilizer. However, it is possible that by scrubbing gas mixture from the digester, water droplets containing some other dissolved salts could also be removed along with ammonia. In this case, the RO process to concentrate ammonium sulfate should also take into consideration the presence of other inorganic salts that could be found in the anaerobic digester.

In a previous iteration of this work it was suggested that LPRO membranes should be tested for the concentration of ammonium sulfate from aqueous solutions, and that the solution-diffusion model did not adequately describe the transport in the investigated RO membranes [24], which was attributed to the presence of convective transport through the membranes. In this study, three LPRO membranes have been characterized using ammonium sulfate, tripotassium phosphate, and multi-ion aqueous solutions in order to provide much-needed information on membrane performance in terms of ammonium ion rejection. Tests using tripotassium phosphate were conducted because the constituent ions can be found in anaerobic digestate in significant proportions. The multi-ion aqueous solution used comprised NH_4^+, K^+, SO_4^{2-}, and PO_4^{3-} in the same concentration ratios as found in anaerobic digestate.

4.2 Theoretical Background

The LPRO membranes selected in this study were characterized with single-salt (ammonium sulfate and tripotassium phosphate) aqueous solutions. Assuming stoichiometric transport of ions solvent and solute permeances were determined using the Kedem-Katchalsky model that accounts for both convective and diffusive transport through the membrane. The possibility of the convective solute transport was hinted at in the previous study using RO membranes [24]. It should also be noted that the effects of concentration polarization have not been factored into the analysis of the experimental results for reasons given in the experimental section.

The permeate flux across a membrane for a given pressure is given by the following equation:

$$J_V = \overline{P_{M,W}}(\Delta P - \sigma \Delta \pi) \quad (1)$$

where J_V [kg.m^{-2}.s^{-1}] is the solvent flux across the membrane; $\overline{P_{M,W}}$ [kg.m^{-2}.s^{-1}.Pa^{-1}] is the solvent permeance; ΔP [Pa] is the applied pressure gradient; $\Delta\pi$ [Pa] is the osmotic pressure gradient across the membrane and is a function of the feed and permeate concentrations, and; σ is the reflection coefficient of the salt for a given pressure across a particular membrane and accounts for imperfections within the membrane [25]. When σ = 1 the Kedem-Katchalsky model becomes the solution-diffusion model.

The osmotic pressure, $\Delta\pi$ [Pa], can be determined experimentally or by calculations using a modified van't Hoff equation for dilute concentrations. The van't Hoff equation is given as:

$$\Delta\pi = iRT(\phi_f c_f - \phi_p c_p) \tag{2}$$

where i is the number of ions produced by a given salt during dissociation; ϕ is the osmotic coefficient for a given salt at given molalities and temperature, and can be experimentally determined or found in literature; c_f [mol.m^{-3}] is the feed concentration of a given salt; c_p [mol.m^{-3}] is the solute concentration in the permeate stream; R [J.mol^{-1}.K^{-1}] is the universal gas constant, and; T [K] is the experimental temperature. The osmotic coefficients used in this paper are taken from Refs. [26] and [27].

The solute flux is calculated from experimentally determined parameters by the following equation:

$$j_i = c_p \times J_V \tag{3}$$

The relationship between the solute flux and the solute permeance is given by the following equation:

$$j_i = \overline{P_{M,S}}(c_f - c_p) + \left[\frac{(1-\sigma)c_{avg}J_V}{\rho}\right] \tag{4}$$

where j_i [mol.m^{-2}.s^{-1}] is the solute flux; $\overline{P_{M,S}}$ [m.s^{-1}] is the solute permeance for a given salt for a particular membrane; ρ is the density [kg.m^{-3}], and; c_{avg} [mol.m^{-3}] is the average concentration across the membrane pores, measured as a log-mean concentration difference.

Experimental variations in permeate fluxes were accounted for by determining the fractional uncertainty using the standard error equations.

4.3 Experimental

4.3.1 Permeation and separation experiments

The experimental setup used for the experiments, shown in Fig. 4.1, was described in our earlier study [24]. The permeation experiments were conducted using flat-sheet membranes housed in static cells and feed stored in a 20 l high-density polyethylene tank. Solutions in the tank were fed to the static cells using a centrifugal pump. Three membranes, with an active area of 14.5 cm^2 each, were tested simultaneously to obtain average performance for a given type of membrane. The membrane inlet temperature was measured at the membrane cell inlet points. Constant temperature during experiments was maintained using a Haake cooling bath. Pressure readings were taken at the membrane cell inlets and the retentate rotameter inlet. The permeate sample was collected at atmospheric pressure, so the pressure differential needed for Eq. (1) is essentially the feed pressure. The feed flow rate was 3 $l.min^{-1}$ while the highest permeate flow rate recorded was 6 $ml.min^{-1}$. Owing to the large differences between feed and permeate flow rates, zero stage-cut was assumed in each experiment. In addition, because of a large linear velocity of the feed stream in the membrane cell, the effects of concentration polarization were considered negligible and have not been factored into the calculations.

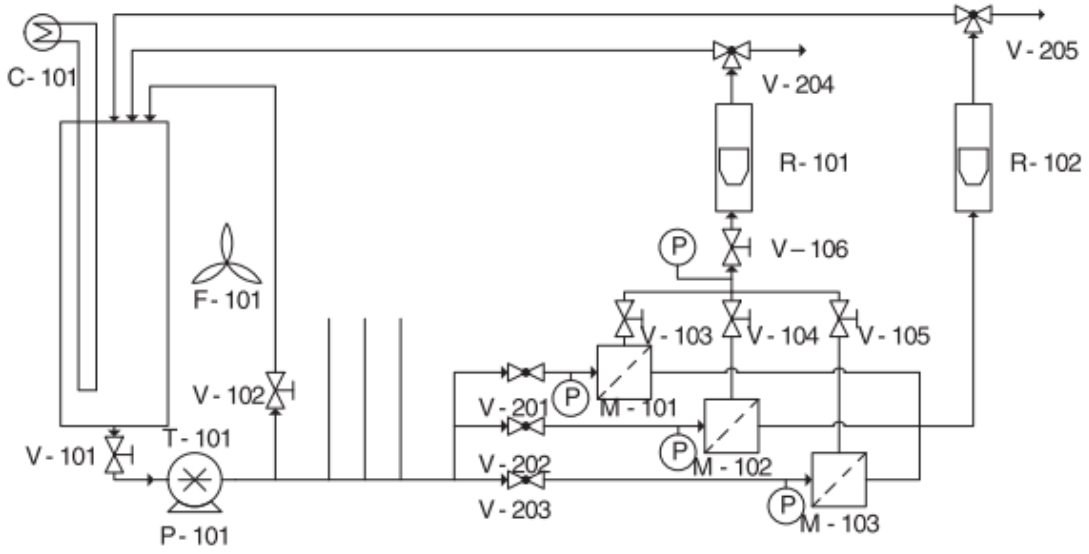

Figure 4.1: Schematic of the laboratory experimental setup for the concentration of ammonium sulfate using reverse osmosis. V-100 series valves are metering valves, and V-200 series valves are globe valves. M-101, M-102, and M-103 are static cells housing membrane elements. R-101 and R-102 are rotameters on the retentate and permeate side, respectively. F-101 is a 4-foot standing fan used to cool down the diaphragm pump, P-101. T-101 is the feed tank. The three vertical lines are a replacement for a flow regulator and are used to even out irregularities in flow to the membranes.

The solvent flux required for membrane characterization was determined by weighing the collected permeate (m_p) at constant time intervals (Δt):

$$J_V = \frac{m_p}{A_m \Delta t} \tag{5}$$

where A_m [m^2] is the active membrane area. The observed solute rejection, R, is calculated using the following equation:

$$R = 1 - \frac{c_p}{c_f} \tag{6}$$

where c_p and c_f are the permeate and feed concentrations, respectively. The feed and standard solutions for calibration of a conductivity meter were prepared using deionized water from a MilliPore system. The permeate concentrations were determined using an Oakton COND6+ conductivity meter. The conductivity measurements were converted to concentration values using calibration curves prepared for the individual

salts. Ionic concentrations for determining the stoichiometry of ions in the permeate were determined using inductively coupled plasma mass spectrometry (ICP-MS) for K^+, SO_4^{2-}, and PO_4^{3-} ions and a colorimetric method for NH_4^+. The chemicals used in the preparation of the calibration curves were purchased from Sigma-Aldrich and were analytical-grade unless noted otherwise.

4.3.2 Investigated membranes and experimental design

The membranes used in this study are commercially available membranes, selected for their abilities to provide high permeate fluxes at low pressures without a marked decrease in their rejection abilities. Flat sheet coupons were purchased from Sterlitech, each with an active diameter of 43 mm. The properties of the membranes used in this study are summarized in Table 4.1.

First, the membranes were tested with deionized water at pressures ranging from 3.5 x 10^5 Pa to 28 x 10^5 Pa. The separation experiments carried out were grouped in two broad classes: single-salt experiments and mixed-salt experiments. The single-salt experiments were conducted using $(NH_4)_2SO_4$ and K_3PO_4 for a feed concentration range of 2.5 to 40 g.l^{-1}. The experimental feed pressures ranged from 3.5 x 10^5 Pa to 28 x 10^5 Pa The limits of the feed concentrations were dependent on the osmotic pressure of the salt used.

Table 4.1: Properties of LPRO membranes used in this study.

Membrane	**DOW XLE**	**TriSep ACM4**	**TriSep X201**
Material	Polyamide	Polyamide	Polyamide-Urea
Solvent flux [kg.m^{-2}.s^{-1}] [a]	0.0138	0.0184	0.0142
Applied pressure [× 10^5 Pa] [a]	6.90	15.50	15.50
NaCl rejection [%] at 2 g.l^{-1} [a]	98.7	99.2	99.5
pH Range [a]	2 - 11	2 - 11	2 - 11
Water contact angle	66.3 [b]	35 [c]	55.0 ± 1.8 [d]

[a] As reported by Sterlitech, 2015 for a 2 g.l^{-1} NaCl feed solution at 25 ºC [28]
[b] As measured by Xu, et al., 2006 [29]

[c] As reported by Nghiem, L. D., 2005 [30]
[d] As measured by Comerton, 2008 [31]

The mixed-salt experiments class was subdivided into two groups: increasing total feed concentrations at a fixed $(NH_4)_2SO_4$:K_3PO_4 ratio of 3.12:1, and variable mass percentage contributions to a total feed concentration of 20 $g.l^{-1}$. The fixed-ratio experiments were intended to mimic increasing feed concentrations in a membrane process that would occur with larger membrane areas assuming that both salts were similarly rejected by the tested membranes. The fixed total salt concentration experiments are designed to investigate the relationships between the dominance of a given ion in the solution and its resulting rejection. All mixed-salt experiments were carried out at 13.80 $\times 10^5$ Pa. Table 4.2 summarizes the experiments conducted in this study.

Table 4.2: Experimental plan for determining the feasibility of using LPRO membranes to concentrate ammonium ions in anaerobic digestate.

Feed	**$\Delta P \times 10^5$ [Pa]**	**c_f [$g.l^{-1}$]**	**Ratio**
H_2O	3.5, 7, 13.8, 30	-	-
$(NH_4)_2SO_4$	13.8	2.5, 5, 10, 20, 25	-
K_3PO_4	3.5, 7, 13.8, 30	2.5, 20, 40	-
$(NH_4)_2SO_4 + K_3PO_4$	13.8	3.3, 6.6, 13.2, 26.4	$(NH_4)_2SO_4$:K_3PO_4 3.12:1
$(NH_4)_2SO_4 + K_3PO_4$	13.8	20	$(NH_4)_2SO_4$:K_3PO_4 1:3, 1:1, 3:1

4.4. Results and Discussion

4.4.1 Deionized water permeation tests

The membranes were initially characterized using deionized water as feed. These experiments were carried out to determine the solvent permeances of the membranes as a function of feed pressure and to observe membrane compaction, if any. Fig. 2 presents the effect of ΔP on the water flux for the membranes investigated in this study.

It is evident that water fluxes increase with an increase in the pressure differential. Except for the DOW XLE at $\Delta P = 30 \times 10^5$ Pa, all fluxes fall on the respective straight lines passing through the origin. The observed downward deviation of experimental flux

of the DOW XLE membrane at the highest feed pressure is attributed to membrane compaction and can be confirmed by a reduction in water permeance through the membrane. Membrane compaction occurs when an increase in applied pressure leads to a restructuring of the membrane polymers to accommodate the increase in pressure, which leads to a reduced membrane porosity [32].

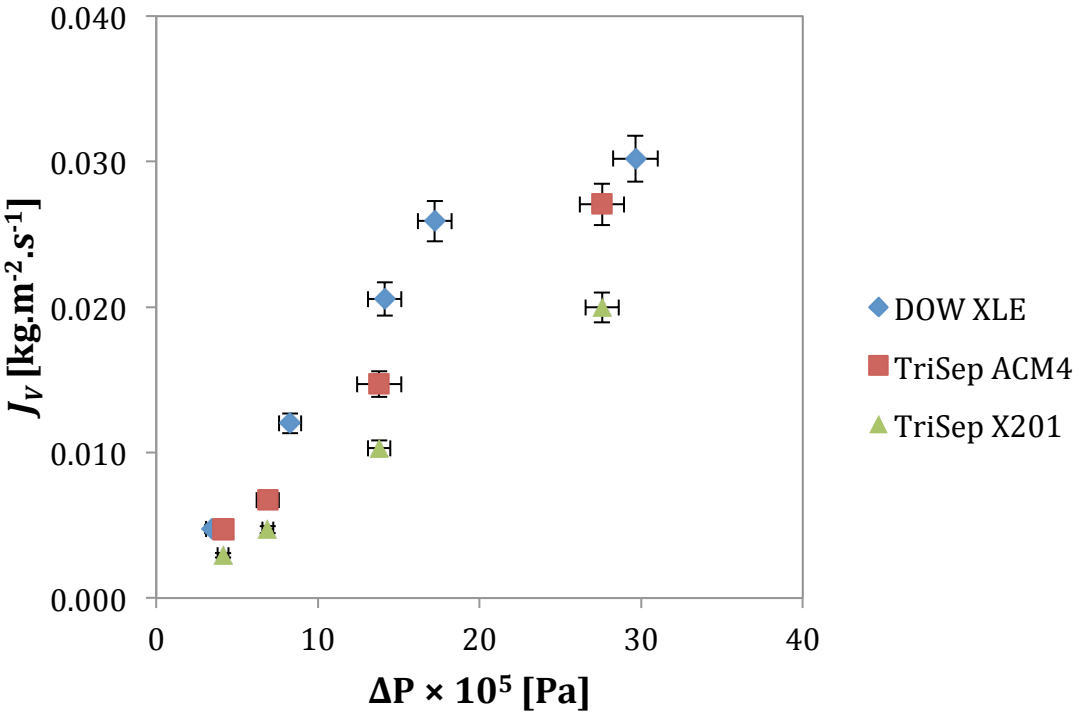

Figure 4.2: Plot of permeate fluxes versus pressure differential for the membranes using deionized water as feed. The average experimental temperature was 21 ± 2 ºC.

Figure 4.2 also shows that the DOW XLE membrane displays the highest permeate fluxes at a given pressure differential, followed by the TriSep ACM4 and the TriSep X201 membranes. Uncertainties in pressure differentials are derived from the oscillations of the pressure gauges. Permeate flux uncertainties are derived using standard error equations. This trend confirms the manufacturer-specified fluxes for the three membranes. It is also noted that the DOW XLE and TriSep X201 membranes show permeate fluxes slightly lower than those specified by the manufacturer, although the TriSep ACM4 membrane shows fluxes close to manufacturer specifications.

Using Eq. (1), the pure water permeances for the DOW XLE membrane is 1.45×10^{-8} $kg.m^{-2}.s^{-1}.Pa^{-1}$, while the TriSep ACM4 has a permeance of 1.042×10^{-8} $kg.m^{-2}.s^{-1}.Pa^{-1}$ and the TriSep X201 membrane has a permeance of 0.717×10^{-8} $kg.m^{-2}.s^{-1}.Pa^{-1}$. The pure water permeances reported are at pre-compaction pressures, and for the DOW XLE membrane the compacted permeance is 1.02×10^{-8} $kg.m^{-2}.s^{-1}.Pa^{-1}$ at the highest feed pressure.

4.4.2 Single salt separation experiments

Single-salt separation experiments were carried out with aqueous solutions of $(NH_4)_2SO_4$ and K_3PO_4, respectively. The experiments with $(NH_4)_2SO_4$ were performed at a fixed feed pressure of 13.80×10^5 Pa and five different feed concentrations ranging from 2.5 to 25 $g \cdot l^{-1}$. On the other hand, the experiments with K_3PO_4 were performed with three different feed concentrations of 2.5, 20 and 40 $g \cdot l^{-1}$ at four different feed pressures ranging from 3.50×10^5 Pa to 30×10^5 Pa.

Salt rejections

To our best knowledge, the LPRO membranes used in this study have not been characterized with aqueous solutions of $(NH_4)_2SO_4$ and K_3PO_4. The NaCl rejections of the selected membranes that are provided in Table 4.1 refer to brackish water (2 $g.l^{-1}$ of NaCl). On the one hand, the salts investigated in this study are larger than NaCl, which should help their rejection, but on the other hand, the lowest feed concentration, 2.5 $g \cdot l^{-1}$, considered in this study is slightly greater than that of brackish water, which might lower their rejections in comparison.

Figure 4.3 presents the effect of $(NH_4)_2SO_4$ concentration in the feed stream on solute rejection at the feed pressure of 13.80×10^5 Pa. The horizontal reference lines show the respective rejections of brackish water. As expected, the rejection $(NH_4)_2SO_4$ decreases with feed concentration. At the lowest feed concentration of 2.5 $g \cdot l^{-1}$ the rejections of $(NH_4)_2SO_4$ are comparable (TriSep ACM 4 and TriSep X201 membranes) or even greater (DOW XLE membrane) than the respective rejections of brackish water. The effect of feed concentration on solute rejection is strongest for the TriSep ACM 4 membrane, for which the rejection at 25 $g \cdot l^{-1}$ drops to 93%. On the other hand, while the rejections of $(NH_4)_2SO_4$ by the TriSep X201 and DOW XLE membranes decrease with

increase in feed concentration, the lowest experimental rejections are just slightly below 98%. It is important to emphasize that although the rejection of brackish water by the DOW XLE membrane is smaller than that of the TriSep ACM 4 membrane, the former appears to be much better for the rejection of $(NH_4)_2SO_4$ than the latter. This indicates that while the manufacturer specified NaCl rejections provide a useful guide, they are not necessarily indicative of the rejections of different solutes. In addition, the TriSep ACM 4 membrane shows the worst solute rejections despite the fact that this membrane was tested at a slightly greater feed pressure (15.50×10^5 Pa) than the other two membranes (13.80×10^5 Pa). The effect of feed pressure is further explored with the other solute considered in this study, which is discussed next.

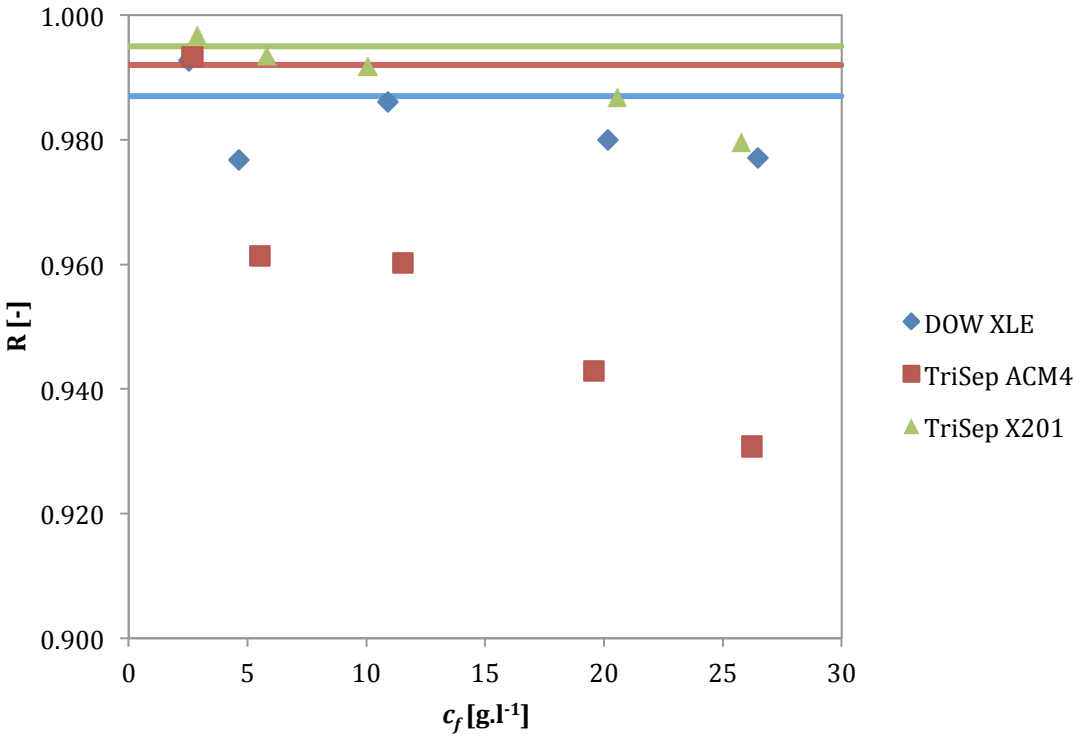

Figure 4.3: $(NH_4)_2SO_4$ rejections as a function of increasing $(NH_4)_2SO_4$ concentrations in feed. All reported values are at an average temperature of 22±1.5 ºC. DOE XLE and TriSep X201 membranes were tested at 13.8 x 10^5 Pa while TriSep ACM 4 at 15.5 x 10^5 Pa. The horizontal lines are specified NaCl rejections from the membrane vendor, Sterlitech, and can be found on their website. All manufacturer rejections refer to a 2 g.l^{-1} NaCl feed concentration at 25 ºC.

Figure 4.4 presents the effect of feed pressure on the rejection of K_3PO_4 at two different feed concentrations of 2.5 and 20 g·l^{-1}. In addition, the membranes were also

tested with a concentrated feed solution of 40 $g \cdot l^{-1}$ at 13.8 x 10^5 Pa. As expected, the solute rejection increases with an increase in feed pressure. The effect of feed pressure is much stronger for the concentrated feed solution for which the rejection increases from just 83% to 96%. Interestingly, the TriSep ACM4 membrane, which is clearly the worst membrane for the rejection of $(NH_4)_2SO_4$, shows rejections of K_3PO_4 similar to or even better than the other membranes. With the exception of the TriSep ACM4 membrane, which rejects K_3PO_4 better than $(NH_4)_2SO_4$, the TriSep X201 and DOW XLE membranes reject better $(NH_4)_2SO_4$ better than K_3PO_4. This is more evident at the higher than at the lower feed concentration. At the lower feed concentration of 2.5 $g.l^{-1}$ and the similar feed pressure the rejections of K_3PO_4 and $(NH_4)_2SO_4$ are comparable. It is also interesting to note that the most concentrated feed solution of 40 $g \cdot l^{-1}$ tested at 13.8 x 10^5 Pa shows a better solute rejection than 20 $g \cdot l^{-1}$ tested at 7 x 10^5 Pa. This is because of the lowered effect of the osmotic pressure at 13.80 × 10^5 Pa for K_3PO_4.

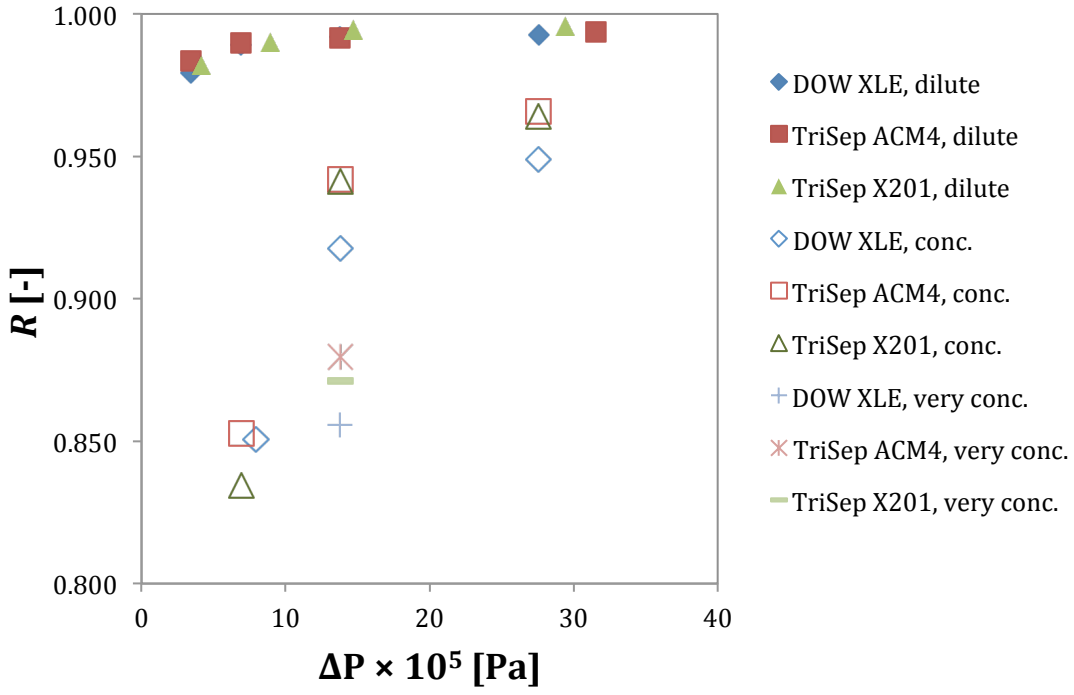

Figure 4.4: Solute rejections as a function of increasing pressure differentials for K_3PO_4 permeation experiments at 2.5 $g.l^{-1}$ (dilute), 20 $g.l^{-1}$ (concentrated), and 40 $g.l^{-1}$ (very concentrated) feed concentration. All experiments were conducted at 13.80 × 10^5 Pa. The average temperature for the experiments shown was 21.5±1.5 ºC.

Solvent fluxes and reflection coefficients

Fig. 4.5 presents the effect of the osmotic pressure gradient on water fluxes in experiments carried out at constant feed pressures with aqueous solutions of ammonium sulfate (Fig. 4.5a) and tripotassium phosphate (Fig. 4.5b). The variation in the osmotic pressure gradient results from different feed concentrations and consequently different permeate concentrations. The osmotic pressure gradients required to construct the plots in Fig. 4.5 were calculated from Eq. (2) using the experimentally measured permeate concentrations.

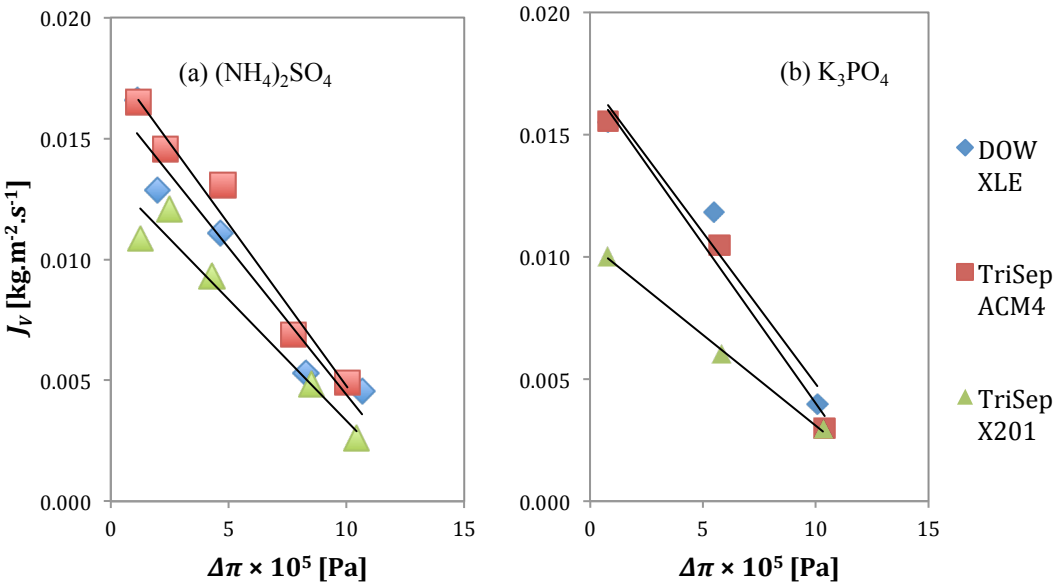

Figure 4.5: Permeate fluxes as a function of the osmotic pressure gradients. All experiments were carried out at 13.80 × 10^5 Pa, except the $(NH_4)_2SO_4$ ACM4 experiments, which were at 15.50 × 10^5 Pa. All experiments were at 22±1.5 ºC.

It is evident that as expected from Eq. (1) the solvent fluxes decrease with an increase in the osmotic pressure gradient, i.e., an increase in feed concentration. For both solutes, the relationships between the water flux and the osmotic pressure gradient for each membrane are approximately linear. The corresponding slopes (S) are then used to evaluate the reflection coefficient for each salt in the investigated membranes. Rearranging Eq. (1), the slope in N_w versus $\Delta\pi$ is given by:

$$S = -\overline{P_{MW}}\sigma \Rightarrow \sigma = -\frac{S}{\overline{P_{MW}}} \tag{7}$$

Such calculated reflection coefficients are summarized in Table 4.3.

Table 4.3: Selected characterization properties for three commercially available membranes used in ammonium rejection experiments.

Membrane	**σ, K_3PO_4**	**σ, $(NH_4)_2SO_4$**
DOW XLE	0.827	0.968
TriSep ACM4	1.21*	0.961
TriSep X201	0.977	0.977

*The σ-value of 1.21 is outside the expected σ range: $0 < \sigma < 1$.

Except for the TriSep ACM4 membrane for K_3PO_4 the reflection coefficients in Table 4.3 are just slightly lower than unity. For $(NH_4)_2SO_4$, the reflection coefficients are based on five different feed concentrations while for K_3PO_4 they are based only on three different feed concentrations. This is most likely the reason for more consistent reflection coefficients of $(NH_4)_2SO_4$ compared to K_3PO_4. The same argument could be used to explain to explain the physically impossible $\sigma > 1$ for K_3PO_4 in the TriSep ACM4 membrane. On the other hand, it is important to keep in mind that the Kedem-Katchalsky model assumes a stoichiometric transport of ions through the membrane, which will be discussed further in the next section on the mixed-salt separation.

With σ close to 1, the Kedem-Katchalsky model is equivalent to the solution-diffusion model, i.e. the contribution of the convective transport to the overall transport of through the membrane is practically negligible. This would suggest a lack defects/imperfection in the membranes investigated in this study. On the other hand, it is possible that minor imperfections and consequently convective transport may occur through without the model accounting for it, as has been documented in literature [33].

In addition to experiments at constant feed pressure and varying feed concentrations, the experiments with aqueous solution of K_3PO_4 were also carried out with increasing pressure differentials at a constant feed concentration. The summary of

these experiments showing the effect of feed pressure for two different feed concentrations of 2.5 $g.l^{-1}$ and 20 $g.l^{-1}$ of K_3PO_4 on the water flux is shown in Fig. 6.

It is evident from Fig. 4.6 that similarly to Fig. 4.2 the water flux increases almost linearly with the applied feed pressure for all membranes at both feed concentrations. Moreover, for a given membrane the resulting slopes appear to be independent of the feed concentration. Some deviation from linearly, seen at the highest feed pressure of 30 x 10^5 Pa, could be attributed to membrane compaction. Unlike Fig. 4.2, the compaction effects are seen for all membranes, not only for the DOW XLE membrane. At the same time, they are not as pronounced as in Fig. 4.2 for the DOW XLE membrane. While the water flux in both Fig. 4.2 and Fig. 4.6 appears to be linearly related to the feed pressure, it should be noted that the corresponding straight lines would not pass through the origin in Fig. 4.6 as they do in Fig. 4.2. This is because of the effect of the osmotic pressure gradient, which increases with an increase in feed pressure. As a matter of fact, the intercept with the pressure axis could be used to evaluate the experimental osmotic pressure [24].

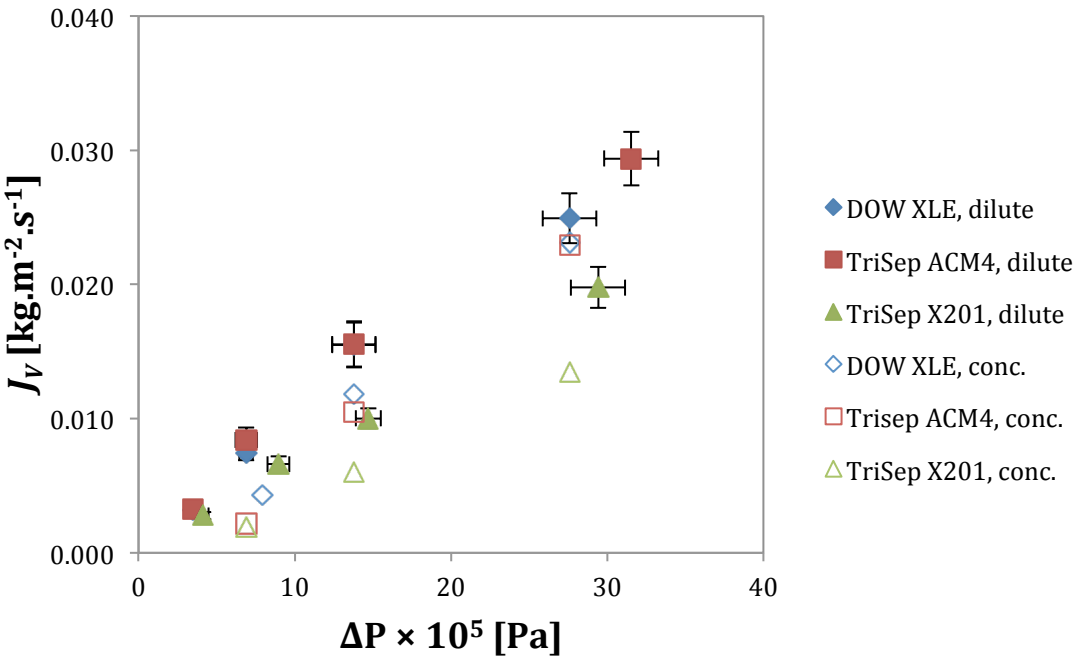

Figure 4.6: Experimental permeate fluxes as a function of increasing pressure differentials for K_3PO_4 permeation experiments at 2.5 $g.l^{-1}$ (dilute) and 20 $g.l^{-1}$ (concentrated) feed concentrations.. For the sake of clarity, the experimental permeate fluxes obtained at 40 $g.l^{-1}$ have not been shown. The average temperature for the experiments shown was 21.5±1.5 ºC.

Solute and solvent permeances

The transport through the membrane is commonly characterized by the permeances of both solvent and solute. In this subsection, the solvent and solute permeances are presented as a function of the feed concentration and feed pressure. Solvent permeances were calculated from Eq. (1) using the reflection coefficients listed in Table 4.3, except for the TriSep ACM4 membrane tested with K_3PO_4 solution, for which $\sigma = 1$ was used. Solute permeances were calculated from Eq. (4) using the experimental solute fluxes calculated from Eq. (3) and the reflection coefficients listed in Table 4.3. For the TriSep ACM4 membrane tested with K_3PO_4 solution, $\sigma = 1$ was assumed. Figure 4.7 presents the effect of feed concentration on solvent permeances in the experiments with $(NH_4)_2SO_4$ (Fig. 4.7a) .and with K_3PO_4 (Fig. 4.7b). The solvent permeances at $c_f = 0$ correspond to those presented in Fig. 4.2 for the same feed pressure.

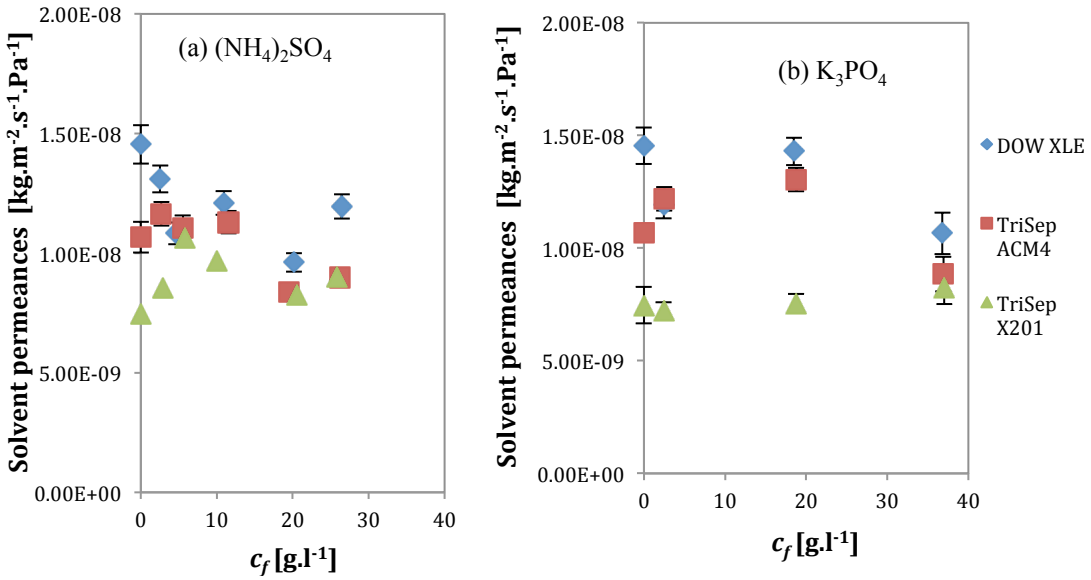

Figure 4.7: Solvent permeances as a function of increasing feed concentrations using Kedem-Katchalsky model. For comparison, the pure water permeances are presented at the 0 $g.l^{-1}$ feed concentration. All experiments were carried out at 13.80×10^5 Pa except the $(NH_4)_2SO_4$ experiments with ACM4, which was carried out at 15.50×10^5 Pa.

It is evident that there is a significant variation in solvent permeances in Fig. 4.7, which is due to random experimental errors. At the same time, there is no clear trend between solvent flux and feed concentration. The respective solvent permeances with pure water are in the range of those determined with salt solutions. Moreover, the solvent

permeances for a given membrane in the experiments with $(NH_4)_2SO_4$ and K_3PO_4 are comparable. Consequently, it is safe to conclude that solvent permeance is independent on solute concentration and the nature of solute in feed solution. Fig. 4.7 also validates the use of Kedem-Katchalsky model for membrane characterization by means of solvent permeance. At the same time, since the reflection coefficients used to determine the solvent permeances reported in Fig. 4.7 were close to unity, one could draw a similar conclusion with the applicability of the solution-diffusion model to describe the solvent transport across the membrane.

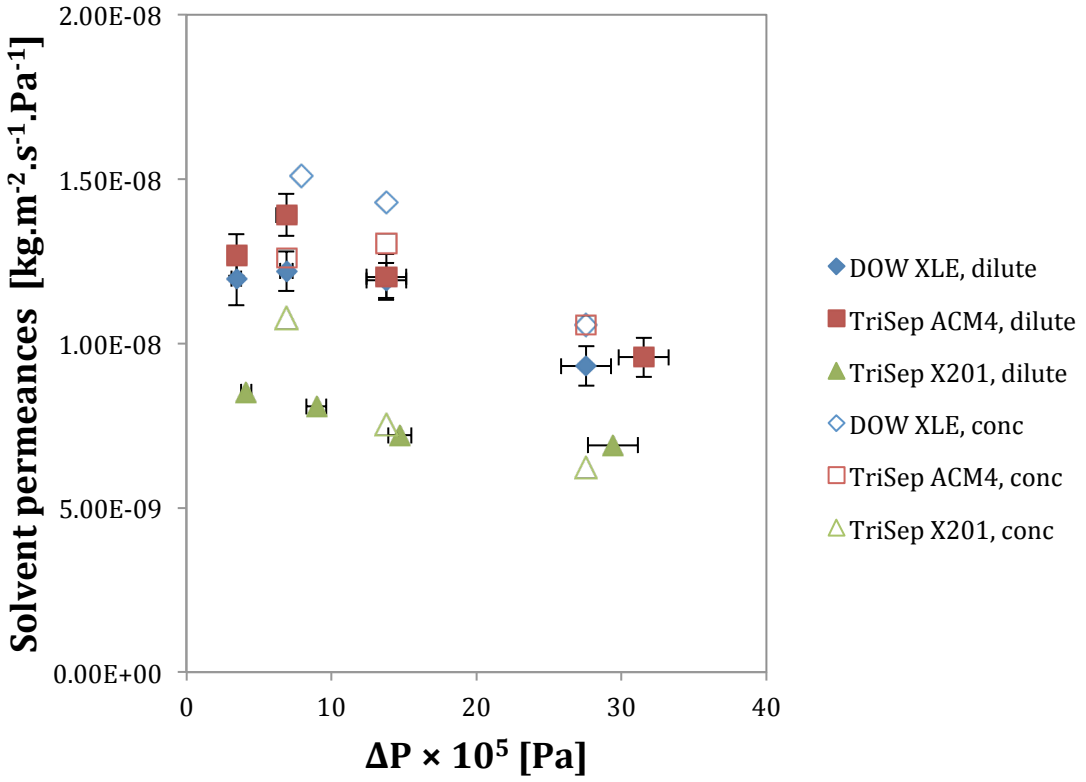

Figure 4.8: Solvent permeances as a function of increasing pressure differentials for K_3PO_4 permeation experiments at 2.5 $g.l^{-1}$ (dilute) and 20 $g.l^{-1}$ (concentrated) feed concentrations. All solvent permeances are calculated using the Kedem-Katchalsky model. For the sake of clarity, the solvent permeances obtained at 40 $g.l^{-1}$ have not been shown. The average temperature for the experiments shown was 21.5±1.5 ºC.

Figure 4.8 presents the effect of feed pressure on water permeance in two series of experiments with K_3PO_4 solutions at 2.5 $g.l^{-1}$ and 20 $g.l^{-1}$ feed concentrations corresponding to the water fluxes presented in Fig. 4.6. Solvent permeances decrease

with an increase in feed pressure, which is a result of compaction occurring in the membranes. The extent of compaction with feed pressure appears to be similar in all investigated membranes regardless of the feed concentration. For the TriSep ACM 4 and X201 membranes, the solvent permeances for both dilute and concentrated feed solutions appear to be similar at a given feed pressure. On the other hand, for the DOW XLE membrane for a given feed pressure, the solvent permeances with the more concentrated feed solution appear to be greater than for dilute feed solution, which is inconstant with what was observed in Fig. 4.7. Again, random experimental errors could lead to this inconsistency.

Figure 4.9 presents the effect of feed concentration on solute permeances in the experiments with $(NH_4)_2SO_4$ (Fig. 4.9a) and with K_3PO_4 (Fig. 4.9b). Unlike solvent permeances, which were independent of feed concentration, the solute permeances either decrease, increase, or are independent of feed concentration depending on the membrane and solute.

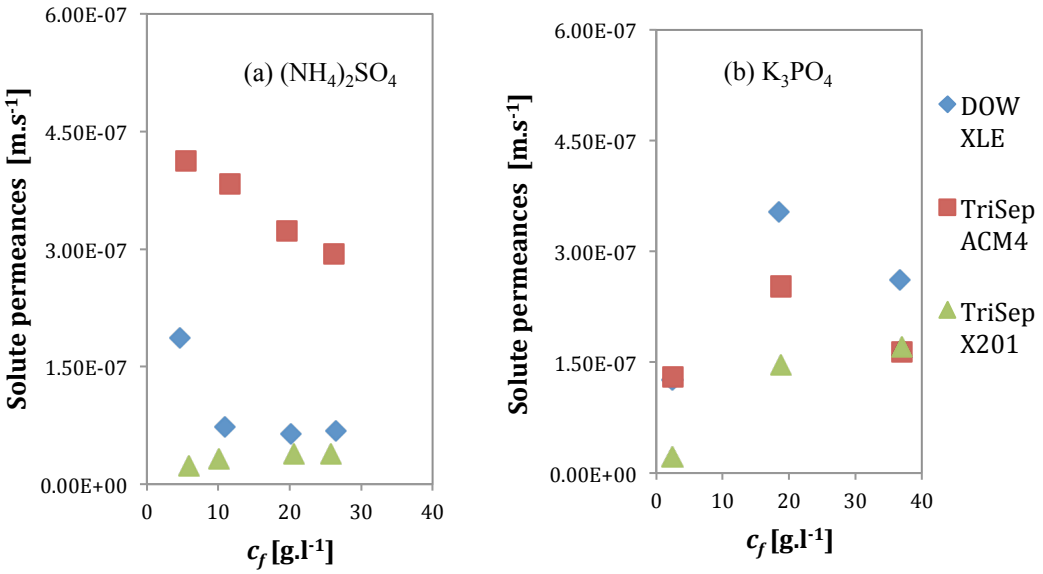

Figure 4.9: Solute permeances as a function of increasing feed concentration using Kedem-Katchalsky model. All experiments were carried out at 13.80×10^5 Pa except the TriSep ACM4 data for $(NH_4)_2SO_4$, which was carried out at 15.50×10^5 Pa. The K_3PO_4 σ value for the TriSep ACM4 membrane was assumed to be unity.

Figure 4.9a shows a marked decrease in the $(NH_4)_2SO_4$ permeance in two of the membranes as the feed concentration increases. A similar result was observed in our

previous study with RO membranes, and the decrease in solute flux at increasing feed concentrations was attributed to the convective solute transport across the membrane [24]. It was thought that using the Kedem-Katchalsky model would eliminate the variation of solute permeance with feed concentration. However, it is clear that except for the TriSep X201 membrane for which $(NH_4)_2SO_4$ permeance is independent of feed concentration, the Kedem-Katchalsky model did not alleviate the dependence of solute permeance of feed concentration. Interestingly, in the experiments with K_3PO_4 solution with the TriSep X201 membrane, permeance of solute increases with an increase in feed concentration. For the other two membranes, since there are only three experimental points, it is difficult to conclude about any specific trend. Comparing the rejections of two solutes in Figs. 4.9a and 4.9b the only clear conclusion can be made with regard to the TriSep ACM4 membrane, which shows a smaller solute permeance (greater rejection) of K_3PO_4 compared to $(NH_4)_2SO_4$. For the other two membranes, because of variation in solute permeance with feed concentration, it is difficult to conclude which solute has a greater permeation in which membrane.

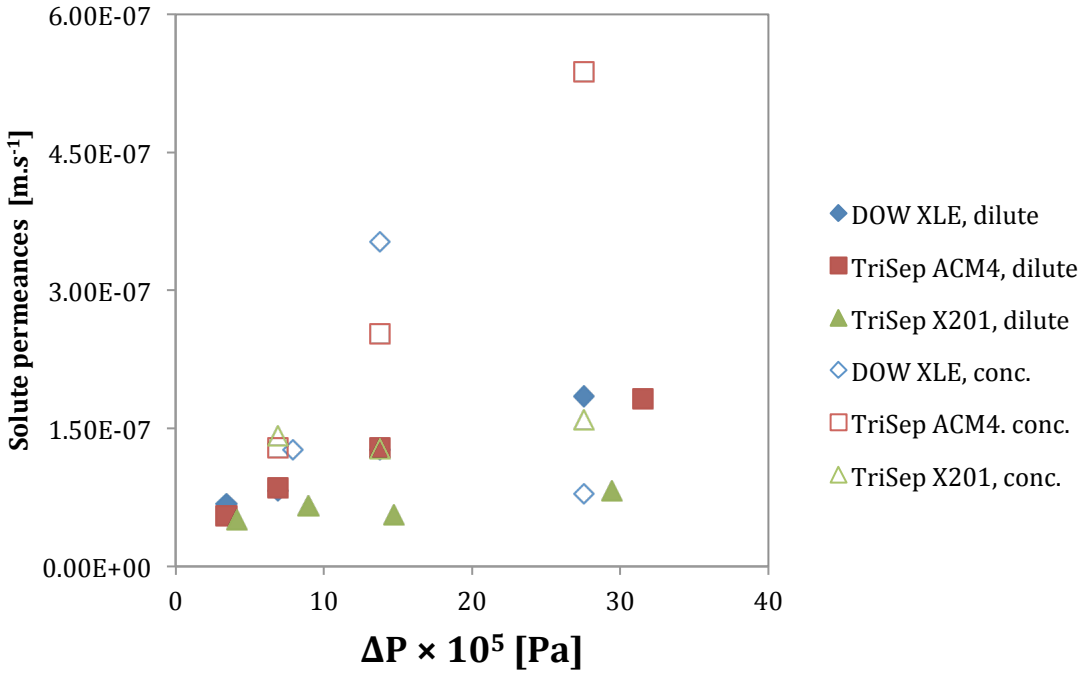

Figure 4.10: Solute permeances as a function of increasing pressure differentials for K_3PO_4 permeation experiments at 2.5 $g.l^{-1}$ (dilute) and 20 $g.l^{-1}$ (concentrated) feed concentrations. All solute permeances are calculated using the Kedem-Katchalsky model. For the sake of clarity, the solute permeances obtained at 40 $g.l^{-1}$ have not been shown. The average temperature for the experiments shown was 21.5±1.5 ºC. The K_3PO_4 σ value for the TriSep ACM4 membrane was assumed to be unity.

Figure 4.10 presents the effect of feed pressure on the permeance of K_3PO_4 in two series of experiments carried at feed concentration of 2.5 and 20 $g.l^{-1}$. Aside from the TriSep X201 data at either concentration the solute permeances increase with increasing pressure differential. The TriSep X201 data indicates its solute permeances are independent of the pressure differential for that membrane, which would confirm the suitability of the Kedem-Katchalsky model to describe the transport in that membrane, especially for the experiments with the dilute feed solution. However, the increase in solute permeance for the other membranes indicates that this model cannot adequately account for solute transport, and more rigorous models must be applied to characterize the membranes.

While the $(NH_4)_2SO_4$ solute permeances decrease with an increase in concentration in both Fig. 4.9 and the previous paper [24], the K_3PO_4 solute permeances generally increase with an increase in solute concentration. Increasing the pressure differential increases the solute permeance of both salts. However, solvent permeances for both salts were shown to be relatively independent on feed concentration and applied pressure provided no membrane compaction occurred. It can therefore be concluded that while the Kedem-Katchalsky model (and solution diffusion model) adequately describe solvent transport through LPRO membranes, they are not suitable to describe the solute transport through the membrane. This is most likely caused by the non-stoichiometric nature of the rejections, a phenomenon that is investigated in the next section.

4.4.3 Mixed-salt experiments

Permeation experiments were carried out using a combination of $(NH_4)_2SO_4$ and K_3PO_4 salts to determine NH_4^+ rejection trends in the presence of other ions found in anaerobic digestate. In preparing the increasing total salt concentration experiments, linear changes in ionic concentrations for NH_4^+ and K^+ were assumed and the initial NH_4^+:K^+ stoichiometric ratio found in anaerobic digestate was provided by a local company, CHFour Biogas.

All ionic concentrations except NH_4^+ were measured using ICP-MS, and NH_4^+ concentrations were measured using a colorimetric method. The distinct measurement of individual ions enabled the verification or otherwise of the stoichiometric assumptions for the phenomenological models. The properties of the ions in the system are given in Table 4.4. The K^+ and NH_4^+ cations have comparable radii (r_s) and the diffusivities at infinite dilution (D_∞) despite the fact that the molecular weight (MW) of the former is twice that of the latter. In turn, although the MW of SO_4^{2-} and PO_4^{3-} are comparable, the r_s of the former is significantly smaller while D_∞ is considerably larger than those of the latter. It is also important to note, that both monovalent cations are smaller and have greater D_∞ than the multivalent anions.

Table 4.4: Diffusivities at infinite dilution, solute radii, and molecular weights of ions used in mixed-salt experiments.

Ion	MW [g.mol^{-1}]	Solute radius, r_s [nm]	D_∞, [m^2.s^{-1}]
K^+	39.09	0.125	1.96×10^{-9}
NH_4^+	18.04	0.128	1.98×10^{-9}
SO_4^{2-}	96.06	0.207	1.07×10^{-9}
PO_4^{3-}	94.97	0.343	0.70×10^{-9}

4.3.1 Mixed-salt permeation results: Permeate fluxes

The effect of the total salt concentration for a fixed ratio of the constituent salts on permeate flux and the effect of different ratios of the constituent salts for the fixed total salt concentration on the permeate flux are presented in Figs. 11 and 12, respectively.

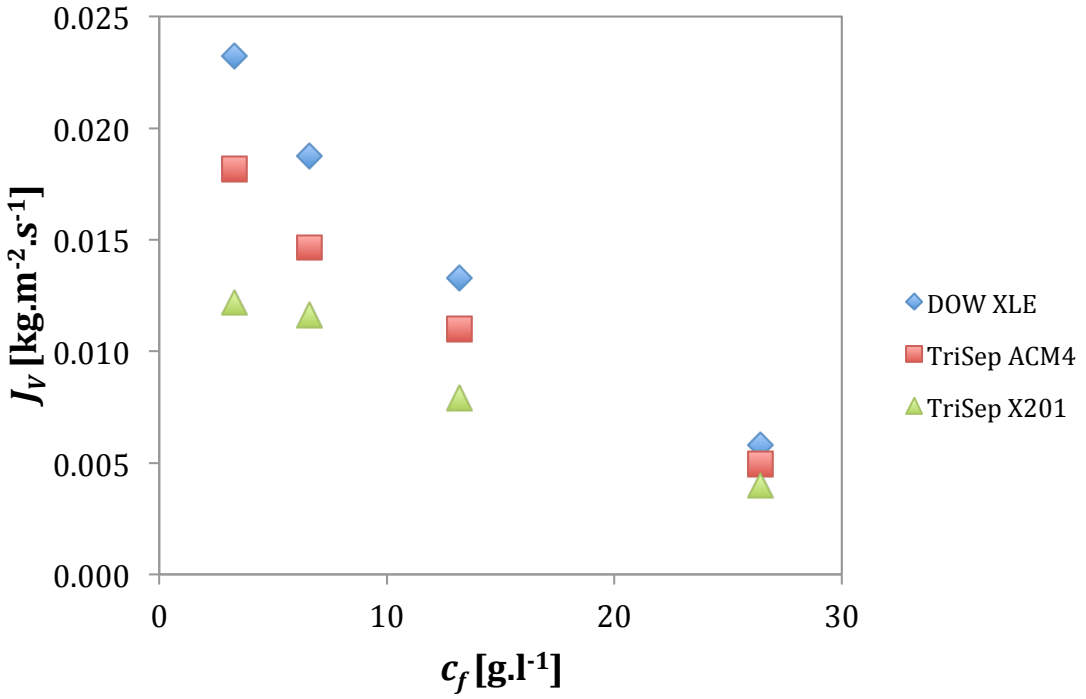

Figure 4.11: Permeate fluxes as a function of increasing total feed concentrations at a constant NH_4^+: K^+ molar ratio of 3.3:1 found in anaerobic digestate. All experiments were carried out at 13.80×10^5 Pa and at 23 ± 1.5 ºC.

It is evident from Fig. 4.11 that as the total salts concentration increases while the feed pressure is constant, the permeate flux decreases, which follows the single-salt permeate flux-feed concentration trends found for single salts (Fig. 4.3). This is because when the total salt concentration increases, the osmotic pressure gradient, which counterbalances the pressure driving force, also increases. However, since the molecular weights of $(NH_4)_2SO_4$ and K_3PO_4 are different and the two produce different number of ions upon dissociation, their contributions to the total osmotic pressure gradient cannot be deducted from Fig. 4.11. To better understand the contributions of either salt to the total osmotic pressure gradient, Fig. 4.12 presents the effect of changing ratio $(NH_4)_2SO_4$ to K_3PO_4 in the feed solution when both the total salt concentration (20 $g.l^{-1}$) and the feed pressure (13.80×10^5 Pa) are constant. According to Eq. (2), the osmotic pressure of the 20 $g.l^{-1}$ $(NH_4)_2SO_4$ solution is greater than that of the 20 $g.l^{-1}$ K_3PO_4 solution, which is consistent with a smaller permeate of the former compared to latter seen in Fig. 4.12. On the other hand, the permeate flux does not decrease monotonically with increasing concentration ratio of $(NH_4)_2SO_4$ to K_3PO_4 in the feed solution, but rather the maximum permeate flux is observed for the ratio 1:3. This is unexpected, as the lower osmotic pressure feed should have higher permeate fluxes according to Eq. (1), and is best attributed to experimental errors.

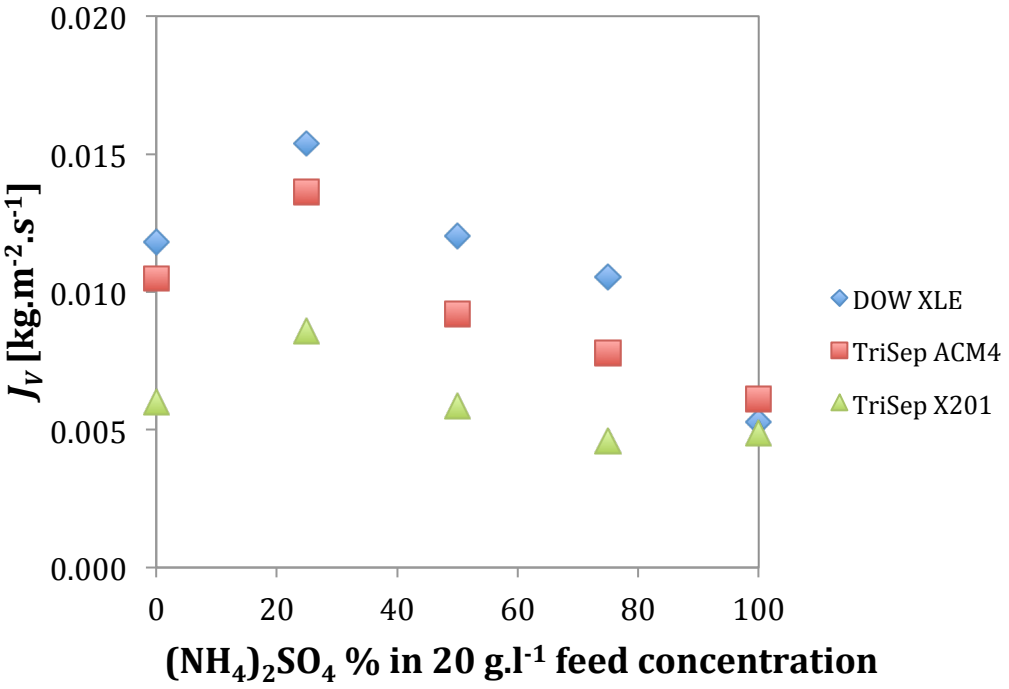

Figure 4.12: Permeate fluxes as a function of the mass percentage contribution of $(NH_4)_2SO_4$ in a 20 g.l^{-1} feed solution. At a total contribution of 0 % pure K_3PO_4 permeate fluxes are presented. All experiments were carried out at 23 ± 1.5 ºC.

Mixed-salt rejections

The ionic rejections were measured using ICP-MS and colorimetric methods. Conductivity measurements were not used, as they could not account for individual ions to the measured conductivity. The measurement of unique ionic concentrations in the permeate stream allows verification of stoichiometric transport of ions that was assumed when analyzing single salt separation experiments.

Table 4.5: The ionic feed and permeate concentrations from mixed-salt permeation experiments at total salt concentrations in feed of 3.3, 6.6, 13.2, and 26.4 $g.l^{-1}$. The $(NH_4)_2SO_4$:K_3PO_4 mass concentration ratio in the feed was kept constant at 3.12:1. Numbers in parentheses on the permeate side are ionic rejections.

Memb.	Feed					Permeate			
	pH	NH_4^+ mol/l	K^+ mol/l	PO_4^{3-} mol/l	SO_4^{2-} mol/l	NH_4^+ mol/l	K^+ mol/l	PO_4^{3-} mol/l	SO_4^{2-} mol/l
XLE	8.3	0.0378	0.0113	0.0038	0.0189	0.0016 (0.957)	0.0001 (0.990)	0 (1)	0.0014 (0.924)
	8.8	0.0757	0.0226	0.0075	0.0378	0.0029 (0.961)	0.0003 (0.987)	0.0001 (0.990)	0.0017 (0.955)
	9.0	0.1514	0.0452	0.0151	0.0757	0.0036 (0.976)	0.0009 (0.981)	0.0002 (0.984)	0.0025 (0.967)
	9.6	0.3027	0.0904	0.0302	0.1514	0.0025 (0.992)	0.002 (0.978)	0.0006 (0.981)	0.0045 (0.970)
ACM4	8.3	0.0378	0.0113	0.0038	0.0189	0.0018 (0.952)	0.0003 (0.974)	0.0001 (0.979)	0.0017 (0.911)
	8.8	0.0757	0.0226	0.0075	0.0378	0.0035 (0.953)	0.0012 (0.945)	0.0004 (0.950)	0.0032 (0.916)
	9.0	0.1514	0.0452	0.0151	0.0757	0.0032 (0.979)	0.0012 (0.971)	0.0004 (0.975)	0.0032 (0.957)
	9.6	0.3027	0.0904	0.0302	0.1514	0.0019 (0.994)	0.0075 (0.917)	0.0026 (0.913)	0.0172 (0.886)
X201	8.3	0.0378	0.0113	0.0038	0.0189	0.0012 (0.969)	0.0001 (0.991)	0 (1)	0.0014 (0.927)
	8.8	0.0757	0.0226	0.0075	0.0378	0.0032 (0.957)	0.0002 (0.993)	0 (1)	0.0014 (0.963)
	9.0	0.1514	0.0452	0.0151	0.0757	0.0032 (0.979)	0.0023 (0.949)	0.0008 (0.945)	0.0049 (0.935)
	9.6	0.3027	0.0904	0.0302	0.1514	0.0019 (0.994)	0.0051 (0.944)	0.0018 (0.941)	0.0116 (0.924)

Table 4.5 presents the summary of the results of the experiments in which the ratio of the constituent salts was kept constant while the total salt concentration in feed solution was changed. Table 4.5 corresponds to permeate-flux results shown in Fig. 4.11. Table 4.6 presents the summary of the second series of experiments in which the total salt concentration was kept constant while the ratio of the constituent salts was varied. Table 4.6 corresponds to permeate-flux results shown in Fig. 4.12. It is important to note that the concentrations of individual ions in both tables are in $mol.l^{-1}$, and these concentrations were used to calculate the ionic rejections from Eq. (6); the latter are shown as numbers in parentheses underneath the respective ionic concentrations in permeate. In addition, both tables show experimentally measured pH of the respective feed solutions.

Table 4.6: The ionic feed and permeate concentrations from mixed-salt permeation experiments at a varying $(NH_4)_2SO_4$:K_3PO_4 ratios of 1:3, 1:1, and 3:1 for a total feed concentration of 20 $g.l^{-1}$. Numbers in parentheses on the permeate side are ionic rejections.

		Feed				Permeate			
Memb.	pH	NH_4^+ mol/l	K^+ mol/l	PO_4^{3-} mol/l	SO_4^{2-} mol/l	NH_4^+ mol/l	K^+ mol/l	PO_4^{3-} mol/l	SO_4^{2-} mol/l
XLE	10.5	0.076	0.212	0.071	0.038	0.001 (0.983)	0.004 (0.983)	0.0004 (0.994)	0.001 (0.960)
	9.6	0.151	0.141	0.047	0.076	0.002 (0.988)	0.008 (0.947)	0.003 (0.945)	0.005 (0.936)
	9.0	0.227	0.071	0.024	0.114	0.003 (0.986)	0.002 (0.977)	0.0005 (0.980)	0.004 (0.969)
ACM4	10.5	0.076	0.212	0.071	0.038	0.002 (0.979)	0.015 (0.930)	0.005 (0.933)	0.003 (0.909)
	9.6	0.151	0.141	0.047	0.076	0.002 (0.988)	0.026 (0.816)	0.010 (0.796)	0.018 (0.759)
	9.0	0.227	0.071	0.024	0.114	0.001 (0.993)	0.010 (0.853)	0.004 (0.839)	0.021 (0.815)
X201	10.5	0.076	0.212	0.071	0.038	0.002 (0.978)	0.006 (0.969)	0.001 (0.981)	0.002 (0.952)
	9.6	0.151	0.141	0.047	0.076	0.002 (0.989)	0.007 (0.952)	0.002 (0.950)	0.004 (0.941)
	9.0	0.227	0.071	0.024	0.114	0.002 (0.990)	0.006 (0.917)	0.002 (0.909)	0.012 (0.890)

Analysis of the rejections of ions in Tables 4.5 and 4.6 reveal that for a given salt, the rejections of the cation and anion are different, in particular in the case of $(NH_4)_2SO_4$ for which regardless of the membrane and feed composition, the rejection of NH_4^+ is considerably greater than the rejection of SO_4^{2-}. In the case of K_3PO_4, while the rejections of PO_4^{3-} and K^+ are different, they no not differ significantly. Moreover, for a given membrane in some experiments PO_4^{3-} shows higher and in other cases lower rejection than K^+. Considering consistently greater rejections of NH_4^+ compared to SO_4^{2-} it can be concluded that transport of ions in mixed salt experiments is not stoichiometric. This phenomenon has been observed in literature [34] and can be accounted for by the creation of an electric charge on the membrane surface due to the feed pH [35]. Moreover, in this case the contribution of electromigration to the transport of ions across the membrane should be included. It is important to keep in mind that the solution-diffusion model considers only a diffusion driven by the concentration gradient while the Kedem-Katchalsky model also accounts for the convective transport of ions. However, none of

these models considers electromigration of ions. The latter can be accounted for by the extended Nernst-Planck equation as used in the Donnan Steric Pore (DSPM) Model [36].

Considering the measured pH values summarized in Tables 4.5 and 4.6 it is evident that in all experiments the feed solution was weakly basic. Consequently, as seen in Tables 4.5 and 4.6 as the concentration of K_3PO_4 increases the pH of feed solution increases. It is well documented in literature that a membrane charge is created by the pH of the feed solution, and that the membrane charge is dependent on the isoelectric point (IEP) [37], [38]. From the results presented in Tables 4.5 and 4.6 it can be concluded that the membranes tested are positively charged to counterbalance the excess negative ions in the solution. This implies that the operating conditions are below the IEP and the electrostatic repulsion between the cations and the positively charged membrane surface is strong, leading to increased cation rejection [35]. As a result, the negatively charged PO_4^{3-} and SO_4^{2-} are attracted to the membrane surface, and electromigration will enhance their transport through the membrane while lowering their rejection. This is why, despite a two-fold greater diffusivity of K^+ and NH_4^+ compared to PO_4^{3-} and SO_4^{2-} the former are equally or even better rejected by the membranes than the latter. In turn, a more than 30% greater diffusivity of SO_4^{2-} compared to PO_4^{3-} is probably responsible for significantly lower rejections of SO_4^{2-} compared to PO_4^3.

According to Table 4.4, the solute radius of NH_4^+ is slightly larger than the solute radius of K^+. This is probably why the diffusivity of the former is slightly lower than that of the latter. Considering the rejections of the two cations from different mixed salt solutions an interesting behavior of K^+ can be observed. On the one hand, for the fixed ratio of $(NH_4)_2SO_4$ and K_3PO_4 and the increasing total salts concentration, the rejection of K^+ slightly decreases (Table 4.5). However, at the highest total salt concentration as the ratio of $(NH_4)_2SO_4$ and K_3PO_4 increases (Table 4.6), i.e. as the concentration of K_3PO_4 decreases, the rejection of K^+ appears to decrease. On the other hand, the corresponding rejections of NH_4^+ appear to be more independent of the composition and the concentration of the mixed-salt feed solution.

From the practical point of view, the rejections of NH_4^+ from the mixed-salt solutions are of a great interest, because they indicate the potential of the investigated LPRO membrane for the removal and concentration of ammonium ion, which is the

ultimate objective of this work. The rejections of NH_4^+ reported in Tables 4.5 and 4.6 are presented graphically in Figs. 4.13 and 4.14, respectively.

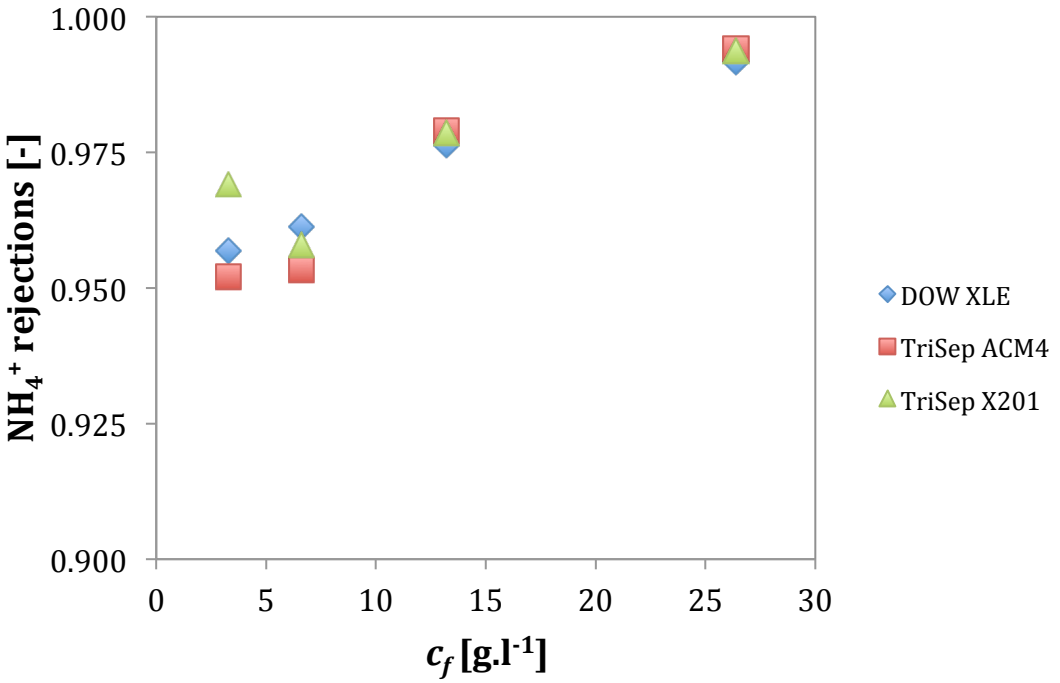

Figure 4.13: NH_4^+ rejections as a function of increasing total feed concentrations following the NH_4^+: K^+ ratio found in anaerobic digestate. The rejections were calculated after conversion of NH_4^+ concentrations from $g.l^{-1}$ to $mol.l^{-1}$. All experiments were carried out at 23 ± 1.5 ºC.

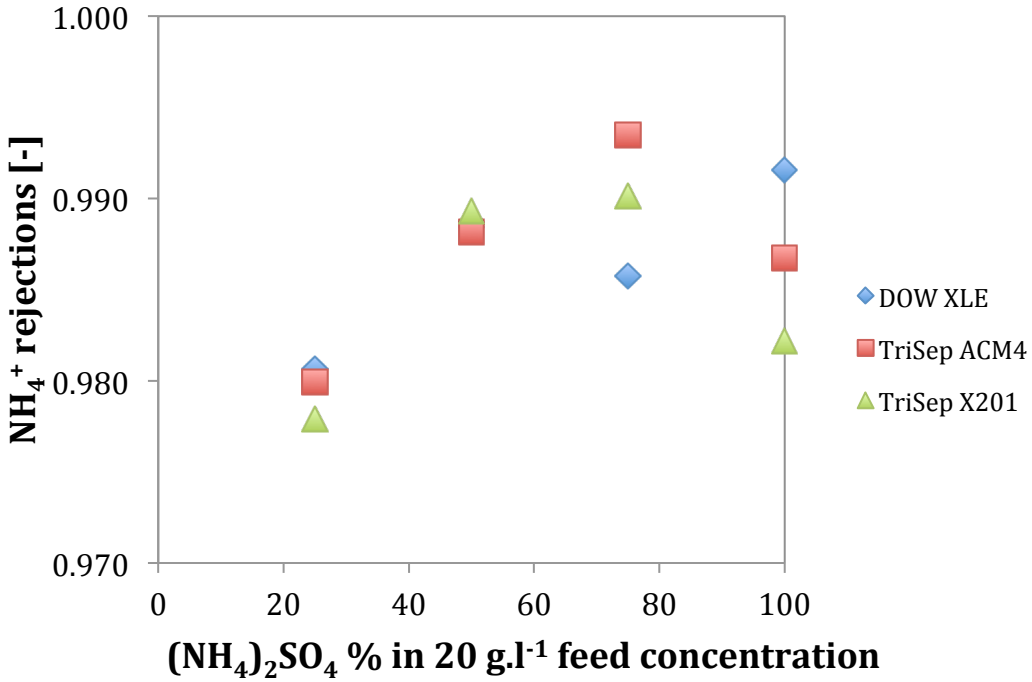

Figure 4.14: NH_4^+ rejections as a function of the mass percentage contribution of $(NH_4)_2SO_4$ to a 20 g.l^{-1} feed solution. All experiments were carried out at 23 ± 1.5 ºC.

It appears that in general as the concentration of $(NH_4)_2SO_4$ in feed solution increases, either the increase in the total salt concentration for the fixed ratio of $(NH_4)_2SO_4$ and K_3PO_4 – Fig. 4.13, or by increasing the ratio of $(NH_4)_2SO_4$ to K_3PO_4 for the fixed total salt concentration – Fig. 4.14, the rejection of NH_4^+ increases. This is exactly the opposite trend to that shown in Fig. 4.3 for the rejection of $(NH_4)_2SO_4$ in single-salt experiments at an increasing solute concentrations. It should be emphasized that the results presented in Fig. 4.3 were determined assuming a stoichiometric transport of ions across the membrane, which might not be the case. This could be confirmed by repeating single-salt experiments and determining the permeate composition by focusing on each ion separately, as it was the case for the mixed-salt experiments. Regardless of the outcome of the repeated single-salt experiments, the results shown in Figs 4.13 and 4.14 are extremely promising for the ultimate objective of this study. They indicate that if the membrane process were scaled-up and thus carried out at non-zero stage cut conditions, as the concentration of NH_4^+ ion on the high pressure-side of the membrane were increasing, its rejection would not decline but rather increase. This would allow a

very efficient concentration of the NH_4^+ ions in the reject stream, even in relatively low-stage cut conditions.

Considering the rejection of NH_4^+ by different membranes in Figs 4.13 and 4.14, there is no consistent trend with respect to which membrane shows the highest rejection. It can be seen that although TriSep X201 appears to be the best at the lowest total feed concentration in Fig. 4.13, it is the worst one for the lowest ratio of $(NH_4)_2SO_4$ to K_3PO_4 in Fig. 4.14. It is important to note that although it is difficult to rank the investigated membranes on the basis of NH_4^+ rejection, they all show excellent rejections for this cation. It is easier to rank the investigated membranes on the basis of the permeate flux (Figs. 4.11 and 4.12), according to which DOW XLE appears to be the best, followed by TriSep ACM4 and TriSep X201. However, despite some differences in permeate flux all of these membranes would be suitable for the concentration NH_4^+ ion from the mixed-salt solutions containing $(NH_4)_2SO_4$ and K_3PO_4.

4.5 Conclusions

In this paper the characterization of membranes using the solution-diffusion and Kedem-Katchalsky models for feed solutions of $(NH_4)_2SO_4$ and K_3PO_4 have been carried out, and it has been concluded that both models are inadequately equipped to explain the observed results. A previous paper carried out by the team members also found evidence of solute transport by mechanisms other than diffusion through RO membranes, and it concluded that the basic solution-diffusion model was inadequately equipped to explain the observed results. This was attributed to the possibility of non-stoichiometric passage of ions through the membranes owing to the creation of a membrane surface charge, a phenomenon caused by the pH of the feed solution. Further investigation using mixed-salt solutions showed the presence of non-stoichiometric rejections for all experiments, indicating that models that do not consider the effect of individual ions in the system on total membrane performance may not be able to fully explain the transport mechanisms. Advanced mechanistic models are therefore recommended for further characterization purposes.

The use of membranes in the concentration of ammonium ions in feed solutions comprising two salts has been shown to be very efficient, with a minimum NH_4^+ rejection of 95.7%. The DOW XLE membrane showed high rejections for both $(NH_4)_2SO_4$ and

NH_4^+ ion and had the highest permeate fluxes for both single salt and mixed salt experiments, which makes it the best membrane for NH_4^+ concentration in anaerobic digestate. The DOW XLE membrane also has the highest average rejections for all the ions in the mixed-salt system. Further tests using this membrane with mixed-salt solutions and other single-salt solutions are strongly recommended.

It is recommended that the single salt experiments should be redone with a focus on ascertaining the stoichiometric nature or otherwise of membrane rejections. This can be done using two or more salts, and the feed pH of all experiments should be monitored to better understand the effect of feed pH on membrane surface charge, which affects membrane performance. If non-stoichiometric rejections are observed, the mixed-salt experiments should be characterized using mechanistic models based on the extended Nernst-Planck equation or the Maxwell-Stefan equation.

4.6 Acknowledgements

This research project was conducted in collaboration with CHFour Biogas Ltd, and was financially supported through the NSERC (Natural Sciences and Engineering Research Council) Engage Plus program.

Nomenclature

Symbol	Title	Units
σ	Reflection coefficient	-
ϕ	Osmotic coefficient	-
ΔP	Pressure differential	Pa
$\Delta\pi$	Osmotic pressure differential	Pa
π_f	Osmotic pressure on feed side of membrane	Pa
π_p	Osmotic pressure on permeate side of membrane	Pa
ω	Solute permeability coefficient	$mol.m^{-2}.s^{-1}.Pa^{-1}$
A_m	Membrane area	m^2
c_{avg}	Average solute concentration across the membrane	$mol.m^{-3}$
c_f	Solute concentration in feed	$mol.m^{-3}$
c_p	Solute concentration in permeate	$mol.m^{-3}$

ENP	Extended Nernst-Planck	
ICP-MS	Inductively coupled plasma mass spectrometry	
IEP	Isoelectric point	
j_i	Solute flux across the membrane	$mol.m^{-2}.s^{-1}$
J_V	Permeate/solvent flux across the membrane	$kg.m^{-2}s^{-1}$
LPRO	Low-pressure reverse osmosis	
ρ	Density	$kg.m^{-3}$
$\overline{P_{M,S}}$	Solute permeance across the membrane	$m.s^{-1}$
$\overline{P_{M,W}}$	Solvent permeance across the membrane	$kg.m^{-2}.s^{-1}.Pa^{-1}$
R	Solute rejection	-
RO	Reverse osmosis	
UF	Ultrafiltration	
V_P	Permeation rate through the membrane	$kg.s^{-1}$

4.7 References

[1] W. R. Bowen, a. W. Mohammad, and N. Hilal, "Characterisation of nanofiltration membranes for predictive purposes - Use of salts, uncharged solutes and atomic force microscopy," *J. Memb. Sci.*, vol. 126, no. 1, pp. 91–105, 1997.

[2] B. Van der Bruggen, M. Mänttäri, and M. Nyström, "Drawbacks of applying nanofiltration and how to avoid them: A review," *Sep. Purif. Technol.*, vol. 63, no. 2, pp. 251–263, 2008.

[3] V. K. Gupta, S.-T. Hwang, W. B. Krantz, and A. R. Greenberg, "Characterization of nanofiltration and reverse osmosis membrane performance for aqueous salt solutions using irreversible thermodynamics," *Desalination*, vol. 208, no. 1–3, pp. 1–18, 2007.

[4] V. Silva, V. Geraldes, a. M. Brites Alves, L. Palacio, P. Prádanos, and a. Hernández, "Multi-ionic nanofiltration of highly concentrated salt mixtures in the

seawater range," *Desalination*, vol. 277, no. 1–3, pp. 29–39, 2011.

[5] X. Jin, X. Huang, and E. M. V Hoek, "Role of specific ion interactions in seawater RO membrane fouling by alginic acid," *Environ. Sci. Technol.*, vol. 43, no. 10, pp. 3580–3587, 2009.

[6] a. M. Hidalgo, G. León, M. Gómez, M. D. Murcia, D. S. Barbosa, and P. Blanco, "Application of the solution-diffusion model for the removal of atrazine using a nanofiltration membrane," *Desalin. Water Treat.*, vol. 51, no. 10–12, pp. 2244–2252, 2013.

[7] F. N. Ahmed, "Modified Spiegler-Kedem Model to Predict the Rejection and Flux of Nanofiltration Processes at High NaCl Concentrations," University of Ottawa, 2013.

[8] W. R. Bowen and J. S. Welfoot, "Modelling the performance of membrane nanofiltration-critical assessment and model development," *Chem. Eng. Sci.*, vol. 57, no. 7, pp. 1121–1137, 2002.

[9] M. Mondor, L. Masse, D. Ippersiel, F. Lamarche, and D. I. Massé, "Use of electrodialysis and reverse osmosis for the recovery and concentration of ammonia from swine manure," *Bioresour. Technol.*, vol. 99, no. 15, pp. 7363–7368, 2008.

[10] R. Einav, K. Harussi, and D. Perry, "The footprint of the desalination processes on the environment," *Desalination*, vol. 152, no. 1–3, pp. 141–154, 2003.

[11] S. Sridhar, A. Kale, and a. a. Khan, "Reverse osmosis of edible vegetable oil industry effluent," *J. Memb. Sci.*, vol. 205, no. 1–2, pp. 83–90, 2002.

[12] L. F. Greenlee, D. F. Lawler, B. D. Freeman, B. Marrot, and P. Moulin, "Reverse osmosis desalination: Water sources, technology, and today's challenges," *Water Res.*, vol. 43, no. 9, pp. 2317–2348, 2009.

[13] A. Little, "Can Desalination Counter California's Drought? - The New Yorker," *New Yorker*, 2015. [Online]. Available: http://www.newyorker.com/tech/elements/can-desalination-counter-the-drought. [Accessed: 13-Oct-2015].

[14] I. D. Association, “Desalination by the Numbers | IDA,” *Desalination 101*, 2014. [Online]. Available: http://idadesal.org/desalination-101/desalination-by-the-numbers/. [Accessed: 13-Oct-2015].

[15] D. M. Babson, K. Bellman, S. Prakash, and D. E. Fennell, “Anaerobic digestion for methane generation and ammonia reforming for hydrogen production: Athermodynamic energy balance of a model system to demonstrate net energy feasibility,” *Biomass and Bioenergy*, vol. 56, pp. 493–505, 2013.

[16] L. Appels, J. Baeyens, J. Degrève, and R. Dewil, “Principles and potential of the anaerobic digestion of waste-activated sludge,” *Prog. Energy Combust. Sci.*, vol. 34, no. 6, pp. 755–781, 2008.

[17] J. H. Kim, D. H. Um, and O. C. Kwon, “Hydrogen production from burning and reforming of ammonia in a microreforming system,” *Energy Convers. Manag.*, vol. 56, pp. 184–191, 2012.

[18] T. Wirthensohn, F. Waeger, L. Jelinek, and W. Fuchs, “Ammonium removal from anaerobic digester effluent by ion exchange,” *Water Sci. Technol.*, vol. 60, no. 1, pp. 201–210, 2009.

[19] J. Desloover, A. Abate Woldeyohannis, W. Verstraete, N. Boon, and K. Rabaey, “Electrochemical resource recovery from digestate to prevent ammonia toxicity during anaerobic digestion,” *Environ. Sci. Technol.*, vol. 46, no. 21, pp. 12209–12216, 2012.

[20] B. Lauterböck, M. Ortner, R. Haider, and W. Fuchs, “Counteracting ammonia inhibition in anaerobic digestion by removal with a hollow fiber membrane contactor,” *Water Res.*, vol. 46, no. 15, pp. 4861–4869, 2012.

[21] M. L. Gerardo, N. H. M. Aljohani, D. L. Oatley-Radcliffe, and R. W. Lovitt, “Moving towards sustainable resources: recovery and fractionation of nutrients from dairy manure digestate using membranes,” *Water Res.*, vol. 80, pp. 80–89, 2015.

[22] D. . Nurdan Doruk, “A Novel Solution for Biogas Applications in Poultry

Industry: CLAMBS approach," *J. Bioprocess. Biotech.*, vol. 05, no. 02, 2015.

[23] S. H. Byeon, B. K. Lee, and B. Raj Mohan, "Removal of ammonia and particulate matter using a modified turbulent wet scrubbing system," *Sep. Purif. Technol.*, vol. 98, pp. 221–229, 2012.

[24] D. Carter, L. Rose, T. Awobusuyi, M. Gauthier, F. H. Tezel, and B. Kruczek, "Characterization of commercial RO membranes for the concentration of ammonia converted to ammonium sulfate from anaerobic digesters," *Desalination*, vol. 368, pp. 127–134, 2015.

[25] K. S. Spiegler and O. Kedem, "Thermodynamics of hyperfiltration (reverse osmosis): criteria for efficient membranes," *Desalination*, vol. 1, no. 4, pp. 311–326, 1966.

[26] M. El Guendouzi, a. Mounir, and a. Dinane, "Water activity, osmotic and activity coefficients of aqueous solutions of Li2SO4, Na2SO4, K2SO4, (NH4)2SO4, MgSO4, MnSO4, NiSO4, CuSO4, and ZnSO4 at T = 298.15 K," *J. Chem. Thermodyn.*, vol. 35, no. 2, pp. 209–220, 2003.

[27] M. El Guendouzi and A. Benbiyi, "Thermodynamic properties of binary aqueous solutions of orthophosphate salts, sodium, potassium and ammonium at T=298.15K," *Fluid Phase Equilib.*, vol. 369, pp. 68–85, 2014.

[28] Sterlitech, "Reverse Osmosis Membranes," 2015. [Online]. Available: http://www.sterlitech.com/reverse-osmosis-ro-membrane-ymxle3001.html.

[29] P. Xu, J. E. Drewes, T. U. Kim, C. Bellona, and G. Amy, "Effect of membrane fouling on transport of organic contaminants in NF/RO membrane applications," *J. Memb. Sci.*, vol. 279, no. 1–2, pp. 165–175, 2006.

[30] L. D. Nghiem, "Removal of emerging trace organic contaminants by nanofiltration and reverse osmosis," University of Wollongong, 2005.

[31] A. M. Comerton, R. C. Andrews, D. M. Bagley, and C. Hao, "The rejection of endocrine disrupting and pharmaceutically active compounds by NF and RO membranes as a function of compound and water matrix properties," *J. Memb.*

Sci., vol. 313, no. 1–2, pp. 323–335, 2008.

[32] K. M. Persson, V. Gekas, and G. Trägårdh, "Study of membrane compaction and its influence on ultrafiltration water permeability," *J. Memb. Sci.*, vol. 100, no. 2, pp. 155–162, 1995.

[33] A. E. Yaroshchuk, "The role of imperfections in the solute transfer in nanofiltration," *J. Memb. Sci.*, vol. 239, no. 1, pp. 9–15, 2004.

[34] Y. Zhao, J. T. Ã, and S. Hong, "Combined influence of membrane surface properties and feed water qualities on RO / NF mass transfer , a pilot study," vol. 39, pp. 1233–1244, 2005.

[35] J. Luo and Y. Wan, "Effects of pH and salt on nanofiltration-a critical review," *J. Memb. Sci.*, vol. 438, no. July 2015, pp. 18–28, 2013.

[36] W. R. R. Bowen and a W. A. W. Mohammad, "Characterization and prediction of nanofiltration membrane performance-a general assessment," *Chem. Eng. Res. Des.*, vol. 76, no. November, pp. 885–893, 1998.

[37] S. Szoke, G. Patzay, and L. Weiser, "Characteristics of thin-film nanofiltration membranes at various pH-values," *Desalination*, vol. 151, pp. 123–129, 2003.

[38] M. R. Teixeira, M. J. Rosa, and M. Nyström, "The role of membrane charge on nanofiltration performance," *J. Memb. Sci.*, vol. 265, no. 1–2, pp. 160–166, 2005.

Chapter 5: Characterization of Low Pressure RO membranes for Removal and Concentration of Ammonia from Anaerobic Digestate using Donnan Steric Pore Model

Tolulope D. Awobusuyi, F. Handan Tezel, Boguslaw Kruczek

Department of Chemical and Biological Engineering, University of Ottawa, 161 Louis Pasteur, Ottawa, Ontario K1N 6N5, Canada

Abstract

Membrane technology is the preferred separation method for a wide selection of industries, including the agriculture and desalination industries. This is due to a number of advantages: higher separation efficiencies at lower costs, environmentally benign processes and materials, and low capital costs. However, engineers' understanding of the solute and solvent behavior within membranes is an emerging field, and most of the models available are limited as to the parameters they can adequately describe. Membrane characterization is also difficult, and inconsistencies in physical properties across membrane sheets have been observed in literature.

In this paper, three low-pressure reverse osmosis membranes have been characterized using the Donnan Steric Pore model (DSPM), which accounts for diffusive, convective, and electromigration contributions to ionic transport through the membranes. The membranes are to be used for the removal and concentration of ammonium ions in anaerobic digestate, and have been tested using separate solutions of ammonium sulfate and tripotassium phosphate salts. The parameters by which the membranes have been characterized are the pore radius, r_p; the effective membrane thickness, L/A_k; and the membrane surface charge, X. The presence of a membrane surface charge has been shown and its effects on non-stoichiometric ionic rejections have also been examined.

Keywords: DSPM (Donnan Steric Pore model), Nernst-Planck equation, Membrane characterization, non-stoichiometric rejections, effects of feed pressure and pH on membrane performance, removal and concentration of ammonium ions in anaerobic digestate.

5.1 Introduction

Membrane separation processes are applied in many industries [1] for a variety of separation processes: desalination [2]–[5], agriculture [2], [6], [7], and healthcare industries [3], [7], [8] are some examples. These industries are generally involved in the production of high-purity chemical compounds and/or the production of waste that are considered hazardous to the environment. Therefore, efficient separation processes–as production and treatment steps–are a necessity [9]–[11]. In this paper three low pressure reverse osmosis (LPRO) membranes have been characterized using ammonium sulfate and tripotassium phosphate and the Donnan steric pore model. These membranes will be used in the concentration of ammonium ions in anaerobic digester effluent, which contains the ions that comprise $(NH_4)_2SO_4$ and K_3PO_4.

The models available for characterizing membranes used in solute/solvent separations do not always provide adequate descriptions of the membrane properties. Literature written on the subject agree that sieving, electrical and dielectric effects govern the rejection abilities of reverse osmosis (RO), LPRO and nanofiltration (NF) membranes [1], [7], and any model used in characterization must take these into consideration. In general, reverse osmosis membranes display higher solute rejections than nanofiltration membranes primarily because of size exclusion [12], but the effects of electrostatic interactions on the overall rejections cannot be ignored in either case. The effects of the membrane surface charge on ionic rejections, especially in cases of multiple ions being present in the feed, is also important [13]. The most common method for incorporating these effects is the extended Nernst-Planck (ENP) equation [1], [7], which is used in combination with a number of models: the pore model, the space charge model, and the Teorell-Meyer-Sievers model [1], [14]. The widespread use of the extended Nernst-Planck equation is due to its provision of ionic species transportation terms for each of the transportation modes [15]. Ion-ion interaction and ion-membrane interaction also play an important role in membrane performance and are accounted for using models based on the extended Nernst-Planck equation.

Models used in general are grouped in two categories: mechanistic and phenomenological models. In case of membranes, the mechanistic models account for ion transport through the membrane via the different transportation modes. The

phenomenological models can be described as “mechanism-independent” [7], and do not account for ionic transport, as the membrane is assumed to be near to equilibrium as a black box during solvent transport [8], [15]. There is the solution-diffusion model which, while being the most common model used in the characterization of polymeric membranes, has been shown to have limitations with respect to characterizing nanofiltration membranes as it does not account for convective transport through the membranes [2], [6]. This problem is rectified by the use of the Kedem-Katchalsky model or modifications to this model, such as the Spiegler-Kedem-Katchalsky model or a combination of the Spiegler-Kedem combination with liquid film theory [7], [15]. Models with the extended Nernst-Planck equation as a fundamental equation are commonly referred to as mechanistic models.

The effects of feed pH and applied pressure on membrane rejections cannot be understated. Changes in pressure affect the significant contributions of diffusion, convection, and electromigration to overall solute flux, and overall solute rejection. Effects of the feed pH may include an increase in estimated pore sizes and effective membrane thickness [16], [17], changes in membrane surface charge from positive to negative as the pH increases, although this is also affected by the nature of the solution [18], [19]. These have significant effects on overall membrane performance and should be taken into consideration when carrying out membrane characterization.

In this paper the results from permeation experiments for the removal and concentration of ammonia from anaerobic digestate using three low-pressure reverse osmosis (LPRO) membranes have been characterized using the Donnan Steric Pore Model (DSPM), which is based on the extended Nernst-Planck equation. The membranes were tested using separate solutions of ammonium sulfate and tripotassium phosphate solutions in a reverse osmosis process. The objectives of these tests were to determine the effects of feed pH and pressure changes on membrane activity and to determine the stoichiometric nature of the ionic rejections. A previous paper submitted for publication had shown non-stoichiometric rejections for feed solutions containing two salts and it was proposed to observe if the same behavior held true for single-salt solutions. The effect of pH on the stoichiometry of the rejections will provide important information for

the final application, which is the concentration of ammonium in anaerobic digester effluent using membranes.

5.2 Theoretical background

Ionic transport through polymeric membranes is dependent on a number of factors: the pore radius, r_p; the nature of the membrane polymer; the concentration of the feed; and the effective membrane thickness, L/A_k. Phenomenological models do not account for these in great detail, as it is assumed that the membrane functions as a "black box" in which the transport observed cannot be adequately explained from our existing fundamental knowledge [8], [15]. However, innovations in computational analysis [20]–[22] and greater understanding of the complex interrelationships between ions, polymeric materials, and solutes has led to the rise of mechanistic models that predict both transport parameters and the effective contribution of the individual transport mechanisms to the total solute flux. These models are based on either the Maxwell-Stefan or extended Nernst-Planck equations, although the extended Nernst-Planck equation is the more commonly used one of the two.

The extended Nernst-Planck equation describes the contributions of diffusion, electromigration, and convection, respectively, to the solute flux of a given ion through a membrane, as follows [1], [23]:

$$j_i = -D_{i,p}\frac{dc_i}{dx} - \frac{z_i c_i D_{i,p}}{RT} F \frac{d\psi}{dx} + K_{i,c} c_i J_v \tag{1}$$

where j_i is the flux of a given ion i, z_i is the valence charge, c_i is the concentration of an ion i within the membrane, F is the Faraday's constant, R is the universal gas constant, T is the temperature, J_v is the measured solvent flux, and $D_{i,p}$ is the ionic diffusivity of ion i. $D_{i,p}$ is given as:

$$D_{i,p} = K_{i,d} \times D_{i,\infty} \tag{2}$$

where $D_{i,\infty}$ is the ionic diffusivity at infinite dilution. Diffusive, electromigration, and convective transport are corrected for hindrances to transport for systems with ionic radii comparable to pore radii [25]–[27]. These hindrance factors, $K_{i,d}$ and $K_{i,c}$, are dependent on the solute radius to pore radius ratio, λ [1], and are applied as corrections to the ionic

diffusivity at infinite dilution and the solute volume carried through the membrane by the permeate flux, respectively. Bowen et al. [1] provides the formula for calculating the hindered factors, which are based on previous work done by Deen [28] and Bowen and Sharif [29] for $0 < \lambda < 0.8$. They have studied these hindrance factors for different ions and have found that the following equations applied for all the ions they studied:

$$K_{i,d} = 1.0 - 2.30\lambda + 1.154\lambda^2 + 0.224\lambda^3 \tag{3}$$

$$K_{i,c} = 1.0 + 0.054\lambda - 0.988\lambda^2 + 0.441\lambda^3 \tag{4}$$

It must be noted that these relationships work on the assumptions of an incompletely-developed solute velocity and homogeneous transport velocity across the membrane [1], [30].

The diffusion and electromigration terms in Eq (1) have driving forces of concentration gradient, $\frac{dc_i}{dx}$, and an electric potential difference, $\frac{d\psi}{dx}$, respectively. In the case of uncharged solutes, the electromigration term is taken to be nonexistent [1], [16], [24].

The use of an electric potential gradient to calculate the electromigration contribution is facilitated by the assumption of a constant electric field within the membrane pores and electroneutrality in both the bulk solutions and inside the membrane [1], [15]. The zero current condition is expressed as:

$$I = F\sum_{i=1}^{n} z_i j_i = 0 \tag{5}$$

The conditions of electroneutrality are expressed as follows:

$$\sum_{i=1}^{n} z_i C_i = 0 \tag{6a}$$

$$\sum_{i=1}^{n} z_i c_i = -X \tag{6b}$$

where C_i is the bulk concentration of a given ion i, c_i is the concentration of ion i inside the membrane, and X is the membrane surface charge, which is assumed to be constant throughout the membrane [1].

For systems operating under a low stage cut (ratio of permeate to the feed), the solute flux, j_i, can also be expressed as:

$$j_i = C_{i,p} \times J_V \tag{7}$$

where $C_{i,p}$ is the permeate concentration and J_v is the water (solvent) flux through the membrane. The concentration gradient of an ion i through the membrane is derived by substituting Eq. (7) into Eq. (1) and by rearranging it, as follows:

$$\frac{dc_i}{dx} = \frac{J_v}{D_{i,p}}(K_{i,c}c_i - C_{i,p}) - \frac{z_i c_i}{RT} F \frac{d\psi}{dx} \tag{8}$$

By assuming that the conditions of electroneutrality are applicable to the segments inside the membrane the electric potential, $\frac{d\psi}{dx}$, can be calculated by rearranging equation (1) for all the ions *i* in the system. The electric potential gradient is cumulative for all ions in the system and can thus be derived from Eq. (8):

$$\frac{d\psi}{dx} = \frac{\sum_{i=1}^{n} \frac{z_i J_v}{D_{i,p}}(K_{i,c}c_i - C_{i,p})}{\frac{F}{RT}\sum_{i=1}^{n}(z_i^2 c_i)} \tag{9}$$

Using the boundary conditions and satisfying the conditions of electroneutrality through the membrane for all ions can solve Equations 8 and 9 and give the concentration and electric potential gradients. To determine the concentration just inside the membrane at the membrane-solution interface, $c_{i,1}$ and $c_{i,n}$, the following equation is used with the boundary conditions specified for the feed and permeate sides in Eq. (10) [1]:

$$\frac{c_i}{C_i} = \varphi \exp\left(-\frac{z_i F}{RT}\Delta\psi_D\right) \tag{10}$$

where C_i is the bulk concentration on the side being considered. The bulk concentration, C_i, on either side of the membrane is given as:

$$x = 0; C_i = C_{i,f}, \qquad x = L; C_i = C_{i,p} \tag{11}$$

where $C_{i,f}$ and $C_{i,p}$ are the feed and permeate ion concentrations at the membrane-solution interface in the bulk phase, respectively. In Eq. (10), $\Delta\psi_D$ is the Donnan potential at the interface, F is the Faraday's constant, and ϕ is the steric partitioning coefficient, given by the following equation [1]:

$$\phi = (1-\lambda)^2 \tag{12}$$

where λ is the ratio of the solute radius to the pore radius. The Donnan potential is calculated using the following equation [31]:

$$\psi_D = -\frac{k_B T}{z_i e} \arcsin h\left(\frac{X}{2 z_i C_i}\right) \tag{13}$$

where k_B is the Boltzmann constant, e is the elementary charge, and X is the membrane surface charge. When ψ_D is calculated on either side of the membrane using $C_{i,f}$ and $C_{i,p}$ in Eq. (13), $\Delta\psi_D$ is calculated to be used in Eq. (10) by taking the difference between the two sides of the membrane.

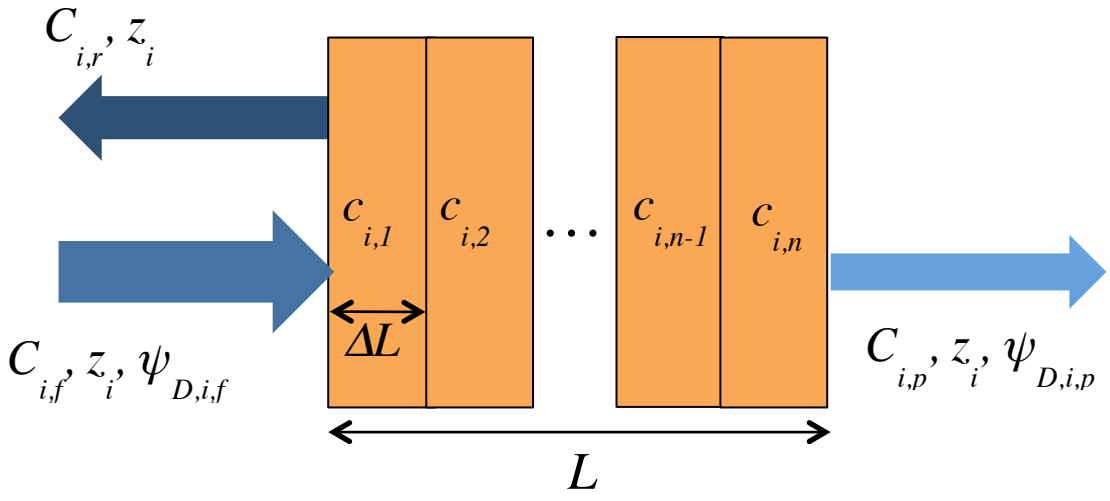

Figure 5.1: Schematic of the membrane detailing the locations of the bulk concentrations, donnan potentials, and concentrations inside the membrane, as used in the Donnan steric pore model.

Figure 5.1 shows the direction of flow and the locations of the bulk concentration and concentrations inside the membranes. Using this schematic as a basis, the DSPM model was applied for characterization of the LPRO membranes with Microsoft Excel 2011. The feed and permeate ionic concentrations were determined experimentally in a reverse osmosis system, along with the solvent flux, J_V, and using the equations outlined above, the pore radius, r_p, and membrane surface charge, X, were determined iteratively, as follows:

The membrane was conceptually divided into a number of segments (see Fig. 5.1) and the initial values of X and r_p were guessed. Then, the Donnan potentials at the feed

and permeate ends of the membrane were determined by using Equation 13 and $\Delta\psi_D$ is determined. The concentrations inside the membrane segment closest to the membrane-solution interface, c_i, are determined at both the feed and permeate ends using Equation 10 with the guessed value of r_p and the value obtained for $\Delta\psi_D$ for the guessed X. The value of c_i at the last segment next to the permeate is determined by using Eq. (10). Then, c_i in each of the subsequent membrane segments was determined using the one-step central difference method using Equations (8) and (9). Eq. 9 was solved for $\frac{d\psi}{dx}$ for each segment using the calculated c_i. This value of $\frac{d\psi}{dx}$ was used in Eq. (8) for each segment to calculate $\frac{dc_i}{dx}$. Then, all the calculated parameters with the guessed values of r_p and X are substituted into Eq. (1) and Eq. (6b) to solve for the improved values of r_p and X. This iteration is continued for each segment, until the values of r_p and X converge.

The calculated r_p and the experimentally determined J_V were used to determine the effective membrane thickness, L/A_k, using the Hagen-Poiseuille equation [23] as follows:

$$J_V = \frac{r_p^2 \Delta P}{8\mu(L/A_k)} \tag{14}$$

5.3 Experimental

Three low-pressure reverse osmosis membranes were characterized using two different solutions of a salt comprising ions found in anaerobic digestate. The salts used were $(NH_4)_2SO_4$ and K_3PO_4, and these were selected on the basis of their comprising ions found in anaerobic digestate and for their significant contributions to the total osmotic pressure exerted by the digestate on a membrane. The salts used were analytical-grade and were purchased from Sigma-Aldrich Canada (Oakville, Ontario). All standard solutions were prepared using deionized water from a Super-Q Plus Water Purification system (Etobicoke, Ontario). The permeate concentrations of K^+, SO_4^{2-}, and PO_4^{3-} were determined using an Agilent 8800 QQQ ICP-MS spectrometer (purchased from Santa

Clara, California, USA), and the permeate concentrations for NH_4^+ were determined using an indophenol colorimetric method developed at the Advanced Research Complex, University of Ottawa.

The ionic and salt properties are presented in Table 5.1. The diffusivities at infinite dilution are given in literature cited in the table caption, and the corresponding solute radii are calculated using the Stokes-Einstein equation, which is given as [28]:

$$D_{i,\infty} = \frac{k_B T}{6\pi\eta r_s} \tag{15}$$

The properties of the LPRO membrane characterized in this study are given in Table 5.2.

Table 5.1: Diffusivities at infinite dilution, solute radii, feed pH, and molecular weights of ions and salts used in the experiments in this study. The solute radii for individual ions were determined using the Stokes-Einstein equation and the ionic diffusivities were determined from literature. The feed pH was determined at a 20 $g.l^{-1}$ for both salts using a handheld pH meter.

	MW [$g.mol^{-1}$]	**Solute radius, r_s [nm]**	**pH**	**$D_{i,\infty}$, [$m^2.s^{-1}$]**
K^+	39.09	0.125	-	1.96×10^{-9}[a]
NH_4^+	18.04	0.128	-	1.98×10^{-9}[a]
SO_4^{2-}	96.06	0.207	-	1.07×10^{-9}[a]
PO_4^{3-}	94.97	0.343	-	7.00×10^{-10}[b]
$(NH_4)_2SO_4$	132.14	-	5.9	-
K_3PO_4	212.27	-	10.7	-

[a] As determined by Li and Gregory, 1974 [32]
[b] As determined by Krom and Berner, 1980 [33]

The acidic pH reported for $(NH_4)_2SO_4$ is a result of its being the product of a weak base, NH_4OH, and a strong acid, H_2SO_4. The alkaline pH of K_3PO_4 is a result of its being the product salt of a strong base, KOH, and a weak acid, H_3PO_4.

Table 5.2: Properties of LPRO membranes used in this study.

Membrane	DOW XLE	TriSep ACM4	TriSep X201
Material	Polyamide	Polyamide	Polyamide-Urea
Solvent flux [$kg.m^{-2}.s^{-1}$] [a]	0.0138	0.0184	0.0142
Applied pressure [$\times 10^5$ Pa] [a]	6.90	15.50	15.50
NaCl rejection [%] at 2 $g.l^{-1}$ [a]	98.7	99.2	99.5
pH Range [a]	2 - 11	2 - 11	2 - 11
Water contact angle	66.3 [b]	35 [c]	55.0 ± 1.8 [d]

[a] As reported by Sterlitech, 2015 for a 2 $g.l^{-1}$ NaCl feed solution at 25 ºC [34]
[b] As measured by Xu, et al., 2006 [35]
[c] As reported by Nghiem, L. D., 2005 [36]
[d] As measured by Comerton, 2008 [37]

5.4 Results

Ionic transport through LPRO membranes is dependent on the valence charge of the ion, the ionic radius, the pH of the feed solution, and the interactions between ions of the same or different valence charges in the solution surrounding the membrane [1], [21], [38], [39]. The focal points of this paper are the effects of pH on ionic transportation and membrane characterization using the DSPM model, both of which have been reported here. The effects of ionic properties like diffusivity and solute radius on ionic rejections are also briefly discussed.

5.4.1 Effect of feed pressure and pH on membrane performance: Non-stoichiometric rejections

Permeation tests were carried out for K_3PO_4 and $(NH_4)_2SO_4$ at two pressures (1.38 and 2.76 MPa), and the individual ionic concentrations in the permeate were measured. These ionic concentrations were plotted for 2 different applied pressures and have been presented in Figures 5.1 and 5.2 for K_3PO_4 and $(NH_4)_2SO_4$, respectively.

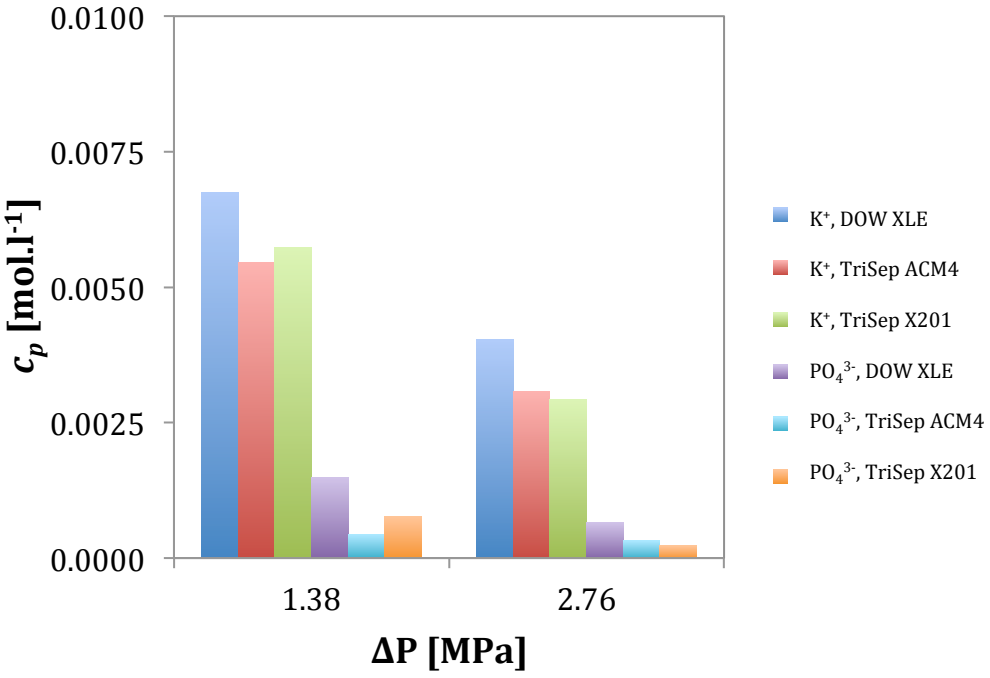

Figure 5.2: K^+ and PO_4^{3-} concentrations in permeate as a function of applied pressure differential. The feed concentration was 0.094 mol.l^{-1} K_3PO_4, and all experiments were carried out at 23.3 ± 0.7 ºC. The feed pH was 10.7.

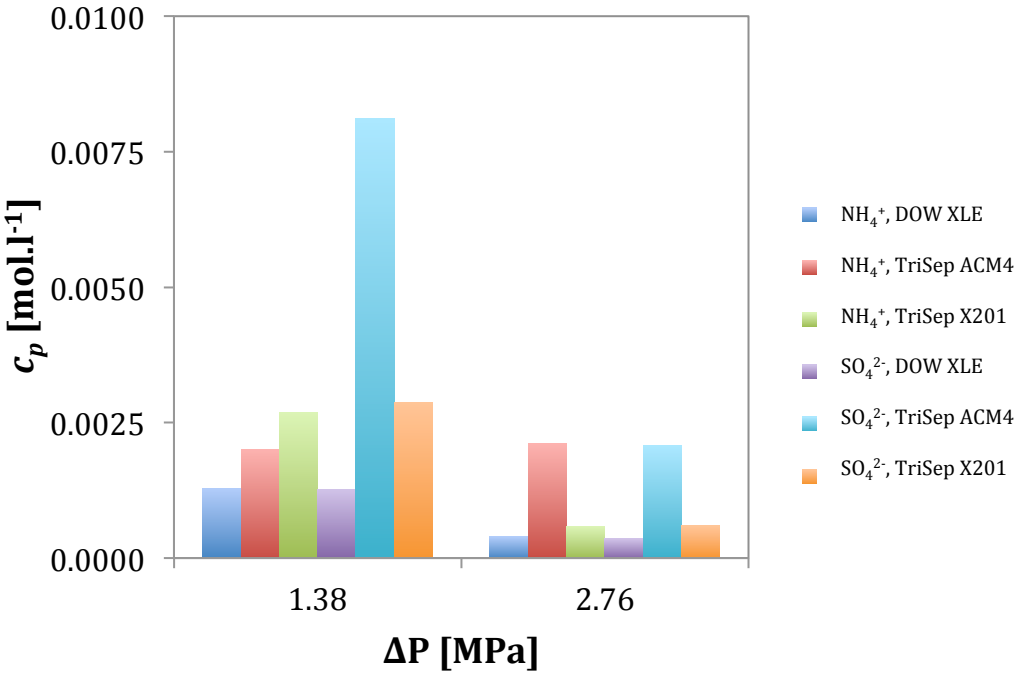

Figure 5.3: NH_4^+ and SO_4^{2-} concentrations in permeate as a function of applied pressure differential. The feed concentration was 0.151 mol.l^{-1} $(NH_4)_2SO_4$, and all experiments were carried out at 23.3 ± 0.7 ºC. The feed pH was 5.9.

Figure 5.2 shows that ionic concentrations of K^+ and PO_4^{3-} in the permeate do not follow the stoichiometric ratios of the feed salt, K_3PO_4, from which the ions were derived, as the concentrations of K^+ in the permeate are much higher than those of PO_4^{3-}. For the DOW XLE membrane, the K^+ concentration at 1.380 MPa is 0.007 mol.l^{-1}, while the corresponding PO_4^{3-} concentration at that pressure is 0.0014 mol.l^{-1}. The stoichiometric K^+:PO_4^{3-} ratio is 3:1, as 1 mole of K_3PO_4 gives 3 moles of K^+ and 1 mole of PO_4^{3-}. The stoichiometric ratio of K^+:PO_4^{3-} at 1.380 MPa is 5:3, while at 2.76 MPa the ratio is 2:1 in favor of K^+. This variation in concentration ratios are observed for all membranes as pressure increases, showing that increases in pressure affect both concentration and molar ratio of ions present in the permeate stream. In Figure 5.2 the K^+:PO_4^{3-} ratio is seen to increase with increasing pressure for all membranes.

The non-stoichiometric transport is influenced by the differences in solute sizes and ionic diffusivities, ion-membrane interaction, feed pH, and direction of ion transport

by electromigration. Size exclusion plays an important role in membrane rejection, and as K^+ ions are almost three times smaller than PO_4^{3-} ions (See Table 5.1), the rejections for K^+ are lower. The specific ion-membrane interaction between K^+ and reverse osmosis membranes leads to a favorable passage of K^+ ions. This has been documented in literature [40]. The preferential passage of cations through the membranes suggests an electrostatic attraction between the cations and the membrane surface, indicating a negatively charged membrane surface. Dielectric effects also play a role in ion rejection, as the presence of different dielectric charges for both the ions and membrane results in polarization charges at the solution-membrane interface [27]. This is accounted for in the electromigration term of the extended Nernst-Planck equation in the DSPM model.

Figure 5.3 also shows non-stoichiometric rejections for NH_4^+ and SO_4^{2-} for all experiments. Unlike the results presented in Fig. 5.2, however, anionic passage through the membrane is higher than cationic passage. The stoichiometric NH_4^+:SO_4^{2-} ratio is 2:1, as 1 mole of $(NH_4)_2SO_4$ gives 2 moles of NH_4^+ and 1 mole of SO_4^{2-}. For the DOW XLE, the stoichiometric ratio of NH_4^+:SO_4^{2-} at 1.380 MPa is 1:2, while at 2.76 MPa the ratio is 1:2 in favor of SO_4^{2-}. The preferential passage of SO_4^{2-} indicates a positively charged membrane surface that attracts SO_4^{2-}, as the solute radius and diffusivities at infinite dilution (see Table 5.1) favor NH_4^+ passage through the membrane. The effects of applied pressure on NH_4^+ and SO_4^{2-} rejections are also shown in Fig. 5.3, and while rejections increase for either ion (as can be seen with decreased concentrations in the permeate) at higher applied pressures, there is no effect on the ionic ratio of the rejections except for the ACM4 membrane.

From Figs. 5.2 and 5.3 it can be concluded that there is a preferential passage of ions through the membranes: K^+ in Fig. 5.2 and SO_4^{2-} in Fig. 5.3. It is suspected that this is due to the effects of feed pH on the membrane surface charge, a phenomenon also reported in available literature [41]. Permeate fluxes, pore structure, and membrane charges are also directly affected by pH, and literature on the subject also show that changes in pH bear directly on the electromigration of ions through the membrane [17], [42], [43]. More importantly, membrane surface charges are known to change signs as the pH of the feed solution changes, assuming a negative charge at a higher pH value beyond

the isoelectric point [44]. Kaya et al. [41] explain this as "the influence of the pH on the dissociation of the functional groups of the membranes." Fig. 5.2 shows a lower valence cation being passed preferentially when compared to its higher valence anionic counterpart. The higher diffusivity and the lower solute radius of the cation with respect to the anion (see Table 5.1) also aids preferential passage of K^+ through the membrane. The reverse behavior is observed in Fig. 5.3, where higher valence anion (SO_4^{2-}) preferentially passes through a membrane in the presence of a lower valence cation with a smaller solute radius and a higher diffusivity. These can be best explained as a change in membrane surface charge, which preferentially attracts certain ions. The membrane surface charge is likely a function of the feed pH, and lower feed pH are known to cause positively charged membrane surfaces and vice versa [17], [45].

The exposure of membranes to alkaline solutions has been shown to increase average pore size and the membrane thickness/porosity ratio [16], [46]. This corresponds to a decrease in rejections, and this can be enhanced by an increase in the salt concentrations [17], [24]. Overall, K_3PO_4 rejections (Figure 5.2) are lower than $(NH_4)_2SO_4$ rejections (Figure 5.3) at a feed concentration of 20 $g.l^{-1}$. Increases in applied pressure differentials also increase overall rejections, as seen in Figs. 5.2 and 5.3. The implications of these results for practical purposes are that ionic rejections can be influenced by the manipulation of the pH to create a membrane surface charge favorable to the desired ion. In the concentration of NH_4^+ ions in anaerobic digester effluent it is desirable to have a positively charged membrane, as seen in Figure 5.3, which repels positively charged ions. This can be done by lowering of the overall pH of the anaerobic digester effluent.

5.4.2 Effect of ionic properties on rejection

Table 5.1 provides the diffusivities and solute radii of the ions comprising the salts used in this study. Smaller ions have higher diffusivities and this may have an effect on ionic rejections, as disproportionately paired ions (K^+ and PO_4^{3-}) are seen to show disproportionate passage through the membranes, with the smaller ion displaying preferential passage. However, the feed pH determines the membrane surface charge, and valence charge of the ion determines its attraction or repulsion to the membrane surface.

From both Figures 5.2 and 5.3 ionic passage through the membrane is seen to decrease with increasing applied pressures. This is attributed to a drop in ion permeance through the membrane and is directly related to a decreasing ion diffusivity with increasing pressures [47]. This drop in ion permeance is also a result of the lowered porosity caused by compaction [48]. The differences in ionic passage as a result of applied pressure are best observed with the K^+ and NH_4^+ results in Figures 5.2 and 5.3, which show large drops in permeate concentrations for both ions for all membranes tested. Solute radii also contribute to the ionic passage through the membranes. Larger ions encounter greater resistance to passage through the membrane, and this is a probable cause of the low anionic permeate concentrations seen in Figures 5.2 and 5.3.

A combination of the membrane surface charges, applied pressure differential, valence charges, ion diffusivities and solute radii work together to determine ionic passage through the membranes. The feed pressure is seen to directly influence the rejection of ions within the system, and the creation of the membrane surface charge explains the preferential passage of ions through the membrane.

5.4.3 Membrane characterization using DSPM model

The ionic rejections obtained from the experiments conducted were used in fitting runs with the DSPM model until optimum solutions of r_p, X, and L/A_k were obtained. Using a sequence in which the differences between the predicted and actual ionic fluxes were minimized, r_p and X could be estimated with the observed rejection data.

Tables 5.3 and 5.4 show the results of fittings for K_3PO_4 and $(NH_4)_2SO_4$ using the DSPM model at two applied pressures, 1.380 and 2.76 MPa.

Table 5.3: Membrane parameters determined by the DSPM model using K_3PO_4 salt at the specified pressures.

	r_p [nm]		L/A_k [µm]		X [mol.m^{-3}]	
Pressure, MPa	1.380	2.76	1.380	2.76	1.380	2.76
XLE	0.475	0.5	21.79	32.07	-188	-263.2
ACM4	0.5	0.5	32.95	35.79	-282	-291.4
X201	0.45	0.397	38.09	30.56	-188	-197.4

From Table 5.3 the average pore radius for all membranes is determined to be 0.47 nm. The negative membrane surface charges predicted by the model confirm the suspected effect of pH on the membrane surface and on rejections in Section 5.4.1. The results also show a relationship between water permeances, which can be derived from Table 5.2, and membrane thickness, where the membranes with larger water permeances are predicted to have lower effective membrane thicknesses by the model. This is also shown in literature using the DSPM model for other membranes [23]. This effect is seen most clearly in the difference between the calculated effective membrane thicknesses for the XLE membrane at the two pressures and is a result of the lowered porosity A_k. A previous study showed that the XLE is susceptible to compaction at pressures as high as 2.76 MPa, and at compaction water permeance and membrane porosity are lowered.

Table 5.4: Membrane parameters predicted by the DSPM model using $(NH_4)_2SO_4$ solution at the specified pressures.

	r_p [nm]		L/A_k [μm]		X [mol.m^{-3}]	
Pressure, MPa	1.380	2.76	1.380	2.76	1.380	2.76
XLE	0.45	0.45	19.56	27.92	172.5	174.8
ACM4	0.49	0.51	31.64	37.23	208.9	208.2
X201	0.45	0.45	38.09	39.26	171.1	174.4

The results predicted using the DSPM model and $(NH_4)_2SO_4$ solution agree with the results presented in Table 5.3 and the effect of feed pressure and pH as discussed in the preceding section. The large increase in effective membrane thickness, post-compaction, for the XLE membrane is also confirmed in Table 5.3. However, Table 5.4 shows the membranes to be positively charged as a result of the slightly acidic pH of the feed solution. The relationship between pure water permeances and membrane thickness also holds and will be presented in detail in Table 5.5.

The membrane parameters for the three LPRO membranes used in this study are presented in Table 5.5. The average membrane thickness for the XLE membrane was calculated using the pre-compaction averages of the predicted membrane thickness.

Table 5.5: Average membrane properties as predicted by the DSPM model using K_3PO_4 and $(NH_4)_2SO_4$ salts. The pure water permeances have been calculated in a paper submitted for publication.

	Average r_p [nm]	Average L/A_k [µm]	P_{MW} [$kg.m^{-2}.s^{-1}.Pa^{-1}$]
XLE	0.47	20.68	1.45×10^{-8}
ACM4	0.5	34.40	1.042×10^{-8}
X201	0.44	36.50	0.717×10^{-8}

The pore radii shown in Table 5.5 are averaged across the pore radii obtained at pre-compaction pressures. From Table 5.5 it is seen that the X201 membrane has the smallest pore radii, corresponding to a lower flux through the membrane as seen in Table 5.2. Any attempt to describe a relationship between the pore radius and the permeance is inconclusive from the data, however. The distinct relationship between pure water permeance and $r_p^2/(L/A_k)$, which is shown by Equation 14, can be deduced from the results. Changes in L/A_k were seen to have no effect on the contributions of the diffusive, convective and electromigration transport modes to the overall solute flux and have not been reported. However, Bowen et al. [1] have reported that "the L/A_k value obtained from the pure water permeability is much larger than those obtained from the fitting of the rejection data." It should be noted that this was reported for uncharged solutes and may be considered as applicable to charged solutes.

5.5 Conclusions

The use of mechanistic models in membrane characterization has been shown to be an adequate tool for describing the pore radius and the membrane surface charges of LPRO membranes. A relationship between reductions in water permeances and increases in effective membrane thickness as a result of lowered membrane porosity has also been confirmed. However, changing the effective membrane thickness in the model has no effect on the solute flux contributions of the diffusive, convective, and electromigration transport modes. The effective membrane thickness predicted by the Hagen-Poiseuille equation was found to be exaggerated when compared to values observed in literature, which limits the effectiveness of this method of membrane characterization. The

characterization of these membranes using uncharged solutes should also be considered in order to give accurate predictions of the effective membrane thickness.

A relationship between feed pH and membrane surface charge has also been proven to exist, and a relationship between feed pH and stoichiometry of ions in the permeate steam has also been shown. The feed solution with slightly acidic pH (ammonium sulfate) was found to have a positively charged membrane and the alkaline pH feed solution (tripotassium phosphate) had negatively charged membrane surfaces. This was observed in the repulsion and attraction of positively charged ions in the feed, respectively, and is important information for the final application of these membranes, which is the concentration of ammonium ions in anaerobic digester effluent. Extensive measurements of the effects of feed pH on pore radius, membrane surface charge, and effective membrane thickness should also be considered for future work. The determination of the isoelectric point for all the membranes tested should also be considered.

The average pore radius of the LPRO membranes predicted by the developed model is 0.47 ± 0.009 nm. The variation in predicted pore radii across different solutes is relatively small, and so an average value of r_p can be reported with confidence. The predicted effective membrane thickness ranges from 19 – 39 μm, although the actual values may be much lower had the membranes been characterized using uncharged solutes. The increase in effective thickness due to the effect of membrane compaction has also been shown for the DOW XLE membrane.

5.6 Acknowledgements

This research project was conducted in collaboration with CHFour Biogas Ltd, and was financially supported through the NSERC (Natural Sciences and Engineering Research Council) Engage Plus program.

Nomenclature

Symbol	Title	Units
A_k	Membrane porosity	-

C_i	Bulk concentration of ion i	$mol.l^{-1}$
c_i	Concentration inside the membrane	$mol.l^{-1}$
$C_{i,f}$	Concentration on the feed side of the membrane	$mol.l^{-1}$
$C_{i,p}$	Concentration on the permeate side of the membrane	$mol.l^{-1}$
$\frac{dc_i}{dx}$	Concentration gradient	$mol.l^{-1}.m^{-1}$
$D_{i,p}$	Hindered diffusivity of ion	$m^2.s^{-1}$
$D_{i,\infty}$	Bulk Diffusivity	$m^2.s^{-1}$
e	Elementary charge, 1.602×10^{-19}	C
F	Faraday's constant, 96500	$C.mol^{-1}$
I	Ionic strength	M
j_i	Solute flux	$mol.m^{-2}.s^{-1}$
J_V	Solvent flux	$l.m^{-2}.s^{-1}$
k_B	Boltzmann constant, 1.381×10^{-23}	$J.K^{-1}$
$K_{i,c}$	Hindrance factor for convection	-
$K_{i,d}$	Hindrance factor for diffusion	-
$P_{M,W}$	Pure water permeance	$kg.m^{-2}.s^{-1}.Pa^{-1}$
r_p	Pore radius	m
r_s	Solute radius	m
R	Gas constant, 8.314	$J.mol^{-1}.K^{-1}$
T	Temperature	K
x	Distance in the membrane	m
X	Membrane surface charge	$mol.m^{-3}$
z_i	Valence of ion	-

Greek Letters

ξ	Ratio of membrane surface charge to bulk concentration	-
ϕ	Steric partitioning coefficient	-
λ	Ratio of solute radius to pore radius	-
μ	Solution viscosity	Pa.s
ΔP	Applied pressure differential	Pa

$\frac{d\psi}{dx}$	Electric potential gradient across each segment along the membrane	$V.m^{-1}$
$\Delta\psi_D$	Donnan potential	V
L	Membrane thickness	m

List of Abbreviations

DSPM	Donnan Steric Pore model
ENP	Extended Nernst Planck
LPRO	Low pressure reverse osmosis
NF	Nanofiltration
RO	Reverse osmosis

5.7 References

[1] W. R. Bowen, a. W. Mohammad, and N. Hilal, "Characterisation of nanofiltration membranes for predictive purposes - Use of salts, uncharged solutes and atomic force microscopy," *J. Memb. Sci.*, vol. 126, no. 1, pp. 91–105, 1997.

[2] B. Van der Bruggen, M. Mänttäri, and M. Nyström, "Drawbacks of applying nanofiltration and how to avoid them: A review," *Sep. Purif. Technol.*, vol. 63, no. 2, pp. 251–263, 2008.

[3] V. K. Gupta, S.-T. Hwang, W. B. Krantz, and A. R. Greenberg, "Characterization of nanofiltration and reverse osmosis membrane performance for aqueous salt solutions using irreversible thermodynamics," *Desalination*, vol. 208, no. 1–3, pp. 1–18, 2007.

[4] V. Silva, V. Geraldes, a. M. Brites Alves, L. Palacio, P. Prádanos, and a. Hernández, "Multi-ionic nanofiltration of highly concentrated salt mixtures in the seawater range," *Desalination*, vol. 277, no. 1–3, pp. 29–39, 2011.

[5] X. Jin, X. Huang, and E. M. V Hoek, "Role of specific ion interactions in seawater RO membrane fouling by alginic acid," *Environ. Sci. Technol.*, vol. 43, no. 10, pp. 3580–3587, 2009.

[6] a. M. Hidalgo, G. León, M. Gómez, M. D. Murcia, D. S. Barbosa, and P. Blanco, "Application of the solution-diffusion model for the removal of atrazine using a

nanofiltration membrane," *Desalin. Water Treat.*, vol. 51, no. 10–12, pp. 2244–2252, 2013.

[7] F. N. Ahmed, "Modified Spiegler-Kedem Model to Predict the Rejection and Flux of Nanofiltration Processes at High NaCl Concentrations," University of Ottawa, 2013.

[8] W. R. Bowen and J. S. Welfoot, "Modelling the performance of membrane nanofiltration-critical assessment and model development," *Chem. Eng. Sci.*, vol. 57, no. 7, pp. 1121–1137, 2002.

[9] M. Mondor, L. Masse, D. Ippersiel, F. Lamarche, and D. I. Massé, "Use of electrodialysis and reverse osmosis for the recovery and concentration of ammonia from swine manure," *Bioresour. Technol.*, vol. 99, no. 15, pp. 7363–7368, 2008.

[10] R. Einav, K. Harussi, and D. Perry, "The footprint of the desalination processes on the environment," *Desalination*, vol. 152, no. 1–3, pp. 141–154, 2003.

[11] S. Sridhar, A. Kale, and a. a. Khan, "Reverse osmosis of edible vegetable oil industry effluent," *J. Memb. Sci.*, vol. 205, no. 1–2, pp. 83–90, 2002.

[12] Y. Yoon and R. M. Lueptow, "Removal of organic contaminants by RO and NF membranes," *J. Memb. Sci.*, vol. 261, no. 1–2, pp. 76–86, 2005.

[13] C. Bellona, J. E. Drewes, P. Xu, and G. Amy, "Factors affecting the rejection of organic solutes during NF/RO treatment - A literature review," *Water Res.*, vol. 38, no. 12, pp. 2795–2809, 2004.

[14] X.-L. Wang, W.-J. Shang, D.-X. Wang, L. Wu, and C.-H. Tu, "Characterization and applications of nanofiltration membranes: State of the art," *Desalination*, vol. 236, no. 1–3, pp. 316–326, 2009.

[15] J. Wang, D. S. Dlamini, A. K. Mishra, M. T. M. Pendergast, M. C. Y. Wong, B. B. Mamba, V. Freger, A. R. D. Verliefde, and E. M. V Hoek, "A critical review of transport through osmotic membranes," *J. Memb. Sci.*, vol. 454, pp. 516–537, 2014.

[16] M. Dalwani, N. E. Benes, G. Bargeman, D. Stamatialis, and M. Wessling, "Effect of pH on the performance of polyamide/polyacrylonitrile based thin film composite membranes," *J. Memb. Sci.*, vol. 372, no. 1–2, pp. 228–238, 2011.

[17] J. Luo and Y. Wan, "Effects of pH and salt on nanofiltration-a critical review," *J.*

Memb. Sci., vol. 438, no. July 2015, pp. 18–28, 2013.

[18] T. Van Gestel, C. Vandecasteele, A. Buekenhoudt, C. Dotremont, J. Luyten, R. Leysen, B. Van Der Bruggen, and G. Maes, "Salt retention in nanofiltration with multilayer ceramic TiO2 membranes," *J. Memb. Sci.*, vol. 209, no. 2, pp. 379–389, 2002.

[19] M. R. Teixeira, M. J. Rosa, and M. Nyström, "The role of membrane charge on nanofiltration performance," *J. Memb. Sci.*, vol. 265, no. 1–2, pp. 160–166, 2005.

[20] X. Lefebvre, J. Palmeri, and P. David, "Nanofiltration theory: An analytic approach for single salts," *J. Phys. Chem. B*, vol. 108, no. 43, pp. 16811–16824, 2004.

[21] F. Fadaei, S. Shirazian, and S. N. Ashrafizadeh, "Mass transfer modeling of ion transport through nanoporous media," *Desalination*, vol. 281, pp. 325–333, 2011.

[22] J. Garcia-Aleman, J. Dickson, and a. Mika, "Experimental analysis, modeling, and theoretical design of McMaster pore-filled nanofiltration membranes," *J. Memb. Sci.*, vol. 240, no. 1–2, pp. 237–255, 2004.

[23] W. R. R. Bowen and a W. A. W. Mohammad, "Characterization and prediction of nanofiltration membrane performance-a general assessment," *Chem. Eng. Res. Des.*, vol. 76, no. November, pp. 885–893, 1998.

[24] J. Luo and Y. Wan, "Effect of highly concentrated salt on retention of organic solutes by nanofiltration polymeric membranes," *J. Memb. Sci.*, vol. 372, no. 1–2, pp. 145–153, 2011.

[25] X.-L. Wang, T. Tsuru, M. Togoh, S. Nakao, and S. Kimura, "Evaluation of pore structure and electrical properties of nanofiltration membranes," *Journal of Chemical Engineering of Japan*, vol. 28, no. 2. pp. 186–191, 1995.

[26] J. Schaep, C. Vandecasteele, a. W. Mohammad, and W. R. Bowen, "Analysis of the Salt Retention of Nanofiltration Membranes Using the Donnan–Steric Partitioning Pore Model," *Sep. Sci. Technol.*, vol. 34, no. 15, pp. 3009–3030, 1999.

[27] S. Bandini and D. Vezzani, "Nanofiltration modeling: The role of dielectric exclusion in membrane characterization," *Chem. Eng. Sci.*, vol. 58, no. 15, pp. 3303–3326, 2003.

[28] W. M. Deen, "Hindered Transport of Large Molecules in Liquid-Filled Pores,"

AIChE J., vol. 33, no. 9, pp. 1409–1425, 1987.

[29] W. R. Bowen and A. O. Sharif, "Transport through Microfiltration Membranes - Particle Hydrodynamics and Flux Reduction," *Journal of colloid and interface science*, vol. 168, no. 2. pp. 414–421, 1994.

[30] W. R. Bowen and H. Mukhtar, "Characterisation and prediction of separation performance of nanofiltration membranes," *J. Memb. Sci.*, vol. 112, no. 2, pp. 263–274, 1996.

[31] H. Ohshima and S. Ohki, "Donnan potential and surface potential of a charged membrane.," *Biophys. J.*, vol. 47, no. 5, pp. 673–8, 1985.

[32] Y.-H. Li and S. Gregory, "Diffusion of ions in seawater and in deep-sea sediments," *Geochim. Cosmochim. Acta*, vol. 38, pp. 703–714, 1974.

[33] D. Krom and R. A. Berner, "The diffusion coefficients of sulfate , ammonium , phosphate ions in anoxic marine sediments '," vol. 25, no. 2, pp. 327–337, 1980.

[34] Sterlitech, "Reverse Osmosis Membranes," 2015. [Online]. Available: http://www.sterlitech.com/reverse-osmosis-ro-membrane-ymxle3001.html.

[35] P. Xu, J. E. Drewes, T. U. Kim, C. Bellona, and G. Amy, "Effect of membrane fouling on transport of organic contaminants in NF/RO membrane applications," *J. Memb. Sci.*, vol. 279, no. 1–2, pp. 165–175, 2006.

[36] L. D. Nghiem, "Removal of emerging trace organic contaminants by nanofiltration and reverse osmosis," University of Wollongong, 2005.

[37] A. M. Comerton, R. C. Andrews, D. M. Bagley, and C. Hao, "The rejection of endocrine disrupting and pharmaceutically active compounds by NF and RO membranes as a function of compound and water matrix properties," *J. Memb. Sci.*, vol. 313, no. 1–2, pp. 323–335, 2008.

[38] C. Bartels, R. Franks, S. Rybar, M. Schierach, and M. Wilf, "The effect of feed ionic strength on salt passage through reverse osmosis membranes," *Desalination*, vol. 184, no. 1–3, pp. 185–195, 2005.

[39] Y. Zhao and J. S. Taylor, "Incorporation of osmotic pressure in an integrated incremental model for predicting RO or NF permeate concentration," *Desalination*, vol. 174, no. 2, pp. 145–159, 2005.

[40] R. W. Baker, *Membrane Technology and Applications*, 2nd Editio. West Sussex:

John Wiley & Sons, Ltd, 2004.

[41] Y. Kaya, Z. B. Gönder, I. Vergili, and H. Barlas, "The effect of transmembrane pressure and pH on treatment of paper machine process waters by using a two-step nanofiltration process: Flux decline analysis," *Desalination*, vol. 250, no. 1, pp. 150–157, 2010.

[42] K. Kezia, J. Lee, W. Ogieglo, A. Hill, N. E. Benes, and S. E. Kentish, "The transport of hydronium and hydroxide ions through reverse osmosis membranes," *J. Memb. Sci.*, vol. 459, pp. 197–206, 2014.

[43] L. Bruni and S. Bandini, "Studies on the role of site-binding and competitive adsorption in determining the charge of nanofiltration membranes," *Desalination*, vol. 241, no. 1–3, pp. 315–330, 2009.

[44] A. R. D. Verliefde, E. R. Cornelissen, S. G. J. Heijman, J. Q. J. C. Verberk, G. L. Amy, B. Van der Bruggen, and J. C. van Dijk, "The role of electrostatic interactions on the rejection of organic solutes in aqueous solutions with nanofiltration," *J. Memb. Sci.*, vol. 322, no. 1, pp. 52–66, 2008.

[45] S. Szoke, G. Patzay, and L. Weiser, "Characteristics of thin-film nanofiltration membranes at various pH-values," *Desalination*, vol. 151, pp. 123–129, 2003.

[46] A. Al-Amoudi, P. Williams, a. S. Al-Hobaib, and R. W. Lovitt, "Cleaning results of new and fouled nanofiltration membrane characterized by contact angle, updated DSPM, flux and salts rejection," *Appl. Surf. Sci.*, vol. 254, no. 13, pp. 3983–3992, 2008.

[47] V. T. Karathanos, G. K. Vagenas, and G. D. Saravacos, "Water diffusivity in starches at high temperatures and pressures," *Biotechnol. Prog.*, vol. 7, no. 2, pp. 178–184, 1991.

[48] K. M. Persson, V. Gekas, and G. Trägårdh, "Study of membrane compaction and its influence on ultrafiltration water permeability," *J. Memb. Sci.*, vol. 100, no. 2, pp. 155–162, 1995.

6.0 Conclusions and Recommendations

The concentration of ammonium ions in synthetic solutions comprising one ($(NH_4)_2SO_4$ or K_3PO_4) or two ($(NH_4)_2SO_4$ + K_3PO_4) salts was carried out using two RO membranes and three LPRO membranes. This was done as a group of feasibility studies for the application of membrane separation processes to the concentration of ammonium ions found in anaerobic digester effluent. The most important findings from this work were:

1. Ammonium rejections using membranes were in excess of 93% and were generally above 97%. These high rejections are favorable for the intended application to concentrate ammonium ions in the retentate using these membranes.
2. In the presence of multiple ions ammonium rejections are found to increase with increasing feed concentrations and increasing pH. But beyond the suspected isoelectric point, ammonium rejections decrease slightly as the membranes became negatively charged.
3. Solute transport through the membranes occurred via diffusive, convective, and electromigration mechanisms, and in single salt experiments non-stoichiometric rejections were observed.
4. The physical properties of the membranes can be determined using the Donnan steric pore model. The effective membrane thickness, however, was overestimated.

Based on the challenges faced during the process and the limitations observed for both the experiments and modeling the following recommendations can be made:

1. Testing the membranes using uncharged solutes to determine the correct effective membrane thickness;
2. Extensive testing focusing on the effects of feed pH on membrane performance, especially as it relates to ammonium retention;
3. The study of non-stoichiometric rejections in reverse osmosis and the influence of feed concentrations and feed pH on the stoichiometry of the ionic components in the permeate stream;
4. The study of co-ion competition for passage through the membrane as a function of feed concentration and pH.